STUDY OF SEDIMENTAL CHRONOLOGY, ELEMENTAL AND RADIOLOGICAL CONTAMINATION OF THE SUNDARBAN BY NEUTRON ACTIVATION ANALYSIS AND ALPHA SPECTROSCOPY TECHNIQUES

By

SHAIFUL KABIR

Student ID: 18PPHY001P

A thesis submitted in partial fulfillment of the requirements for the degree of

DOCTOR of PHILOSOPHY

Department of Physics

CHITTAGONG UNIVERSITY OF ENGINEERING AND TECHNOLOGY

NOVEMBER 2024

Declaration

I hereby declare that the work contained in this Thesis has not been previously submitted to meet the requirements for an award at this or any other higher education institution. To the best of my knowledge and belief, the Thesis contains no materials previously published or written by another person except where due reference is cited. Furthermore, the Thesis complies with the PLAGIARISM and ACADEMIC INTEGRITY regulations of CUET.

.

SHAIFUL KABIR
Student ID: 18PPHY001P
Department of Physics
Chittagong University of Engineering and Technology (CUET)

DEDICATED TO

MY BELOVED WIFE AND DAUGHTER

List of Publications

Journal Article

Publication 1: Shaiful Kabir, Mohammad Amirul Islam and Mohammad Belal Hossen, Natural radioactivity in soils and medicinal plants of the Sundarban: Concomitant radiological risks and radionuclide transfer factor, Journal of Radiation Research and Applied Sciences, 17(4) (2024) 101071.

Publication 2: Mohammad Amirul Islam, Shaiful Kabir, Ali Arman, Untung Sugiharto, M. Moinul Islam and Mohammad Belal Hossen, ^{210}Pb dating and neutron activation analysis of the Sundarban mangrove sediments: sedimentation rate and metal contamination history, Radiochimica Acta, 112(4) (2024) 273.

Publication 3: Shaiful Kabir, Mohammad Amirul Islam and Mohammad Belal Hossen, Elemental characterization of medicinal plants of the Sundarban by INAA and AAS techniques: health risk assessments and statistical analysis, Journal of Radioanalytical and Nuclear Chemistry, 332 (2023) 3687.

Conference

Conference 1: Shaiful Kabir, Mohammad Amirul Islam, Umma Tamim, Mohammad Belal Hossen, Temporal variation of natural radioactivity and evaluation of radiological hazards in sediment cores of Sundarban, Bangladesh, International conference on "Physics for Sustainable Development & Technology" 8-9-September 23, 2020, CUET.

Conference 2 (Invited Talk): Shaiful Kabir, Mohammad Amirul Islam, U. Tamim, Mohammad Belal Hossen, Elemental Characterization of Medicinal Plants of Bangladeshi Sundarban: Health risk assessments, "BCSIR Congress" 1-3 December, 2022, Dhaka, Bangladesh.

Conference 3: Shaiful Kabir, Mohammad Amirul Islam, Umma Tamim, Mohammad Belal Hossen, Temporal variation of natural radioactivity and evaluation of radiological hazards in sediment cores of Sundarban, Bangladesh, "International Conference on Physics" 19-21 May, 2022, AECD, Dhaka.

Conference 4: Shaiful Kabir, Mohammad Amirul Islam, K. Naher, Mohammad Belal Hossen, Neutron activation analysis for elemental characterization of medicinal plants from the Sundarban mangrove forest, Bangladesh, International conference on "Physics for Sustainable Development & Technology" 22-23 January, 2022, CUET.

Declaration by the Supervisor(s)

This is to certify that Shaiful Kabir, Student ID: 18PPHY001P has carried out this research work under our supervision and, that he has fulfilled the relevant Academic Ordinance of the Chittagong University of Engineering and Technology, so that he is qualified to submit the following Thesis in the application for the degree of DOCTOR of PHILOSOPHY in Physics. Furthermore, the Thesis complies with the PLAGIARISM and ACADEMIC INTEGRITY regulations of CUET.

Dr. Mohammad Belal Hossen
(Supervisor)
Professor
Department of Physics
Chittagong University of Engineering and Technology (CUET)

Dr. Mohammad Amirul Islam
(Co-supervisor)
Chief Scientific Officer
Reactor and Neutron Physics Division
Institute of Nuclear Science and Technology Atomic Energy Research Establishment
Bangladesh Atomic Energy Commission

Acknowledgment

First and foremost, all praise to the *Almighty*, the most Beneficent, and the most Merciful, who led me through this research and sustained me with help, guidance, and the power to complete this.

I am extremely delighted to express my deepest sense of gratitude and honor to my supervisors Dr. Mohammad Belal Hossen, Professor, Department of Physics, Chittagong University of Engineering and Technology (CUET) and Dr. Mohammad Amirul Islam, Chief Scientific Officer, Institute of Nuclear Science and Technology (INST), Atomic Energy Research Establishment (AERE), Bangladesh Atomic Energy Commission for their continuous support, numerous discussions, important suggestions and immense knowledge. They are enthusiastic physicists, from whom I had the privilege of learning not only research work but also basic knowledge of physics. Their unbelievable motivation and guidance helped me to continue and complete my thesis work.

I am pleased to express my deep appreciation to Professor Dr. H. M. A. R. Maruf, Head of the Department of Physics, CUET for his official support, continuous help and valuable scientific discussions during this work.

I also express my respect and thanks to the Director, INST, AERE and Head, Reactor and Neutron Physics Division (RNPD), INST, AERE for their kind permission to carry out my research work there. I am grateful to other scientists and staffs of NAA laboratory, RNPD, INST, AERE for their cordial help during my experimental work.

I also would like to express my gratitude to all faculty members in the Department of Physics, CUET to suggest and help me positively to complete my thesis. Last but not the least I would like to give special thanks to my beloved wife Umme Habiba Binte Islam because of her continuous unconditional supports along with patience towards the completion of this research work.

Abstract

The utilization of nuclear methods has significant potential for human health and sustainable environmental management. This study utilized various nuclear techniques (alpha spectrometry, neutron activation analysis, and gamma-ray spectrometry) to evaluate the sediment accumulation rate, elemental and radiological contamination history, and ecological risks posed by elements in the Sundarban mangrove forest in Bangladesh to develop a sustainable management strategy for the ecosystem. The mass accumulation rates of sediments, determined for the first time in this area by ^{210}Pb dating, varied from 0.068 to 3.20 kg m $^{-2}$ y $^{-1}$, with an average of 0.61 kg m $^{-2}$ y $^{-1}$. The contamination history of 11 metal(loid)s (Al, Ca, V, Cr, Fe, Ni, Cu, Zn, As, Hg, and Pb) for this ecosystem has also been assessed. Different environmental contamination indices suggested that Sundarban mangrove sediments have been contaminated by As. Considering different sediment quality guidelines, it has been observed that Cr, Ni, and As posed occasional adverse biological effects on marine organisms. This study also evaluated the essential and toxic element contents of three widely used medicinal plant leaves (*Acanthus ilicifolius*, *Avicennia officinalis*, and *Xylocarpus mekongensis*) of the Sundarban mangrove ecosystem and the possible health risks associated with the consumption of these plants for long time. The measured concentrations of the elements have been compared with available WHO permissible limits, which indicated that the average concentration of Zn in *A. ilicifolius* (41.2 ± 10.1 mg kg^{-1}) is higher than that of the permissible WHO limit (27 mg kg^{-1}). The average concentrations of Cr in *A. ilicifolius* (3.35 ± 0.37 mg kg^{-1}) and *X. mekongensis* (4.02 ± 2.30 mg kg^{-1}) are also higher than that of the WHO permissible limit (2 mg kg^{-1}). Nevertheless, the average daily intake of the toxic elements is below the maximum tolerable daily intake (MTDI) values. In addition, the natural radioactivity (^{226}Ra, ^{232}Th, and ^{40}K) concentration levels of some medicinal plants and soil cores of the Sundarban mangrove forest in Bangladesh have been assessed using a gamma-ray spectrometry technique. The average activity concentrations at the four cores of this mangrove system are relatively higher than those of their global mean values. Depth-wise activity concentration variations for most of the cores indicate that ^{226}Ra, ^{232}Th, and ^{40}K activities increase from the deeper layer to the surface soils, whereas for other cores, variations are haphazard or overall showed no change over the studied depths. The average activity concentrations of ^{226}Ra, ^{232}Th, and ^{40}K in the studied

medicinal plant leaves varied from 9.03 ± 3.01 to 66.9 ± 8.2 Bq kg^{-1}, 25.3 ± 5.0 to 155 ± 16 Bq kg^{-1}, and 68.1 ± 8.3 to 139 ± 12 Bq kg^{-1}, respectively. For the studied medicinal plants, the soil-to-plant transfer factors of ^{226}Ra, ^{232}Th, and ^{40}K ranged from 0.20 to 1.36, 0.27 to 2.08, and 0.036 to 0.108, respectively. Although some radiological hazard parameters for soils are higher than the global average values, excess lifetime cancer risk values were below the acceptable limit. Different statistical analyses have been performed to find out the origin and behavior of the metals and radionuclides in the mangrove system. This study indicated that the calculated radiological risk parameters for medicinal plants are lower than the acceptable limits prescribed by UNSCEAR. Therefore, the consumption of these medicinal plants by an adult is radiologically safe. Multivariate statistical approaches suggested that sources of metal(loid) pollution are a combination of human activities and natural geological processes. The findings of this study will enhance our understanding of metal pollution and the associated ecological and radiological risks to organisms, hence facilitating the development of novel approaches and management strategies to preserve vulnerable mangrove ecosystems.

বিমূর্ত

মানব স্বাস্থ্য এবং টেকসই পরিবেশ ব্যবস্থাপনার ক্ষেত্রে পারমাণবিক পদ্ধতির ব্যবহারের উল্লেখযোগ্য সম্ভাবনা রয়েছে। এই গবেষণায় বিভিন্ন পারমাণবিক পদ্ধতি (আলফা স্পেকট্রোমেট্রি, নিউট্রন অ্যাক্টিভেশন এনালাইসিস এবং গামা-রে স্পেকট্রোমেট্রি) ব্যবহার করে বাংলাদেশের সুন্দরবন ম্যানগ্রোভ ইকোসিস্টেমে পলিমাটি জমে যাওয়ার হার, দূষণের ইতিহাস, রাসায়নিক মৌল ও তেজস্ক্রিয়তা দ্বারা সৃষ্ট পরিবেশগত এবং রেডিওলজিক্যাল ঝুঁকি মূল্যায়ন করা হয়েছে যেন ইকোসিস্টেমটির একটি টেকসই ব্যবস্থাপনার কৌশল উদ্ভাবন করা যায়। ^{210}Pb ডেটিং পদ্ধতির মাধ্যমে এই এলাকায় প্রথম বারের মতো পলি মাটির ভর জমার হার নির্ণয় করা হয়েছে যা 0.068 থেকে 3.20 kg m^{-2} y^{-1} পর্যন্ত পরিবর্তিত হয়েছে, যার গড় 0.61 kg m^{-2} y^{-1}। এই ইকোসিস্টেমের কিছু ধাতু ও অপধাতু (Al, Ca, V, Cr, Fe, Ni, Cu, Zn, As, Hg, এবং Pb ইত্যাদি) এর দূষণের ইতিহাসও মূল্যায়ন করা হয়েছে। এই গবেষণায় বিভিন্ন পরিবেশ দূষণ সূচক থেকে জানা যায় যে সুন্দরবন ম্যানগ্রোভের পলি As দ্বারা দূষিত হয়েছে। বিভিন্ন পলি মানের নির্দেশিকা বিবেচনা করে এটি প্রতীয়মান হয়েছে যে Cr, Ni এবং As সামুদ্রিক জীবের উপর মাঝে মাঝে প্রতিকূল জৈবিক প্রভাব ফেলে। এই গবেষণায় সুন্দরবন ম্যানগ্রোভ ইকোসিস্টেমের তিনটি বহুল ব্যবহৃত ঔষধি গাছ (*Acanthus ilicifolius*, *Avicennia officinalis*, এবং *Xylocarpus mekongensis*) এর পাতায় প্রয়োজনীয় এবং ক্ষতিকর মৌলের পরিমান এবং উক্ত ঔষধি গাছ সেবনের সাথে সম্পর্কিত সম্ভাব্য স্বাস্থ্য ঝুঁকির মূল্যায়ন করা হয়েছে। মৌলগুলির পরিমাপ করা ঘনত্ব WHO অনুমোদিত সীমার সাথে তুলনা করা হয়েছে যা নির্দেশ করে যে, *A. ilicifolius* এ Zn-এর গড় ঘনত্ব (41.2 ± 10.1 mg kg^{-1}) WHO সীমার (27 mg kg^{-1}) থেকে বেশি; *A. ilicifolius* (3.35 ± 0.37 mg kg^{-1}) এবং *X. mekongensis* (4.02 ± 2.30 mg kg^{-1}) এ Cr-এর গড় ঘনত্বও WHO-এর অনুমোদিত সীমার (2 mg kg^{-1}) চেয়ে বেশি। তা সত্ত্বেও, বিষাক্ত মৌলগুলির গড় দৈনিক গ্রহনের পরিমান সর্বোচ্চ সহনীয় দৈনিক গ্রহণের (MTDI) সীমার নীচে। এছাড়া ও, উক্ত ম্যানগ্রোভ বনের কিছু ঔষধি গাছের প্রাকৃতিক তেজস্ক্রিয়তা (^{226}Ra, ^{232}Th, এবং ^{40}K) এর মাত্রা একটি গামা-রে স্পেকট্রোমেট্রি কৌশল ব্যবহার করে মূল্যায়ন করা হয়েছে। এই ম্যানগ্রোভ সিস্টেমের চারটি মাটির কোরের গড় তেজস্ক্রিয়তার ঘনত্ব তাদের বিশ্বব্যাপী গড় মানের তুলনায় বেশি। বেশিরভাগ কোরের জন্য গভীরতা-ভিত্তিক তেজস্ক্রিয়তা ঘনত্বের বৈচিত্র নির্দেশ করে যে ^{226}Ra, ^{232}Th, এবং ^{40}K এর তেজস্ক্রিয়তা গভীর স্তর থেকে পৃষ্ঠের মাটি পর্যন্ত বৃদ্ধি পেয়েছে, যেখানে অন্যান্য কোরের জন্য তেজস্ক্রিয়তা সামগ্রিকভাবে গভীরতার উপর কোন পরিবর্তন দেখা যায়নি। অধ্যয়নকৃত ঔষধি গাছের পাতায় ^{226}Ra, ^{232}Th, এবং ^{40}K এর তেজস্ক্রিয়তার ঘনত্ব যথাক্রমে 9.03 ± 3.01 থেকে 66.9 ± 8.2 Bq kg^{-1}, 25.3 ± 5.0 থেকে 155 ± 16 Bq kg^{-1}, এবং 68.1 ± 8.3 থেকে139 ± 12 Bq kg^{-1} পাওয়া গিয়াছে। অধ্যয়ন করা ঔষধি গাছের জন্য ^{226}Ra, ^{232}Th, এবং ^{40}K এর মাটি থেকে উদ্ভিদে স্থানান্তর ফ্যাক্টর যথাক্রমে 0.20 থেকে 1.36; 0.27 থেকে 2.08 এবং 0.036 থেকে 0.108 পাওয়া গিয়াছে। এই গবেষণায় যদিও সুন্দরবনের মাটির কিছু রেডিওলজিক্যাল বিপদের মাপকাঠি বিশ্বব্যাপী গড় মানগুলির চেয়ে বেশি, অতিরিক্ত জীবনকাল ক্যান্সার ঝুঁকির মান গ্রহণযোগ্য সীমার নীচে ছিল। এই গবেষণায় ম্যানগ্রোভ সিস্টেমে

ধাতু এবং রেডিওনুক্লাইডের উৎপত্তি এবং তাদের মাটিতে ছড়িয়ে পড়ার আচরণ খুঁজে বের করার জন্য বিভিন্ন পরিসংখ্যানগত বিশ্লেষণ ও করা হয়েছে। এই সমীক্ষাটি নির্দেশ করে যে ঔষধি গাছগুলির জন্য হিসাবকৃত রেডিওলজিক্যাল ঝুঁকির পরামিতিগুলি UNSCEAR দ্বারা নির্ধারিত গ্রহণযোগ্য সীমার নীচে। এতে প্রতীয়মান হয় যে, প্রাপ্ত বয়স্কদের দ্বারা এই ঔষধি গাছ গুলির পাতা ব্যবহার রেডিওলজিক্যালভাবে নিরাপদ। মাল্টিভ্যারিয়েট পরিসংখ্যানগত পদ্ধতির ব্যবহার পরামর্শ দেয় যে, ধাতব দূষণের উৎসগুলি মানুষের কার্যকলাপ এবং প্রাকৃতিক ভূতাত্ত্বিক প্রক্রিয়াগুলির সংমিশ্রণ। এই গবেষণার ফলাফলগুলি ধাতব দূষণ এবং জীবের সাথে সম্পর্কিত পরিবেশগত এবং রেডিওলজিক্যাল বিপদ সম্পর্কে আমাদের জ্ঞানের পরিধি বৃদ্ধি করবে, যা সুন্দরবনের মত সংবেদনশীল ম্যানগ্রোভ ইকোসিস্টেমগুলি সংরক্ষণের জন্য যুগোপযুগী পদ্ধতি এবং পরিচালনার কৌশলগুলির বিকাশকে সহজতর করবে।

Table of Contents

Declaration		I
Declaration by the Supervisor		V
Acknowledgments		VI
Abstract		VII
বিমূর্ত		IX
Table of Contents		XI
List of Figures		XIV
List of Tables		XV
Nomenclature		XVIII
Chapter 1:	**INTRODUCTION**	
1.1	Background	1
1.2	Aims and Objectives	4
1.3	Significance, Scope and Definitions	5
1.4	Thesis Outline	6
Chapter 2:	**LITERATURE REVIEW**	
2.1	Theoretical Background	7
2.1.1	Neutron Activation Analysis	7
2.1.2	Theory of NAA	7
2.1.3	Classification of NAA Method	9
2.1.4	Fundamental Equations for the NAA Method	9
2.1.5	Absolute NAA Method	10
2.1.6	Comparative NAA Method	13
2.2	^{210}Pb Dating Technique	13
2.3	Atomic Absorption Spectrometry	15
2.4	Survey of Some Reported Previous Works	16
2.5	Research Gap	22

Chapter 3: MATERIALS AND METHODOLOGY

3.1	Study Area, Sample Collection and Preparation	24
3 .1.1	Study Area	24
3.1.2	Sample Collection and Preparation	24
3.2	Experimental Techniques	28
3.2.1	Alpha Spectrometry	28
3.2.2	TRIGA Mark II Research Reactor	30
3.2.3	Irradiation and Counting of Samples and Standards by INAA	33
3.2.4	High Purity Germanium Detector	34
3.2.5	Some Important Parameters of HPGe Detector System	35
3.2.6	Gamma Ray Counting	39
3.3	Sample Analysis	41
3.3.1	^{210}Pb Activity Determination	41
3.3.2	Elemental Concentration Determination by INAA	42
3.3.3	Determination of Natural Radioactivity Concentration	42
3.3.4	Elemental Concentration Determination by AAS	42
3.4	Minimum Detectable Activity Concentration	44
3.5	Assessment of Elemental Contamination	44
3.6	Radionuclide Transfer Factor	46
3.7	Radiological Hazard Indices	46
3.8	Quality Control and Quality Assurance	48
3.9	Estimation of Uncertainty	48
3.10	Detection Limits	50

Chapter 4: RESULTS AND DISCUSSION

4.1	Mass Accumulation, Elemental Contamination History and Ecological Risk Assessment of the Sediment of Sundarban	51
4.1.1	Evaluation of Accuracy of the Analysis	51
4.1.2	Sediment Geochronology and Accumulation Rate	53
4.1.3	Spatiotemporal Distribution of Metals in the Sediment Cores	57
4.1.4	Metal Contamination and Ecological Risk Assessment	64

4.1.5	Statistical Analysis for Source Apportionment and Transport Behavior of Metals	69
4.2	Elemental Contamination and Health Risk Assessment of the Medicinal Plants	73
4.2.1	Accuracy Level of the Analysis	73
4.2.2	Health Risk Assessments	79
4.2.2.1	Average Daily Intake	79
4.2.2.2	Target Hazard Quotient	80
4.2.2.3	Target Carcinogenic Risk	80
4.2.2.4	Transfer Factor and Pollution Index	81
4.2.3	Statistical Analysis of the Elemental Data of Medicinal Plants	83
4.3	Natural Radioactivity and Radiological Risk Assessment of the Core Sediments and Medicinal Plants	86
4.3.1	Depth-Wise Radioactivity Concentrations	86
4.3.2	Radiological Hazard Parameters	93
4.3.3	Radioactivity and Associated Radiological Risk of the Medicinal Plants	95
4.3.4	Radionuclide Transfer Factor for the Medicinal Plants	96
4.3.5	Statistical Analysis of Radiological Data	97

Chapter 5: CONCLUSIONS

5.1	Key Findings	100
5.2	Limitation of Study	101
5.3	Practical Implication	101
5.4	Recommendations for Further Study	101

BIBLIOGRAPHY 102-113

List of Figures

Fig. No.	Figure Caption	Page No.
2.1	Probability of occurring nuclear reaction.	8
2.2	Production of supported ^{210}Pb in sediment.	14
2.3	Atomic Absorption Spectrometer-AA6800 used in for the present study in AERE.	16
3.1	Geographical locations of sample collections from the Sundarban.	25
3.2	A typical core sample collected from the Sundarban.	26
3.3	Medicinal plant samples collected from the Sundarban.	26
3.4	Sample preparation for neutron irradiation.	27
3.5	Sample preparation for natural radioactivity measurement.	28
3.6	Alpha spectrometer used in the present study.	29
3.7	Partial view of TRIGA Mark II research reactor.	30
3.8	Inner view of TRIGA Mark II research reactor at AERE, Savar.	32
3.9	Sediment core samples collecting after irradiation in BTRR.	34
3.10	Partial view of HPGe detector system used for this study.	35
3.11	Energy calibration with ^{152}Eu point source.	36
3.12	Energy resolution of the HPGe detector system (1333 keV).	39
3.13	The component of a digital gamma ray spectrometry system.	40
3.14	A typical gamma-ray spectrum of a sediment core sample.	40
3.15	Flowchart of acid digestion method for AAS.	43
4.1	The profiles of $^{210}Pb_{ex}$ vs. depth for the two sediment cores.	54
4.2	Depth (year) vs. mass accumulation rate for the sediment cores.	56
4.3	Vertical metal concentration variations in two cores.	60
4.4	Profiles of EF and I_{geo} values of the elements over time at sediment cores.	65
4.5	Percentage of samples under different SQG values for sediment cores.	68
4.6	Dendogram plot of the metals for sediment cores.	71
4.7	Depth-wise variations of the activity concentrations of the radionucleides ^{226}Ra, ^{232}Th, and ^{40}K.	93

List of Tables

Table No.	Table Caption	Page No.
3.1	Principal design parameters of TRIGA MARK II reactor.	31
3.2	Energy calibration with ^{152}Eu point source.	36
3.3	Data for energy resolution calculation of the HPGe detector system.	37
3.4	Description and equations of the radiological risk indices.	47
3.5	Origin and typical magnitude of uncertainties in INAA.	49
4.1	Accuracy of the analysis by determining ^{210}Pb concentrations in the standard reference materials IAEA-368 (Pacific Ocean sediment) and IAEA-300 (Baltic Sea sediment).	51
4.2	Comparison of measured values with certified values (mg kg^{-1}) in the standard reference materials NIST-SRM-1633b.	52
4.3	Comparison of measured values with certified values (mg kg^{-1}) in the certified reference materials IAEA-CRM-SL-1.	53
4.4	Basic statistics of the metal concentration (% or mg kg^{-1}) data of the C1 core.	57
4.5	Basic statistics of the metal concentration (% or mg kg^{-1}) data of the C2 core.	58
4.6	Basic statistics of the metal concentration (% or mg kg^{-1}) data of the C3 core.	59
4.7	Basic statistics of the metal concentration (% or mg kg^{-1}) data of the C4 core.	59
4.8	Comparison of metal concentrations (% or mg kg^{-1}) in sediments from Bangladeshi and Indian parts of the Sundarban mangrove forest.	63
4.9	Ecological risk factors for the potentially toxic metal(loid)s in sediment cores.	66
4.10	Pearson correlation coefficients for the metal(loid)s in sediment cores.	70
4.11	Varimax rotated factor loading matrix of 11 metal(loid)s	72

(variables) for Sundarban core sediment samples.

4.12 Comparison of measured values with certified values (mg kg^{-1}) in the standard reference materials of SRM-1547 (peach leaves). 74

4.13 Mean values (n = 3) of elemental concentrations (mg kg^{-1}) determined in three medicinal plants by the INAA and AAS. 76

4.14 Elemental concentrations (mg kg^{-1}) in the rhizosphere soil samples. 78

4.15 Comparison of the average daily intake (ADI, mg day^{-1}) of the elements in medicinal plants with the corresponding maximum tolerable daily intake (MTDI) in the Bangladeshi population. 79

4.16 Target hazard quotient (THQ) and target carcinogenic risk (TCR) values of the elements for consuming medicinal plants. 81

4.17 Transfer factor for medicinal plant samples *A. ilicifolius, A. officinalis,* and *X. mekongensis.* 82

4.18 Pollution index value for heavy metals in medicinal plants. 83

4.19 Pearson correlation coefficients for the metals in plant sample (*A. ilicifolius*). 84

4.20 Pearson correlation coefficients for the metals in plant sample (*A. officinalis*). 85

4.21 Pearson correlation coefficients for the elements in plant sample (*X. mekongensis*). 86

4.22 Activity concentrations (Bq kg^{-1}) of radionuclides in the core-1. 87

4.23 Activity concentrations (Bq kg^{-1}) of radionuclides in the core-2. 88

4.24 Activity concentrations (Bq kg^{-1}) of radionuclides in the core-3. 89

4.25 Activity concentrations (Bq kg^{-1}) of radionuclides in the core-4. 90

4.26 Radioactivity concentrations (Bq kg^{-1}) of the naturally occurring radionuclides in the soil core samples. 91

4.27 Comparison of ^{226}Ra and ^{232}Th activities (Bq kg^{-1}) in soils of different mangrove ecosystems of the world. 92

4.28 Radiological hazard indices of core soils of the Sundarban and 94

	the corresponding recommended values.	
4.29	Average activity concentrations (Bq kg^{-1}, n = 3) of the radionuclides in medicinal plant leaves, rhizosphere soils, and transfer factor of the radionuclides in the mangrove ecosystem.	95
4.30	Average radioactivity concentrations and radiological risk parameters for the studied medicinal plants.	96
4.31	Pearson's correlations between radionuclides and associated radiological hazard parameters for core-1.	97
4.32	Pearson's correlations between radionuclides and associated radiological hazard parameters for core-2.	98
4.33	Pearson's correlations between radionuclides and associated radiological hazard parameters for core-3.	98
4.34	Pearson's correlations between radionuclides and associated radiological hazard parameters for core-4.	99
4.35	Factor loadings of the radioactivity and radiological parameters of soils.	99

Nomenclature

Acronyms and Abbreviations

MAR	Mass accumulation rate
INAA	Instrumental Neutron Activation Analysis
AAS	Atomic Absorption Spectrometry
FAAS	Flame Atomic Absorption Spectroscopy
XRD	X-Ray Diffraction
XRF	X-ray Fluorescence
ICP-MS	Inductively Coupled Plasma-Mass Spectrometry
SRM	Standard Reference Material
CRM	Certified Reference Material
HPGe	High Purity Germanium
IAEA	International Atomic Energy Agency
INST	Institute of Nuclear Science and Technology
AERE	Atomic Energy Research Establishment
BAEC	Bangladesh Atomic Energy Commission
EF	Enrichment Factor
PCA	Principal Component Analysis
WHO	World Health Organization
I_{geo}	Geo-accumulation Index
BTRR	BAEC TRIGA Research Reactor
UCC	Upper Continental Crustal
MDAC	Minimum Detectable Activity Concentration
USEPA	United States Environmental Protection Agency
ASV	Average Shale Values
PERI	Potential Ecological Risk Index
THQ	Target hazard quotient
TCR	Target Carcinogenic Risk

Chapter 1: INTRODUCTION

1.1 BACKGROUND

Worldwide, mangrove ecosystems are considered one of the richest stocks of biological and genetic diversity, providing many goods and services such as fisheries, forest products, pollution remediation, and coastal protection (storms and erosion) [1, 2]. Sediments can preserve characteristics of the environment at the time of sediment accumulation and record events that occurred over time. The chemical composition of the sediments mainly depends on the geological structure, geomorphology, and climatic conditions. Sediment analysis provides the ability to reconstruct the environmental conditions of millions of years ago [3-5]. However, heavy metals have become more prevalent in soil as a result of industrialization, urbanization, and contemporary farming methods, posing a serious risk to human health and environmental ecosystems [6-8]. The long-term study of the bulk metal concentration of sediments can help us to identify changes in concentration caused by environmental parameters or paleo-climate indices [9-12]. Over the last few decades, research on plant and sediment cores has proven to be an excellent tool for assessing anthropogenic and natural processes in depositional environments [13-15]. Therefore, plants and sediments have been increasingly used to study the history of pollution in aquatic ecosystems.

The chronological history of environmental impacts can be assessed by dating sedimentary deposits. Generally, various chronology-based techniques are used to determine sediment chronology. For younger sediments (100–200) yr, lead -210 (^{210}Pb) ($T_{1/2}$ = 22.3 years) dating method is common [16]. The isotope ^{210}Pb is a daughter product of ^{222}Rn ($T_{1/2}$ = 3.8 d) and they are members of the ^{238}U natural radioactive series. The ^{210}Pb dating in sedimentary processes is composed of two parts: i) supported ^{210}Pb ($^{210}Pb_{sup}$) that results from the radioactive decay of ^{226}Ra ($T_{1/2}$ = 1600 ± 7 yr) with assumptions that the system has remained closed for sufficient time (>150 yr) and both radionuclides are in the equilibrium state, and ii) excess ^{210}Pb ($^{210}Pb_{ex}$) produced from the radioactive decay of ^{222}Rn in the atmosphere and water column, usually in disequilibrium with ^{226}Ra for less than 150 yr [17-20]. The $^{210}Pb_{ex}$ activity in each sediment layer declines with its age following the usual radioactive decay law, which is used to calculate the age of the sediment in the ^{210}Pb dating method [21, 22]. The Sundarban mangrove forest is the largest single-block mangrove forest (10,000 km^2) in the world.

About 60% of this forest belongs to Bangladesh and the rest of the area is in India. Mangroves are plant communities that can endure in saline to hypersaline environments; they require both freshwater flow and tidal inundation to survive [23]. Moreover, sudden changes in sea currents due to monsoon winds and storms induce the introduction of terrigenous materials and their mixing and transportation, causing a change in intertidal sedimentation rates in the mangrove system [24]. The mangrove ecosystem has been extensively utilized to reconstruct coastal changes because of its high rates of sediment accumulation and stabilized vegetated character, which may make it a particularly effective recorder of environmental changes [25]. The environmental conditions of the Sundarban are deteriorating day by day due to different anthropogenic activities and climate changes [26]. Some recent studies have reported that concentration levels of some toxic metals like V, Cr, and Cd in sediments of the Sundarban are relatively higher than in the world mangrove sediments [27, 28]. Although some studies on metal contamination of the surface sediments of the Sundarban mangrove forest are conducted [28], sediment chronology and historical trends of metal contamination are rare. Therefore, to study whether the increase in metal concentration is part of historical lactogenic concentration, the pollution history of this mangrove ecosystem needs to be explored.

Some plants of mangrove forests are used as herbal medicines. Herbal medicines are getting considerable interest in the global health sector [29]. In developing countries, some issues, like the excessive fee for drug treatments, socioeconomic, wide biodiversity, and the complexity of going through the health system, make herbal medicine more popular day by day. Therefore, stronger use is facilitated by easy access to plants and herbal medicines as alternatives to synthetic drugs [30, 31]. However, recent studies have proven that the toxic metallic contamination of medicinal plants has increased due to numerous human activities, including the use of chemical fertilizers and pesticides, irrigation with wastewater, and other industrialization processes like mining and smelting of non-ferrous metal during production [32-35]. Plants can absorb toxic elements from contaminated soils or deposits on parts of them exposed to the air in polluted environments [36, 37]. For plants, elements can generally be categorized into two types– essential (calcium, zinc, manganese, copper, iron, etc.) and toxic (cadmium, arsenic, lead, nickel, mercury, etc.) [38]. Due to nutritional, chemical, and biological properties, essential elements play a crucial role in the function of the body [39]. On the other hand, human and animal organs may be damaged due to some properties of toxic elements such

as long biological half-lives, high accumulation behavior, and non-biodegradable behavior in diverse body parts [40–42]. Moreover, non-carcinogenic, carcinogenic, and mutagenic effects in the body are led by the accumulation of toxic elements. Sundarban is a rich ecosystem with diverse flora and fauna. Three widely used medicinal plants of the Sundarban mangrove forest are *A. ilicifolius, A. officinalis*, and *X. mekongensis.* Among them, *A. ilicifolius* is a perennial plant, popularly known as “Holy Leaved acanthus" which is locally known as a Hargoja. Phytochemical research on this plant has shown the presence of glycosides, alkaloids, flavonoids, triterpenoids, steroids, fatty acids, and saponins in it [43]. This plant is used as a crude drug to cure diabetes, asthma, dyspepsia, hepatitis, leprosy, paralysis, diuretics, snakebite, and rheumatoid arthritis [44, 45]. Besides this, *A. officinalis is* an evergreen species of mangrove that is mainly found in tropical countries but is not widely introduced elsewhere [46]. It is used as a folk remedy for boils and tumors [47]. The leaves of *A. officinalis* are containing many important phytochemicals [48]. In the presence of such phytochemicals *A. officinalis* may be a source of medicinal properties like analgesic, antioxidant, antimicrobial, or anticancer activities. Another important mangrove medicinal plant is *X. mekongensis,* which contains various essential minerals and phytochemicals [49]. As a result, it has been used traditionally for the treatment of fever, diarrhoea, dysentery, inflammation, and abdominal disorders [49]. Although a few research has been carried out on *A. ilicifolius,* and *A. officinalis* plants in the Indian part of Sundarban and estimated the mangrove ecosystem affected by potentially toxic elements [23], there is no research work on medicinal plants of the Bangladeshi part of Sundarban.

Cosmic radiations and Naturally Occurring Radioactive Materials, (NORMs) (^{238}U, ^{235}U, ^{232}Th, their decay products, ^{40}K) altogether contribute to natural radiation in our environment. Natural background radiation generally originates from NORMs including ^{238}U, ^{232}Th, and ^{40}K. The Earth's surface is covered in NORMs, which differ based on the geological formations of rocks, soils, sediments, water, plants, etc. [50]. Radio-ecological assessment of ionizing radiation exposed to the human body gives information on radiological hazards that may be harmful to human life. Therefore, evaluation of different radiological indices became essential in today’s nuclear era. Sediments in any aquatic ecosystem have the capability of accumulation, transportation, and migration of various contaminants including radioactive materials (^{238}U, ^{232}Th, ^{40}K, ^{137}Cs) thereby acting as significant indicators of radiological contamination [51]. Soil, a significant reservoir for

environmental contaminants, consists of various organic and mineral components [52]. Furthermore, the sediments/soils are used as a vital element for making mud-huts and shelters for human settlements. This is the present scenario of deltaic Sundarbans, which is the center of the current radio-ecological study. The deltaic Sundarbans is situated southwest of Bangladesh, which flows together of the Ganga–Brahmaputra–Meghna river system. The world's biggest contiguous mangrove ecological unit has formed in these estuarine, halophytic areas. The River Ganges is divided into two parts: one is Hooghly flowing through West Bengal (India) and the other part, Padma runs through Bangladesh. The tidal mangrove part beside the Padma estuary is very dynamic with regular deposition and erosion of sediments from several interconnected rivers, channels, etc. Moreover, the Padma estuary is quite significant for the chances of accumulation from industrial wastes, agricultural and domestic effluents, etc. Radionuclides in the soil can be easily transferred to vegetation and animals, including humans. However, the vegetation and saplings in mangrove soils are quite relevant to different layers of soil. In the case of accidents and contamination, this layer would be the first to be affected. In Bangladesh, so far there is no study on the distribution of radionuclides in mangrove sediments and radiometric baseline data. Therefore, it is important to know the variation of radioactivity levels in the Sundarban with time.

1.2 AIMS AND OBJECTIVES

Aims: Research using nuclear techniques for sediment chronology, metal contamination history, and radiological risk assessments has great potential in relation to human health and environments. Neutron Activation Analysis (NAA) along with other nuclear techniques can be used to study the sediment chronology, elemental and radiological contamination history of a mangrove system. In this study, sediment chronology as well as historical trends of the elemental contamination and radiological contamination will be studied at Bangladeshi Sundarban using different nuclear and isotopic techniques.

The main objectives of the present study are as follows:

(i) To assess sediment chronology and sedimentation rate of the rivers of the Sundarban mangrove forest of Bangladesh.

(ii) To study historical elemental distribution and contamination in sediments of the Sundarban using different contamination indices.

(iii) To assess essential and toxic elements in medicinal plant leaves of the Sundarban and their possible health risk due to consumption of these plant leaves.

(iv) To observe the temporal profile of natural radioactivity levels in sediments of the Sundarban.

(v) Finally, to apply multivariate statistical methods to study source apportionment and transport behavior of the elements and natural radionuclides in the Sundarban mangrove system.

Possible Outcomes of the Research:

The main possible outcomes of the research are as follows:

1. For the first time, sedimentation rates of the Sundarddban for the last 150 years will be explored by using the ^{210}Pb dating technique. The depthwise elemental contamination history of this mangrove system will also be assessed.
2. Temporal variations of natural radioactivity concentrations in sediments of the Bangladeshi Sundarban ecosystem will also be reported for the first time.
3. Transfer factors and health risks due to the consumption of studied medicinal plants of the Sundarban will be determined.
4. The source apportionment and transfer behavior of the studied elements and natural radionuclides will be explored out by applying multivariate statistical methods.
5. The elemental and radiological contamination history over the last century of the Sundarban will be used so that proper steps can be implemented to reduce the contamination levels of the sensitive mangrove ecosystem.

1.3 SIGNIFICANCE, SCOPE AND DEFINITIONS

Significance and Scope: It is important to know the pollution status of the Sundarban to save its ecosystem. Some studies have been carried out in the Indian Sundarban, but there is no study on sediment chronology as well as historical trends of the elemental contamination at the Bangladeshi Sundarban. Also, so far there is no historical radiological contamination data for the Bangladeshi Sundarban. The Sundarban mangrove forest consists of vast areas, including Bangladesh and India. The present study will be

able to cover the contamination level of Bangladeshi Sundarban. Besides this, it would be better if this research work were extended up to Indian parts of Sundarban.

Definitions:

Mass accumulation rate (MARs): sediment mass accumulation rates, which are quantified measurements of sediments in kg per meter square per year to the seabed.

Naturally occurring radioactive material: Radionuclides of natural origin contained in or released from process materials may pose a risk to workers, public or the environment. These radioactive elements in minerals and ores originally found in the environment are commonly known as NORM – naturally occurring radioactive material. Some NORM materials require radiation control and regulation.

Ecosystem: An ecosystem is a geographic area where plants, animals, and other organisms, as well as weather and landscapes, work together to form a bubble of life.

1.4 THESIS OUTLINE

Outlines of the thesis are given below:

Chapter–1 presents a brief introduction to the Sundarban mangrove ecosystem and the present research status regarding elemental and radiological contamination of the Sundarban forest.

Chapter- 2 deals with a detailed theoretical background to study this type of research work. This chapter includes different techniques to help readers understand the purposes and goals of the study. It also analyzes previous publications relevant to this study by other researchers, with which these findings could be compared.

Chapter- 3 contains the details of the materials and methodology of the present research.

Chapter- 4 describes the results and discussion of this study.

Chapter- 5 includes the conclusions drawn from the overall experimental results and discussion, along with the scope of future work.

Chapter 2: LITERATURE REVIEW

The Sundarban mangrove forest in Bangladesh is UNESCO declared world heritage site. This forest is contaminated in various ways, such as by increasing anthropogenic activities in the vicinity of its associated areas. To know the historical contamination status and radiological risks in sediments and medicinal plants, some research with different analytical techniques is applied. Neutron Activation Analysis (NAA), Atomic Absorption Spectroscopy (AAS), Flame Atomic Absorption Spectroscopy (FAAS), X-Ray Fluorescence (XRF), X-Ray Diffraction (XRD), Energy Dispersive X-Ray Fluorescence (ED-XRF), Inductively Coupled Plasma Mass Spectroscopy (ICP-MS), Inductively Coupled Plasma Atomic Emission Spectrometer (ICP-AES) etc. For sediment chronology, ^{210}Pb dating, ^{14}C, etc. are commonly used. To analyze samples from different ranges of the mangrove ecosystem, ^{210}Pb dating techniques, research reactor-based NAA and AAS techniques are used. Therefore, some theoretical background on different analytical techniques is given here.

2.1 THEORETICAL BACKGROUND

2.1.1 Neutron Activation Analysis

For the qualitative and quantitative assessment of major, minor, and trace elements in samples from practically every sector of scientific or technical interest, one of the most sensitive and precise methods is neutron activation analysis (NAA). This method was first discovered in 1936 by G. Hevesy and H. Levi [53], who determined the contents of Dy and Eu in a rare earth mixture. The accuracy and precision of the technique are such that NAA is still one of the primary analytical methods for producing Standard Reference Materials (SRMs) or Certified Reference Materials (CRMs) worldwide.

2.1.2 Theory of NAA

Neutron activation analysis has progressed rapidly and has become a versatile and sensitive analytical tool in all branches of science and technology. Based on the highly characteristic and well-defined nuclear properties of the elements, this technique is close to an ideal non-destructive analytical method, capable of handling samples in liquid, solid, and powder form. One type of nuclear reaction is neutron activation. A compound nucleus is created when a target nucleus interacts with a neutron. The high binding energy

and kinetic energy of the incident neutron in the nucleus cause the compound nucleus to remain in a highly excited state for the duration of its finite lifetime (10^{-13}–10^{-15}sec). There exist various methods for de-excitation of the compound nucleus [54] that are not related to the formation process. Based on the nuclear cross-section of each mode and the excitation of the compound nucleus, each of these processes (shown in Fig. 2.1) has a specific probability.

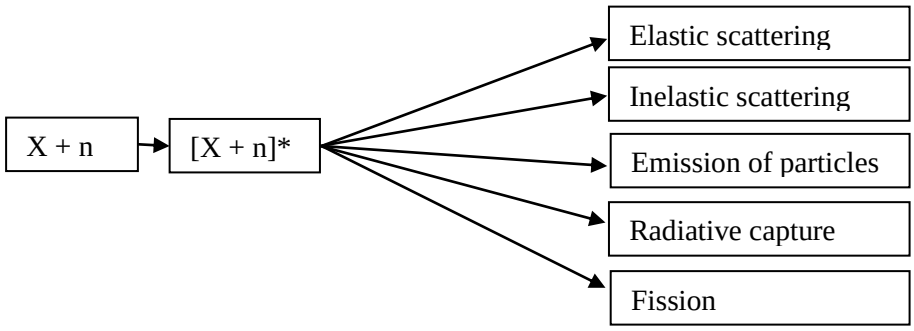

Fig. 2.1: Probability of Occurring Nuclear Reaction.

Elastic scattering:

In this case, the projectile (x) and the expelled particle (y, say) are the same. Since it exits with the same energy and angular momentum as x, the residual nucleus Y and the target nucleus X are identical and remain in the same ground state. The process can be shown as X (x, x) X.

Inelastic scattering:

Here, x and y are equivalent. However, because of its altered energy and angular momentum, the excited state is retained in the residual nucleus Y (= X). X (x, y) X* is one way to write the process.

Emission of particles:

The inverse cross section of the emitted particle the cross section with which the emitted particle would be absorbed if it were incident on the product nucleus resulting from the decay of the compound nucleus determines the type of particle emission (neutrons, protons, or a combination of these). The compound nucleus cross section (in the inverse reaction) and the inverse cross section have the same value. Whether the energy of the input particle is strong enough to excite the compound nucleus to the level required to

produce multiple particles then determines the cross section for the emission of multiple particles.

Radiative capture:

In this instance, the projectile x is absorbed by the target nucleus X, forming the excited compound nucleus (c*), which emits one or more x-ray quanta before falling to the ground state. The procedure can be expressed as X (x, y) Y*. The most advantageous and significant nuclear reaction in NAA is radiation capture.

Fission:

A unique kind of nuclear reaction known as nuclear fission occurs when an excited compound nucleus splits into two pieces with similar mass and atomic numbers. The isotopes of the heaviest elements, such as uranium, thorium, etc., are typically where fission takes place.

2.1.3 Classification of NAA Method

There are various forms of neutron activation analysis, which are as follows:

- ► Instrumental Neutron Activation Analysis (INAA)
- ► Radiochemical Neutron Activation Analysis (RNAA)
- ► Epithermal Neutron Activation Analysis (ENAA)
- ► Prompt Gamma-ray Neutron Activation Analysis (PGNAA)
- ► Fast Neutron Activation Analysis (FNAA) and
- ► Delayed Gamma-ray Neutron Activation Analysis (DGNAA)

2.1.4 Fundamental Equations for the NAA Method

There are two ways in which NAA can be treated mathematically, such as:

1. Absolute NAA method
2. Comparative NAA method

2.1.5 Absolute NAA Method

By irradiating a sample with neutron radiation, the elements to be evaluated become radioactive. The resulting radionuclides, which are identified and measured, based on their characteristics and radiation, such as gamma rays, are subsequently released from the sample. The amount of neutron flux determines how quickly the product grows in a reaction caused by neutrons. The rates of contact increase with increasing neutron flux:

Activation rate $\propto$ Neutron flux (φ)

The activation rate is also directly proportional to the number of target nuclei present i.e.,

Activation rate $\propto$ Number of nuclei present (N)

But the total number of atoms per gram is given by,

$$N = N_A / A \quad \text{……..(2.1)}$$

Where, N_A is Avogadro's number and represents the total number of atoms in the atomic weight A of any element.

The total number of target nuclei for a mass W of the element will be,

$$N = WN_A / A \quad \text{…….....(2.2)}$$

However, when there is more than one isotope present in an element, the number of target nuclei must be corrected for the isotopic abundance (θ).

$$N = W\theta N_A / A \quad \text{…….(2.3)}$$

The relationship between activation rate, the number of target nuclei, and the neutron flux can be expressed in terms of "cross-section" (σ),

$$\text{Activation rate} = \varphi\sigma N \quad \text{……...(2.4)}$$

Where, N is the number of target nuclei in atoms, σ is the cross-section, in barn(b), φ is the neutron flux, in neutrons / cm^2s

Activation rate, in events / s

Substituting equation (3.3) into equation (3.4), we get

$$\text{Activation rate} = \frac{W\theta\sigma N_A}{A} \quad \text{…….....(2.5)}$$

In a neutron-induced reaction, the number of nuclei generated can be simply determined from the activation equation by multiplying by the irradiation duration, t, provided that the resultant nuclide is stable

$$\text{Number of nuclei} = \text{Activation rate} \times \text{irradiation time}$$

$$= \sigma\varphi N\, t \text{ ……..... (2.6)}$$

However there will be a decay rate if the resultant nuclide is radioactive, and this needs to be considered. The generated radionuclide will decay with a characteristic half-life. The rate at which radioactive nuclei decay is proportional to N* if there are N* radioactive nuclei.

$$\text{Decay rate, } \frac{dN^*}{dt} \propto -N^*$$

$$\text{or, } \frac{dN^*}{dt} = -\lambda N^* \text{……(2.7)}$$

Where λ is the decay constant, which has a characteristic value for each nuclide. If the equation is integrated between the limits N_0^* at the time zero and N^* remaining at the time t,

$$N^* = N_0^* \exp(-\lambda t) \text{……..(2.8)}$$

In terms of half-life the equation (3.8) can be written as,

$$\frac{N_o}{2} = N_0^* \exp(-\lambda T_{1/2})$$

$$\text{Where, } T_{1/2} = \frac{\ln 2}{\lambda} = \frac{0.693}{\lambda}$$

The growth of activity is governed by-

$$\text{Production rate} = \text{Activation rate} - \text{Decay rate}$$

$$\frac{dN^*}{dt} = \varphi\sigma N - \lambda N^* \text{ ……..…(2.9)}$$

The solution of the above equation gives

$N^* = \sigma\varphi N \{1 - \exp(-\lambda t)\}/\lambda$ ……(2.10)

The factor $\{1 - \exp(-\lambda t)\}$ is called the saturation factor. The activity or the disintegration rate (A_0) at the end of irradiation time t is then

$$A_0 = \lambda N^*$$

$$= \varphi\sigma N \{1 - \exp(-\lambda t)\} \text{……(2.11)}$$

Substituting equation (2.3) into equation (2.11), we get

$$A_0 = WN_A\sigma\varphi\theta\{1 - \exp(-\lambda t)\}/A \text{……..... (2.12)}$$

This is the basic equation used for NAA calculation in the absolute method.

$$\text{So, } W = \frac{A_0 A}{N_A \varphi\sigma\theta\{1-\exp(-\lambda t)\}} \text{ ……(2.13)}$$

Usually, in neutron activation analysis, the activity of the radionuclide is measured experimentally in a sample to deduce the unknown mass (W) of the element by the above equation.

A correction must be made for the decay period t_d, the cooling time (time from the termination of irradiation to the time of measurement),

$$W = \frac{A_0 A}{N_A \varphi\sigma\theta\{1-\exp(-\lambda t)\}\exp(-\lambda t_d)} \text{ ……..(2.14)}$$

Every element on the right side of the equation above is either measurable or known. As a result, the element's mass may be calculated [55].

The measurement of neutron flux density (φ) is a challenging task due to the difficulty of accurately determining σ. Additionally, the value of φ varies based on time and location in powerful neutron sources such as nuclear reactors, samples, and their containers, resulting in perturbations of neutron flux density (flux depletion and self-shielding of neutrons), which is extremely difficult to assess accurately. Activity A can be obtained from the following relationship:

$$A = \frac{R}{\varepsilon I_\gamma} \quad \text{..... (2.15)}$$

Where I_γ the intensity of gamma rays, ϵ is the absolute counting efficiency of gamma rays, and R is the counting rate of fuel energy peak produced by the gamma rays employed for the activity measurement.

2.1.6 Comparative NAA Method

The comparative method is a more simple and accurate way of quantifying the concentration of an element. The comparison approach involves simultaneously irradiating a known quantity of sample X as a standard and an element X in a sample. The identical radiation detector counts the sample and standard under precisely the same geometrical conditions. This procedure eliminates any uncertainty in the parameters Φ, σ, λ decay scheme, and detection efficiency.

Therefore, the NAA equation for the comparative method is:

$$\frac{W}{W'} = \frac{A_0 \Phi \sigma \theta \, F_i F_d F_c \frac{A}{N_A}}{A_0 \Phi \sigma \, \theta F_i' F_d' F_c' \frac{A'}{N_A}}$$

Here, the contents with' refers to the standard. Since, A_O = (counts per second) / E P exp ($-\lambda t_d$), w = (counts per second) A / $N_A \sigma \phi \theta$ [1- exp ($-\lambda t_i$)] exp ($-\lambda t_d$) $\frac{1-e^{-\lambda t_c}}{\lambda t_c}$

The NAA equation for the comparative method reduces to:

$$\frac{W}{W'} = \frac{\text{Counts per second} \times F_i F_d F_c}{\text{Counts per second}' \times F_i' F_d' F_c'}$$

Using this equation we can get the amount of an element in the sample:

$$W = W' \frac{\text{Counts per second} \times F_i F_d F_c}{\text{Counts per second}' \times F_i' F_d' F_c'}$$

2.2 ^{210}Pb DATING TECHNIQUE

The dating of sedimentary deposits is a popular method for researching the historical timeline of environmental effects. After gaseous ^{222}Rn escapes from the soil surface to the atmosphere, the decay product isotope ^{210}Pb ($T_{1/2}$ = 22.3 y) returns as solid fallout to the surface soil or water reservoirs after a few weeks. Compared to the ^{210}Pb generated inside

the sediment matrix, a portion of the ^{210}Pb activity that is produced as a result of fallout and adsorbed in the surface sediments is referred to as surplus and is only associated with sedimentary processes. In sediments older than 150 years that have been buried by layers deposited later, this radionuclide is basically in radioactive equilibrium with ^{226}Ra, its long-lived precursor. Thus, the difference between the specific activities of these two radionuclides can be used to calculate the excess ^{210}Pb activity in the bottom sediment layers [56]. The radioactive decay law states that the excess ^{210}Pb activity in each sediment layer decreases with sediment layer age. If it is possible to estimate the initial excess ^{210}Pb activity that was present when the sediment was first set down on the marine bed, this law can be used to determine the age of the sediment [56, 57].

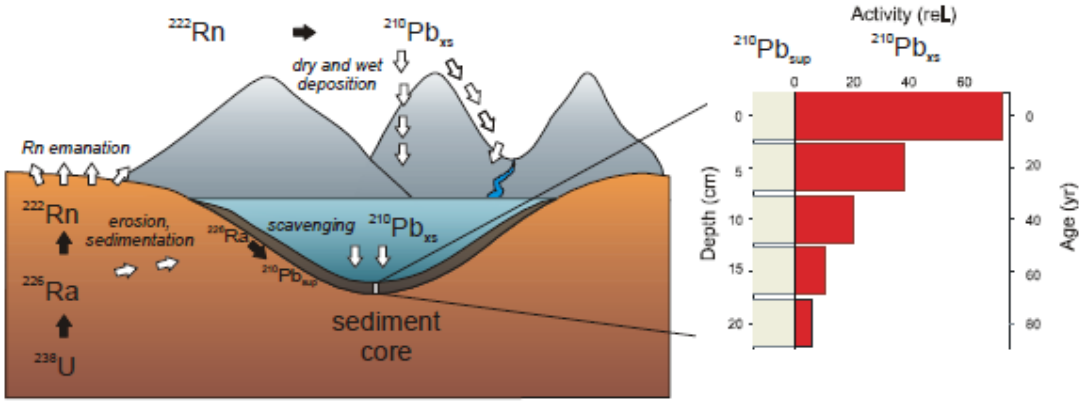

Fig. 2.2: Production of supported ^{210}Pb in sediment [61].

It is plausible to assume that each sediment layer will have the same initial excess ^{210}Pb activity if the catchment's erosive processes are continuous and lead to a constant rate of sediment accumulation. In this instance, the extra ^{210}Pb activity will decrease with sediment depth exponentially. Additionally, the rate at which sediment accumulates in all sediment layers is constant, and this may be easily ascertained by observing the slope of the cumulative dry mass or the semi-logarithmic of the excess ^{210}Pb against depth. This model refers to a constant flux-constant sedimentation rate (CF:CS) model [56, 58]. It is evident in many instances that within the previous 150 years, there have been notable variations in the rates of erosion and sedimentation. The ^{210}Pb profile might be anticipated to be non-linear in this situation.

The constant initial concentration (CIC) model and the constant rate of supply (CRS) model are essentially the two mathematically feasible models for determining ^{210}Pb dates under varying sediment accumulation rates [58-60]. According to the CIC model, a higher flow of sedimentary particles through the water column will extract a correspondingly higher amount of lead (^{210}Pb) from the water and deposit it in the sediments. According to the formula $C = C(0)\, e^{-kr}$, where C(0) is the excess ^{210}Pb concentration of sediments at the sediment-water interface, the excess ^{210}Pb activity will change with depth as shown in Fig. 2.2. Hence, $t = \frac{1}{k} \ln \frac{C(0)}{C}$ is the age (t) of a sediment layer with ^{210}Pb concentration C. Regardless of any fluctuations in the rate at which sediment accumulates, the CRS model assumes that there is continuous fallout of lead (^{210}Pb) from the atmosphere to the seawater, leading to a constant rate of delivery of lead to these sediments proposed this concept. The formula $A = A(0)\, e^{-kt}$ determines the cumulative residual excess ^{210}Pb beneath strata of different ages. Where k is the radioactive decay constant for ^{210}Pb and A(0) is the entire residual excess ^{210}Pb in the sediment column, K is equal to $\ln(2)/T_{1/2}$.
The ^{210}Pb profile is directly numerically integrated to determine A and A(0). Next, we get the age of the sediments at depth x using:

$$t = \frac{1}{k} \ln \frac{A(0)}{A}$$

The formula can be used to demonstrate that the sedimentation rates are directly supplied:

$$r = \frac{kA}{C}$$

2.3 ATOMIC ABSORPTION SPECTROMETRY

Since instrumental NAA cannot reliably determine certain environmentally significant elements, such as Pb, Cd, Cu, Ni, Zn, and Hg, atomic absorption spectrometry (AAS) was utilized to determine these elements, as shown in Fig. 2.3. AAS is a sensitive technique that can measure the concentration of metal ions in a solution, even when other metals are present. This is because each metal atom absorbs a specific wavelength of light. The basic equation to calculate metal concentration using AAS is given below:

$$\text{Metal concentration (mg Kg}^{-1}) = \frac{AAS\ results\ (mg/L)\ x\ Dilution\ Factor}{Mass\ of\ sample\ (Kg)}$$

$$\text{Where, Dilution Factor} = \frac{Final\ volume\ of\ diluted\ solution}{Volume\ of\ aliquote\ taken\ for\ dilution}$$

Fig. 2.3: Atomic Absorption Spectrometer-AA6800 used in for the present study in AERE.

2.4 SURVEY OF SOME REPORTED PREVIOUS WORKS

Research on sediment chronology, elemental and natural radioactivity contamination of sediments are crucial issues worldwide. Several research works have been carried out on different mangrove ecosystems all over the world. The subsequent pages review a number of previous works that are most relevant to the present study.

Radioisotopes like ^{210}Pb and ^{137}Cs have been used in a study by Wren et al. [62] to estimate recent sediment accumulation rates for lake sediments in agricultural watersheds. This could be a useful way to gauge how effective soil conservation measures are at the watershed scale. The application of the Constant Initial Concentration (CIC) model for determining sediment age from the distribution of ^{210}Pb bottom sediments was demonstrated using four sediment cores from Beasley Lake, Mississippi. By offering a benchmark date within the core for the purpose of calibrating the CIC model, the activity of ^{137}Cs was utilized to augment the ^{210}Pb data. In comparison to rates prior to the adoption of soil conservation measures in the watershed, three of the four cores revealed reductions in sediment accumulation rates of at least 50% during the 30 years before core collection in 2008 and 2011. The rates that were most recently resolved were roughly 0.5 cm y^{-1}.

Lubis [18] used the CRS model to calculate the age and rates of sediment accumulation. Since the unsupported ^{210}Pb flux to the sediment is assumed to be constant in this model, the rate of sedimentation can change over time. Two bottom sediment cores from Jakarta Bay (JB 17 and JB 11) were analyzed using the relevant CRS model. According to the data, the rates of sediment accumulation in JBs 17 and 11 were from (0.09 to 1.13) kg m^{-2} y^{-1} and (0.18 to 2.47) kg m^{-2} y^{-1}, respectively.

After the disastrous oil leak event in the Sela River of Sundarban, Islam et al. [28] measured the concentration of 16 trace elements (Al, V, Cr, Mn, Fe, Co, Ni, Cu, Zn, As, Cd, Sb, Hg, Pb, Th, and U) in the sediments of the rivers of the Sundarban mangrove forest. The high quantities of As, Ni, Cr, and Nib that were obtained point to the possibility of unfavorable biological consequences for the ecosystem.

Using sediment quality assessment criteria, Kumar et al. [63] looked into eight trace metals (As, Cd, Cr, Cu, Fe, Mn, Pb, and Zn) in the Bangladeshi portion of the Sundarban mangrove. The average trace metal concentration in the sediments was higher than the crustal abundance, indicating non-natural origins.

Analyzed the levels of seven trace elements (Zn, Cu, Cr, Hg, Pb, Cd, and As) in 14 distinct animal and plant species that were collected in Bangladesh's Sundarbans to examine how they move through the food chain and assess whether the levels in edible species are suitable for human consumption [64]. Zn, Cr, and Cd levels were higher than the suggested health advisory thresholds and could be harmful to human health.

Silva et al.'s study [65] examined the concentrations of key elements (Fe and Al) and specific trace elements (Mn, Zn, Cr, Cu, Ba, As, B, V, and Hg) in intertidal sediment cores from the Sundarban wetland in India. The resulting result was As since it already seemed to be linked to a possible biological danger based on TEL and ERL benchmarks.

Using a graphite furnace atomic absorption spectrophotometer, Bhattacharya et al. [66] calculated the presence of trace metals in the coastal parts of the Sundarban mangrove wetland, which is recognized as a UNESCO World Heritage Site. The findings of the carcinogenic hazards analysis for the metals suggested that dermal absorption of Cr, Pb, and Cd (also known as CDI dermal) could be a cause for concern.

In two study sites in the Indian Sundarban Wetland, Chawdhury et al. [67] examined the capacity of 10 mangrove species for the absorption, storage, and partitioning of trace metal(loid)s in individual plant tissues (leaves, bark, and root/pneumatophore). According to the results, the species may be categorized as an effective metal trap for Cd in aerial portions because of the increased metal accumulation in the leaves as well as the values of the translocation factor and bio-concentration factor.

Ucides cordatus and Callinectes danae, two crab species found in "polluted" mangroves along Brazil's southeast coast, were the subject of physiological investigations in a study conducted by Harris et al. [68]. Cu, Cd, Zn, and Fe concentrations in sediments and crab tissues were analyzed; the results revealed a substantial difference in tissue concentrations between the "polluted" and "unpolluted" populations residing in uncontaminated mangroves within the same geographic area, as well as much greater levels of these elements in the former.

In Bintuni Bay, West Papua Province, Indonesia, Sasmito [69] evaluated the burial rates of soil organic carbon in an undisturbed coastal mudflat and mangrove hydrogeomorphological catena (internal mangrove and fringe mangrove). These results unequivocally show that there is a close relationship between the sequestration and cycling of carbon in mangrove and terrestrial forest ecosystems and that at least some of the carbon losses from terrestrial forests—such as erosion—are buried in mangrove ecosystems.

The Halda River's water and sediments were the subject of a study by Biplob et al. [70] that looked at the origins, ecological concerns, and spatial distribution of eleven metals and one metalloid. Based on this data, it can be said that in order to reduce ecological dangers brought on by toxic metal pollution, efficient management, and restoration efforts should be carried out to protect freshwater fisheries' natural breeding grounds.

Using INAA and AAS techniques, M. Rahman et al. [71] measured the amounts of 15 chemical elements (Al, Br, Ca, Cd, Cl, Cr, Cu, Fe, Hg, K, Mn, Na, Ni, Pb, and Zn) in two different fruit varieties (pomegranate and dragon). Both fruits had greater Pb concentrations than WHO/FAO allowable limits, although the pomegranate had somewhat higher Cd values. This study does show that target hazard quotient values and projected daily intake values were within safe limits when compared to MTDI.

Conversely, the computed TCR values for Cd in pomegranates and Cr in dragon fruit exceeded the upper limit of 1.0×10^{-4} for children. In conclusion, this study indicates that pomegranate and dragon fruits are thought to be possible sources of dietary supplements for human health.

Rahman et al. [72] used INAA and AAS to calculate the total concentrations of seventeen major and trace elements (Al, As, Br, Ca, Cd, Cl, Co, Cr, Fe, K, Mn, Na, Ni, Pb, Sc, V, and Zn) in common spices found in Bangladesh. The chemical element concentrations in the spices under study were compared to global literature data. According to this study, many spices had concentrations of As, Cd, Cr, and Pb that were greater than those recommended by the WHO and FAO. The computed total dietary intake values for Cd, Cr, Mn, and Pb were also greater than the MTDI values, according to this study, indicating a significant danger to consumers. Nonetheless, the total risks of the elements examined from spice consumption did not surpass the THQ recommended value, meaning that individuals would not be at risk if they were exposed to the elements through spice consumption. Taking into account the health dangers to the Bangladeshi people, this study will also make a significant contribution to the field of food safety.

In the surface sediments of the rivers that make up the Sundarban mangrove forest, the level of trace element contamination and distribution estimated by Al-mamun et al. [73] was investigated. The INAA and AAS were used to determine the total concentrations of sixteen environmentally significant major and trace elements (Al, V, Cr, Mn, Fe, Co, Ni, Cu, Zn, As, Cd, Sb, Hg, Pb, Th, and U). The total amounts of V, Cr, Fe, and Cd found in Sundarban sediments are noticeably higher than those found in published research that was gathered from other mangrove sediments across the globe. According to a study of trace element contamination using two separate environmental contamination indices (EF and CF), sediments are moderate to severely contaminated by Cd, but low to moderately contaminated by As, Sb, Th, and U. The gradual degradation of the Sundarban's sediment quality as a result of various human activities is also indicated by the PLI. A number of factors, including port operations, shipbreaking, chemical carrying cargo incidents, and runoff from nearby agriculture and aquaculture, could be contributing to the degradation of the sediment quality. The study area's estimated potential ecological risks for Cd were significant to high, based on potential ecological risk factors and various SQGs.

In contrast, the concentrations of Cr, Ni, Cu, and As were higher than the TEL and ERL values, suggesting that organisms residing in Sundarban sediments may face some ecotoxicological risk. Principal component analysis and Pearson's correlation analysis, two multivariate statistical techniques, provided insight into the origin and behavior of the elements as they moved through the mangrove ecosystem. The results of this study will also be useful in managing future ecological hazards to the vulnerable Sundarban mangrove environment and in measuring the amounts of pollutants, including trace elements.

In a study by Tannus et al. [74], twenty-four elements (essential, non-essential, and potentially toxic) in Brazilian herbal medicines and medicinal plants were identified using axial view ICP OES. This was done following a quick and effective microwave-assisted digestion procedure with suitable detection and quantification limits, precision, and accuracy. *Maytenus ilicifolia* (Mart.) ex Reiss ("espinheira santa"), Cynara scolymus L. (global artichoke), and Harpagophytum procumbens D.C. (devil's claw) are sources of Ca, K, Mg, Na, P, Cu, Fe, Mn, Se, and Zn, according to the results from that study. All samples had high amounts of Al, even though they were much below the maximum suggested doses, and the medicinal plant *Maytenus ilicifolia* (Mart.) ex Reiss displayed Ni. Herbal medications and medicinal plants were the two major groups into which the samples were divided, as demonstrated by PCA and HCA.

According to a study conducted by Chowdhury et al. [75], there was a possible ecological and health concern in the area because the contaminated site had more exchangeable forms of hazardous metals such as Cr, Pb, Cd, and Hg than the unpolluted site. An ecological risk assessment indicated that the study location was under significant pollution strain. Because Cd had the highest exchangeable percentage in the contaminated soil, mangroves absorbed a large amount of this PTE. The potential uptake of Cd, Cr, Zn, and Mn by *A. officinalis* was demonstrated by the bioaccumulation factor. Trace levels of mercury were found in the contaminated rhizosphere. This study also shows that the three mangroves with the highest bioaccumulation factor have considerably accumulated Hg. However, this health risk assessment study shows that there is minimal health risk associated with this harmful metal. *P. coarctata* seeds were found to pose the most risk to human health among the three halophytes (*A. officinalis, A. ilicifolius,* and *P. coarctata*) when consumed.

Plants growing in polluted areas were shown to pose little health risk when consumed orally.

Plants growing in metal-contaminated locations can be used externally, as evidenced by the lack of major health risks observed when plant portions were applied topically. It is necessary to regularly evaluate and monitor the coastal mangrove habitats affected by PTE contamination, taking into consideration the possibility of these hazardous substances bioaccumulating in native flora. It is necessary to take into account the ethnobotanical uses of these plants when putting policy-level pollution mitigation initiatives into action.

Gao et al. [76] found that exposure to large amounts of herbal medicines grown there over an extended period of time—in the form of a medicated diet—may constitute a serious health risk for those exposed to the race metals in contaminated soil. In soil, we discovered that medicinal plants collected from contaminated locations had greater concentrations of Cu, Cr, Pb, and Zn. One of the main goals of the current investigation is to. There were health hazards unrelated to cancer, as indicated by the higher hazard quotient values (HQ > 1) of the AM and CT plants from contaminated areas as compared to standard values. There was a 13.18, 14.33, and 14.01 times greater hazard index for PC, AM, and CT than the safe limit (HI > 1). Cr and Ni provided the highest cancer risk, while soil ingestion and uptake through a medicated meal were the exposure routes that caused the greatest cancer risk. To get herbal medicines free of metals, different metal remediation techniques should be used in the research locations. The transfer rates of toxic elements during the decoction preparation process, as well as the total amount of trace elements in herbal materials, were not taken into account and may have led to safety concerns with these medicinal herbs. It should be emphasized that we only looked at the total number of trace elements in herbal materials. Conducting a systematic health assessment of CHMs thus requires monitoring the entire production process, which includes planting, irrigation, harvesting, processing, and other aspects.

According to a study by Khandaker et al. [77], radioactivity concentrations of U and Th series radionuclides were found in both black and white beach sands in Langkawi. All black sand samples from Pantai Pasir Hitam had elevated levels, which were found to be comparable to high background areas worldwide. Regarding the various radiological

hazard indicators for black sand samples, all of these exceeded the safe values advised by various international organizations.

These indicators included absorbed dose rate, radium equivalent activity, annual effective dose, gamma representative level index, external and internal hazard indices, and lifetime carcinogenic risk. Therefore, even though it would seem sensible to avoid using a lot of black sand in building materials meant for long-term residential habitation, the area's generally low levels of human activity suggest that additional dangers are negligible. The identical sets of indices' results for the beach sands at Cenang demonstrate negligible radiation risk.

While Naskar et al. [78] determined average activities of ^{238}U and ^{232}Th, which were marginally higher than suggested values; activity of ^{40}K is double the global average, which is explained by its native abundance in Sundarbans coastal zones. The hazard indices (H_{ex} and H_{in}), the radiological parameters Ra_{eq}, and the AGDE are below the recommended levels. Studies of correlation indicate that there is no significant relationship or reliance between ^{238}U, ^{232}Th, and ^{40}K. The skewness and kurtosis of univariate statistical analysis demonstrate the frequency of a normal distribution in the absence of a very broad deviation. In contrast to igneous rock systems, the Sundarbans area's deltaic formation has a bedrock pattern that dates to the Holocene and Pleistocene eras and is primarily composed of sedimentary rock, which lowers natural radiation [79]. Since no previous radiological studies have been reported in this area, the current study is noteworthy and could provide baseline data for upcoming radiological aspects. In light of the UNSCEAR report's emphasis on the importance of exposure to natural radiation rather than that from man-made sources, locations rich in monazite, such as the Ganges delta in the India, may also be considered to have relatively high background radiation levels.

2.5 RESEARCH GAP

The Sundarban ecosystem is affected by anthropogenic activities and climate change. Although some studies on metal contamination of the surface sediments of the Sundarban mangrove forest have been conducted, there is no study of sediment chronology and historical trends of metal contamination in Bangladeshi Sundarban.

On the other hand, A few research studies have been carried out on some medicinal plants in the Indian part of Sundarban and estimated that the mangrove ecosystem is affected by potentially toxic elements [80]. There is no comprehensive research work on transfer factors and health risk assessments of the toxic elements of the medicinal plants of the Sundarban. Besides this, there is no research on the temporal variation of radioactivity in the soils and root uptake of radionuclides in the Sundarban mangrove ecosystem. Thus, it is necessary to investigate the mangrove ecosystem's history of pollution in order to determine metal contamination levels in sediments and medicinal plants as well as variations of radioactivity levels with time in the Sundarban to plan a strategy to save the sensitive Sundarban ecosystem from metal and radiological contamination.

Chapter 3: MATERIALS AND METHODOLOGY

3.1 STUDY AREA, SAMPLE COLLECTION AND PREPARATION

3 .1.1 Study Area

The Sundarbans span an approximate 10,000 km^2 region, with 38% of it in India and 62% of it in the interior of Bangladesh. They are situated between 21°32′ to 22°40′N and 88°05′ to 89°51′E [81]. UNESCO has declared the Sundarban mangrove forest a World Heritage site [82]. The freshwater fluxes from the rivers dominate the Sundarbans hydrology. Furthermore, the tidal effect affects this area's eco-geography. The Bay of Bengal is the mouth of numerous rivers and canals, and the freshwater discharge in this delta plain is regulated by the tropical South-West monsoon [83]. The Sundarban has a maximum elevation of 10 meters above mean sea level. In Bangladesh's Sundarban region, the average yearly rainfall varies from approximately 1800 mm in Khulna, situated to the north of the region, to 2790 mm near the coast. The typical temperature range for the climate is 18 to 32 ℃. This forest provides excellent protection against storms, tidal flooding, erosion, and other natural disasters for the coastal communities [84]. Recently, several human-caused events, such as oil spills, industries that kiln bricks, shipbreaking, and the use of excessive chemicals combined straight into water bodies, are steadily worsening the Sundarbans' environmental problems [85], [86]. Moreover, industrial activity has been steadily rising in the area's surroundings. Thus, it is imperative to assess the contamination history in the Sundarbans. In this study, samples were collected from different locations of the Sundarban shown in Fig. 3.1.

3.1.2. Sample Collection and Preparation

Sample Collection

A total of 58 soil samples were collected from four cores (each measuring 26 to 32 cm in length and sliced into 2 cm intervals) from different ranges: one core from the Chandpi Range (C1, length = 32 cm), two cores from the Khulna Range (C2, lengths = 26 cm, and C3, length = 28 cm), and one core from the Satkhira Range (C4, length = 30 cm) of the Bangladeshi Sundarban in 2018.

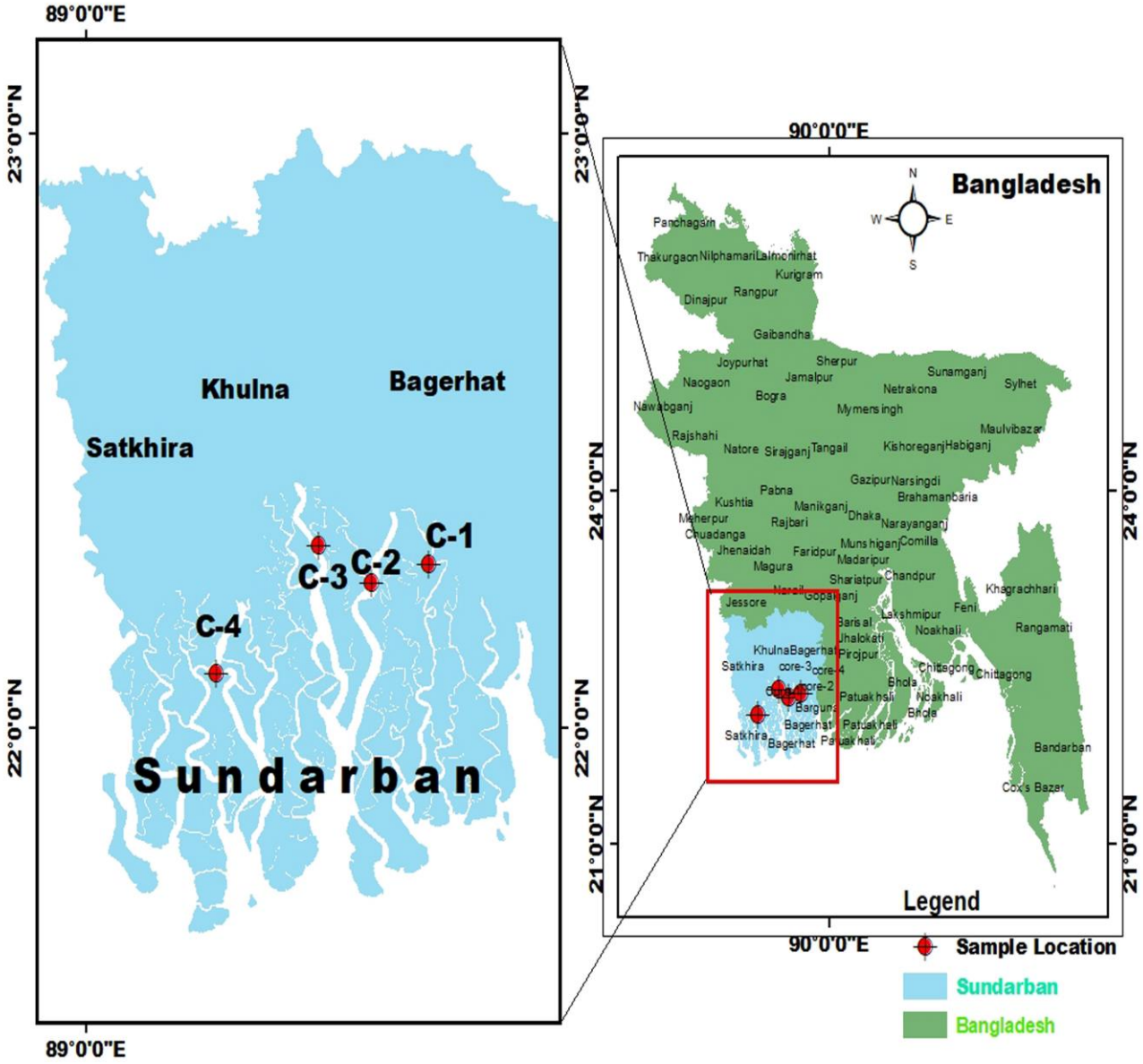

Fig. 3.1: Geographical locations of sample collection from the Sundarban.

Fig. 3.2 shows a typical core sample collected from the Sundarban. The undisturbed river beds were penetrated by the acid-washed coring pipe, and the core was gradually extracted.

Fig. 3.2 : A typical core sample collected from the Sundarban.

For medicinal plant sample collection, leaf samples of three different species (3 samples of each species from each location were used to make a composite sample) of medicinal plants, *A. ilicifolius*, *A. officinalis*, and *X. mekongensis*, and nine corresponding composite rhizosphere soil samples were also collected from 3 different locations of the Bangladeshi Sundarban (Fig. 3.3).

Avicennia officinalis (bine) *Acanthus ilicifolius* (harguza) *Xylocarpus mekongensis* (poshur)

Fig. 3.3: Medicinal plant samples collected from the Sundarban.

Sample Preparation for ^{210}Pb Technique

Two core samples (C1 and C4) were used for ^{210}Pb dating technique. The samples were labelled appropriately and placed in sterile plastic bags. About 5 g of powdered sediment

subsamples from different strata of the two cores were prepared, and ^{209}Po radioisotope tracer was added to the samples for ^{210}Pb alpha spectrometry. A HCl, HNO_3, H_2O_2, and H_2O solution was used to digest the subsamples [87, 88]. Two certified reference materials, IAEA-368 and IAEA-300 (marine sediments), were used to study the accuracy of the analysis.

Sample Preparation for INAA

The collected soil and medicinal plant samples were oven-dried to a consistent weight at 50 °C. The dried samples were ground by a pestle and agate mortar, then sieved, homogenized, and pulverized at NAA lab, INST, BAEC shown in Fig. 3.4.

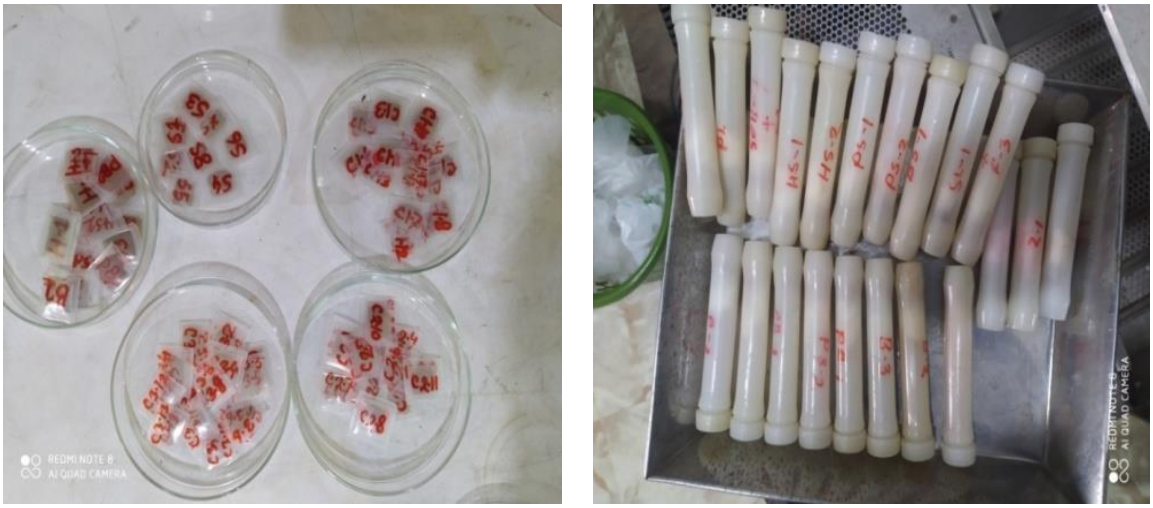

Fig. 3.4: Sample preparation for neutron irradiation.

Different standard reference materials were packed for different samples to ensure quality control and accuracy, such as IAEA-336 (Lichen) and NIST-1547 (Peach Leave) for biological samples and IAEA-Soil-7, IAEA-SL-1, and NIST-1633b for rhizosphere soil samples.

Sample Preparation for AAS

All of the solutions were prepared using Milli-Q System, Millipore's double-de-ionized water. Stock solutions containing 1000 mg/l of each element were diluted to provide the element standard solutions that were used for calibration. USEPA procedure 3051A was

followed to digest 1g of medicinal plant, soil, and the same standards that were used in INAA with 7 ml of HNO3 (65%) in Teflon containers using a microwave accelerator reaction system (MARS 5, CEM, USA) for the purpose of determining the trace element content.

Sample Preparation for Natural Radioactivity

All core samples, medicinal plants, and rhizosphere soil samples were oven-dried and made into homogeneous powder using agate mortar and pestle. The powder soil and plant leaf samples in cylindrical plastic containers were sealed with a cap and wrapped by thick vinyl tape for four to five weeks (>7 half-lives of ^{222}Rn) at room temperature to reach secular equilibrium between parents and their progenies (Fig. 3.5).

Fig. 3.5: Sample preparation for natural radioactivity measurements.

To ensure data quality, two reference materials (IAEA-RM-375) and IAEA-414 were prepared similarly.

3.2 EXPERIMENTAL TECHNIQUES

3.2.1 Alpha Spectrometry

The low activity of a few mBq to several Bq is typical for alpha spectrometry measurements of environmental materials. Therefore, measurement equipment with low background radiation and high counting efficiency is needed for the measurement.

The direct ionizing action of alpha particles can be utilized to measure alpha radiation. A planar silicon semiconductor that was passively implanted was chosen for alpha detection. The rationale for the selection process was to offer points of comparison with the previously discussed, but far less energy-resolving, plastic scintillator cells, which are more widely utilized. Semiconductor detectors are made using PN junctions with depletion zones. By biasing an area with opposing polarities, the depletion zone is formed. Any deposited incident radiation energy in this zone will release electrons from the valence band. The semiconductor material's liberated electrons create a current, which is subsequently sent to the 15 preamplifier for shaping and amplification. An alpha spectrometer is shown in Fig. 3.6.

Fig. 3.6: Alpha spectrometer used in the present study.

Based on the total charge acquired by the preamplifier, information about the energy deposited in the detector is examined. For this reason, the lab purchased a Mirion Technologies PIPS box. This detector's architecture consisted of two silicon detectors encasing a port-equipped, vacant cell that served as the gas testing cell. Both silicon's specifications included an active surface area of 1200 mm^2 and a thickness of 500 µm, which is noticeably thick enough to permit full electron deposition up to 350 keV. Aluminum casing with carbon panes surrounded the detectors and gas cells to exclude external radiation sources (mostly photons). These detectors demonstrated negligible

temperature instability (<100 ppm/^{0}C) within the room temperature range of 0 to 50 °C and did not require any cooling to function. A plastic stand was devised and produced to make it easier to use the detector upright with both windows facing a NaI(Tl) detector.

3.2.2 TRIGA Mark-II Research Reactor

In the present study, core sediment and medicinal plant samples were neutron-irradiated in the TRIGA Mark II research reactor at AERE, Savar of Bangladesh Atomic Energy Commission (BAEC), shown in Fig. 3.7.

Fig. 3.7: Partial view of TRIGA Mark II research reactor at AERE.

BAEC TRIGA Research Reactor (BTRR) is the only nuclear reactor in the country. It is a tank-type research reactor used for training, research, and isotope production [89]. The basic design parameters of the BTRR are given in Table 3.1.

Table 3.1: Principal design parameters of TRIGA Mark II reactor.

Maximum steady state power level	3 MW
Fuel element design: Fuel-moderator material Uranium content Uranium enrichment Burnable poison Shape Overall length of fuel Outside diameter of fuel Cladding material	 U-ZrH 20 wt% 19.7% U-235 0.47wt% Erbium Cylindrical 38cm 3.63cm Type 304 stainless steel
Number of fuel elements	100
Maximum excess reactivity	7.69% Δk/k
Reactivity loss due to equilibrium Xe	2.5% Δk/k
Number of control rods: Shim Regulating Safty/transient	 4 1 1
Total reactivity worth of control rods	12.785 Δk/k
Reactor cooling	Forced down flow of pool water (above500kW)

The reactor has been utilized for study and use in a variety of sectors since it was put into service, including education, training of personnel, radioisotope generation, NAA, neutron radiography, and neutron scattering investigations. Fig. 3.8 depicts the inner view of the reactor core.

Irradiation Facilities: The BTRR is equipped with a number of irradiation facilities for neutron irradiation of the samples, which are listed below:

- Dry Central Thimble (DCT)
- Pneumatic transfer (Rabbit) system
- Rotary specimen rack (Lazy Susan)

- Neutron beam tubes
- Triangular cut-outs in the core
- Thermal column for future use

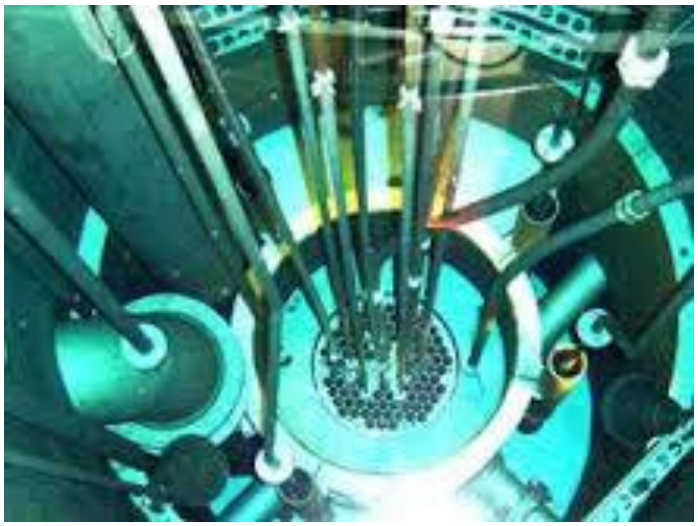

Fig. 3.8: Inner view of TRIGA Mark II research reactor at AERE, Savar.

In the DCT, samples can be irradiated at a maximum thermal neutron flux of about 7.46 x 10^{13} $cm^{-2}s^{-1}$. The pneumatic transfer system has a transfer time of about 4.6 sec is used to irradiate samples that produce short-lived radioisotopes. This system is particularly used for instrumental neutron activation analysis (INAA). In this study, all core sediment and medicinal plant samples were irradiated in this irradiation facility. Four neutron beam tubes (BT), which are named tangential BT, piercing BT, radial BT-1, and radial BT-2, permit the extraction of neutron beams of all energies into the reactor hall for the purpose of neutron and solid-state physics experiments. At present, the piercing BT is being used for triple axes spectrometers, and the tangential BT for neutron radiography. The neutron radiography facility is used for non-destructive testing (NDT), particularly with a view to knowing about hydrogen or neutron absorber material in solid matter. This facility uses neutron irradiation similar to X-ray radiography. The Lazy Susan (LS) or rotary specimen rack is a 'donut'-shaped watertight device placed in the upper part of the graphite reflector assembly around the reactor core. This rack has 41 sample holding tubes. Each of these tubes (except the 1st one) can accommodate two 14cm long and 3.2cm dia standard specimen containers in it. The sample is loaded into the rotary specimen rack through the 3.3cm dia loading tube, which extends up to the top of the reactor shield structure and

terminates at the center channel. A position control mechanism allows the loading of samples in different chambers of the LS. The triangular and hexagonal cutouts in the core allow in-core irradiation of large-diameter samples, which are not suitable for insertion into the dry CT or into the LS.

3.2.3 Irradiation and Counting of Samples and Standards by INAA

Two types of irradiations were performed for the determination of short- and long-lived radionuclides depending on their half-lives.

i) Short irradiation was performed to determine short-lived radionuclides of the elements like Al, Mn, Ti. etc.
ii) Long irradiation was performed to determine relatively long-lived radionuclides of the elements like As, Ba, La, Sm, Th, etc.

i. Short Irradiation

Short irradiation of each sample and standard was performed separately for 60 sec in the rabbit irradiation system of BTRR at 250 kW reactor powers, sediment samples collected after neutron irradiation shown in Fig. 3.9. The outer pack of the irradiated sample was replaced by a new one to reduce radioactive contamination. In the 1st counting of short irradiation, each sample/standard was counted for about 300 sec a 600 sec cooling time. After finishing the 1st count, each sample was counted for 600 sec a 2 hr cooling time. The dead time of the counting system was kept within 10%. In this study, the counting system consisted of a High Purity Germanium (HPGe) detector having an energy resolution of 1.76 keV γ-ray line of ^{60}Co source coupled with MAESTRO-32 (ORTEC) and Genie-2000 (Canberra) software.

ii. Long Irradiation

When it was to perform long irradiation, all the samples and standards were put in the same irradiation vial, and all of them were irradiated at the same time. In that tube, six Al-Au foils (0.1% Au) marked as F-1, F-2, F-3, F-4, F-5, and F-6 were also stacked on the samples. They were used as the flux monitor.

Fig. 3.9: Sediment core samples collecting after irradiation in BTRR.

The irradiation vial containing the samples, standards, and Al-Au foil was irradiated for 7 minutes at 2.4 MW power in the rabbit system of BTRR. After irradiation, the irradiated vial was kept in a lead container for two days to let the short-lived radionuclides decay and reduce the radiation hazard. The 1st count was taken for 3600 sec. After finishing the 1st count, the 2nd count was started (after 7days of irradiation) and was taken for 3600 sec. After taking 1st and 2nd counts, the samples and standards were kept in a radiation-shielded area in a lead cylinder for 1 month before taking the 3rd count. After one month, the 3rd count of the long irradiation of the samples and standards was counted for 7200 sec.

3.2.4 High Purity Germanium (HPGe) Detector

A computer-based multi-channel analyzer, related electronics, and a semiconductor detector typically make up the equipment needed to quantify gamma rays from radioactive substances. The germanium crystal in these detectors is mounted in a vacuum and thermally linked to a copper rod or cold finger in order to function at liquid nitrogen temperatures. The HPGe detector picks up the gamma rays that the product nucleus emits, shown in Fig. 3.10.

Fig. 3.10: Partial view of HPGe detector system used for this study.

Because of its higher resolution than NI crystal, an HPGe detector is a high-quality precision instrument that is frequently employed for gamma spectroscopic measurement. Semiconductor detectors generate free-charge carriers that are useful for measuring and detecting incident radiation.

3.2.5 Some Important Parameters of HPGe Detector System

Some important parameters of the gamma-ray spectrometry system used for this study are calculated and discussed here:

i. Energy Calibration

Energy calibration is defined as the relationship between the energy of the gamma ray and the channel number in the spectrum. As Eu-152 is a multi-gamma emitting radioisotope, ^{152}Eu energy calibration was performed. Later, energy calibration was

confirmed by placing a ^{60}Co source inside the detector. It shows two gamma peaks at 1173.23 keV and 1332.5 keV. Fig. 3.11 shows the gamma energy vs. channel number validating the energy calibration of the detector. Here, Table 3.2 shows three significant gamma peaks of ^{152}Eu used for energy calibration.

Table 3.2: Energy Calibration With ^{152}Eu Point Source.

Gamma Energy (keV)	Channel Number
121.78	533
778.9	3420
1408.01	6188

Three energies of ^{152}Eu were chosen to cover a wide gamma energy range. In Fig. 3.11, these energies with corresponding channel numbers result a in straight line. Thus, it ensures the successful calibration of the detector system.

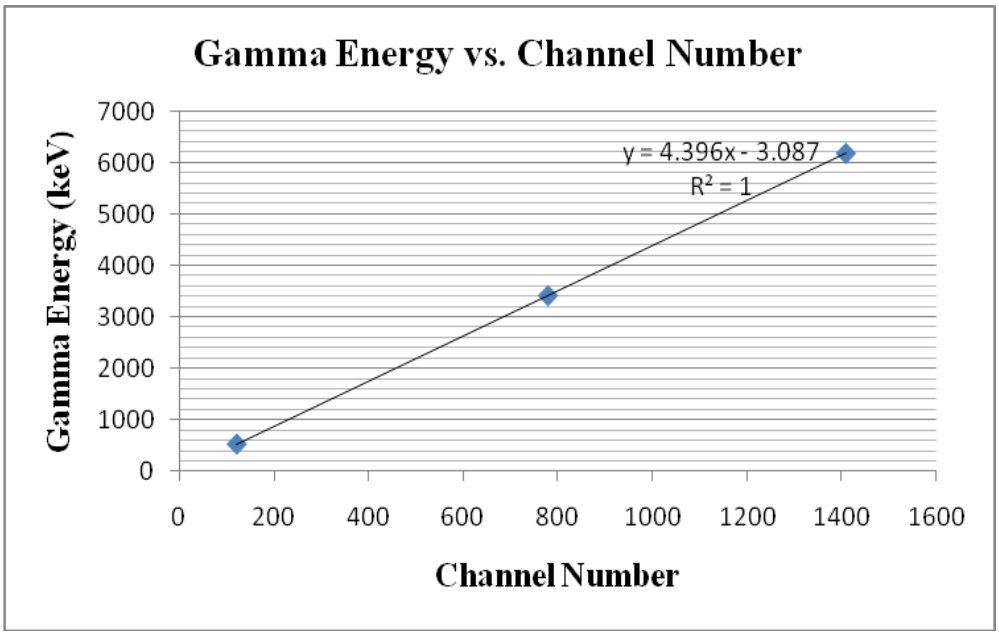

Fig. 3.11: Energy calibration with ^{152}Eu point source.

ii. Measurement of Energy Resolution

To measure the energy resolution of the HPGe detector system, a spectrum was acquired using a ^{60}Co source placed 5 cm away from the surface of the detector. The source was shielded by the lead castle to minimize the background contribution. Two cascades γ -ray

energies of 1173.9 keV and 1333 keV were emitted from ^{60}Co that are 159.1 keV apart. The data used for the measurement of the detector resolution is given in Table 3.3.

$$\text{Energy resolution} = \text{FWHM} \times \frac{E_2 - E_1}{C_2 - C_1}$$

$$= 4 \times \frac{1333 - 1173.9}{3417 - 3008}$$

$$= 1.56 \text{ keV},$$

Where, E_1 = 1173.9 keV, E_2 = 1333 keV, C_1 = 3008, and C_2 = 3417

The energy resolution of the detector obtained in this experiment is 1.56 keV at 1173.9 keV gamma-ray line of ^{60}Co source.

Table 3.3: Data for energy resolution calculation of the HPGe detector system.

Gamma	peak at	1173.9	keV	Gamma	peak at	1333	keV
Channel	Counts	Channel	Counts	Channel	Counts	Channel	Counts
2971	2618	3011	116682	3380	588	3420	82158
2972	2488	3012	47879	3381	562	3421	33129
2973	2519	3013	16143	13382	537	3422	10655
2974	2554	3014	5533	3383	599	3423	2993
2975	2557	3015	2854	3384	587	3424	1034
2976	2490	3016	2242	3385	582	3425	540
2977	2562	3017	2141	3386	610	3426	503
2978	2577	3018	2067	3387	617	3427	447
2979	2571	3019	1989	3388	611	3428	440
2980	2630	3020	2047	3389	607	3429	432
2981	2539	3021	2042	3390	556	3430	375
2982	2584	3022	1994	3391	619	3431	420
2983	2539	3023	1933	3392	595	3432	356
2984	2456	3024	1971	3393	612	3433	331
2985	2615	3025	1903	3394	650	3434	347
2986	2507	3026	1916	3395	600	3435	332
2987	2509	3027	1946	3396	640	3436	353

Gamma peak at 1173.9 keV				Gamma peak at 1333 keV			
Channel	Counts	Channel	Counts	Channel	Counts	Channel	Counts
2988	2569	3028	1911	3397	668	3437	306
2989	2470	3029	1822	3398	651	3438	299
2990	2612	3030	1902	3399	668	3439	323
2991	2547	3031	1797	3400	720	3440	306
2992	2610	3032	1790	3401	653	3441	319
2993	2500	3033	1824	3402	713	3442	268
2994	2613	3034	1808	3403	754	3443	293
2995	2523	3035	1820	3404	747	3444	292
2996	2643	3036	1829	3405	789	3445	304
2997	2643	3037	1704	3406	875	3446	291
2998	2790	3038	1762	3407	921	3447	300
2999	2908	3039	1807	3408	1028	3448	279
3000	2984	3040	1776	3409	1301	3449	283
3001	3493	3041	1765	3410	2220	3450	297
3002	4853	3042	1773	3411	5401	3451	267
3003	10984	3043	1649	3412	16135	3452	300
3004	30851	3044	1688	3413	44467	3453	277
3005	81015	3045	1757	3414	100872	3454	269
3006	168026	3046	1623	3415	183449		
3007	271193	3047	1639	3416	259149		
3008	331927	3048	1652	3417	283943		
3009	308337	3049	1706	3418	241670		
3010	217653	3050	1656	3419	160278		

The energy resolution curve of the HPGe detector is shown in Fig. 3.12 FWHM value was found to be 4 channels at 1173.9 keV peak. The energy resolution is then:

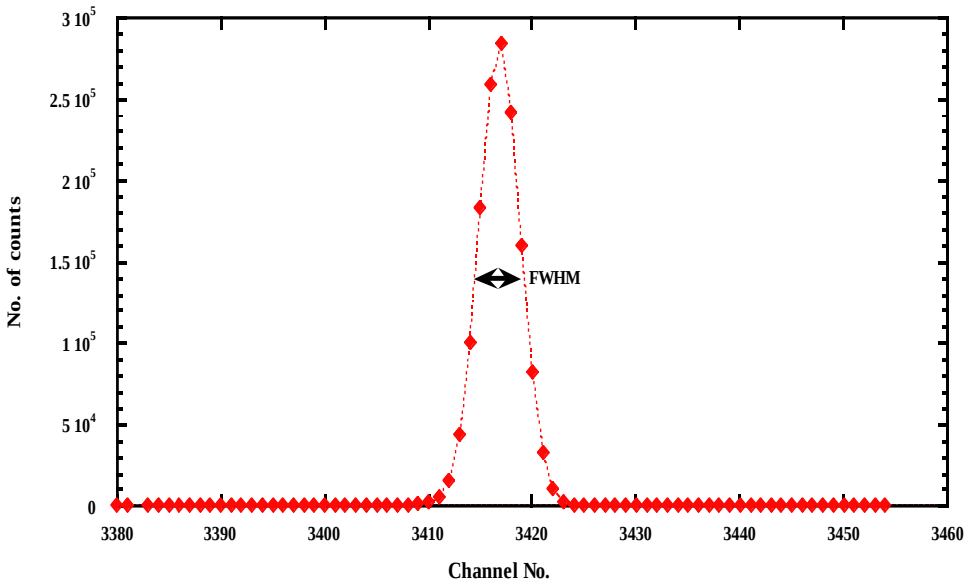

Fig. 3.12: Energy resolution of the HPGe detector system (1333 keV).

iii. Measurement of Detector Efficiency

In this study, elemental concentration was calculated by using the comparative NAA method. For this method, samples and standards were measured in an exactly identical condition. For that reason, the detector shows the same efficiency for a particular gamma peak for a sample and a standard which cancels out the effect of efficiency of the gamma ray peaks at different energies. Therefore, the efficiency of the gamma-ray spectrometry system was not measured in this study.

3.2.6 Gamma Ray Counting

Following the radiation, a digital gamma spectrometer (ORTEC, DSPEC JrTM) shown in Fig. 3.13 and a high purity germanium (HPGe) detector (CANBERRA, 25% relative efficiency, 1.8 keV resolution at 1332.5 keV of ^{60} Co) were used for gamma-ray counting. A gamma-ray spectrum of Sundarban sediment samples is shown in Fig. 3.14. For a short irradiation, two counts were made: one for 300 seconds following a decay time of roughly 300 seconds, and another for 600 seconds following a decay time of two to three hours.

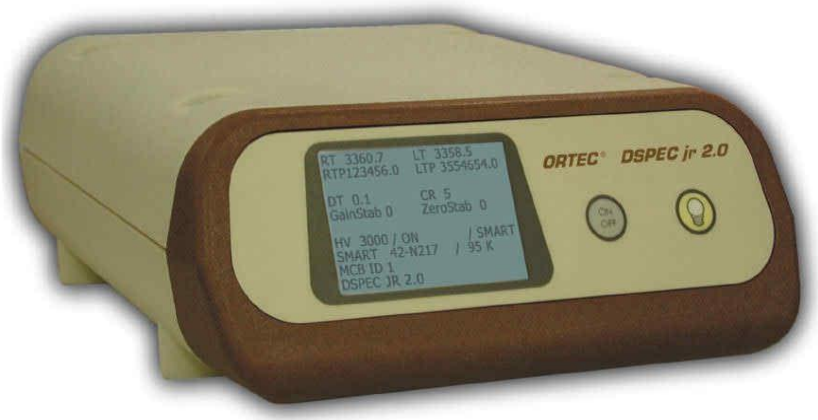

Fig. 3.13: The component of a digital gamma ray spectrometry system.

For long-irradiated samples, the first counting was done for 3600 seconds after a decay period of two to three days; the second counting was done for 7200 seconds after a decay period of seven to ten days; and the third counting was done for eight to twelve hours following a decay period of two to three weeks.

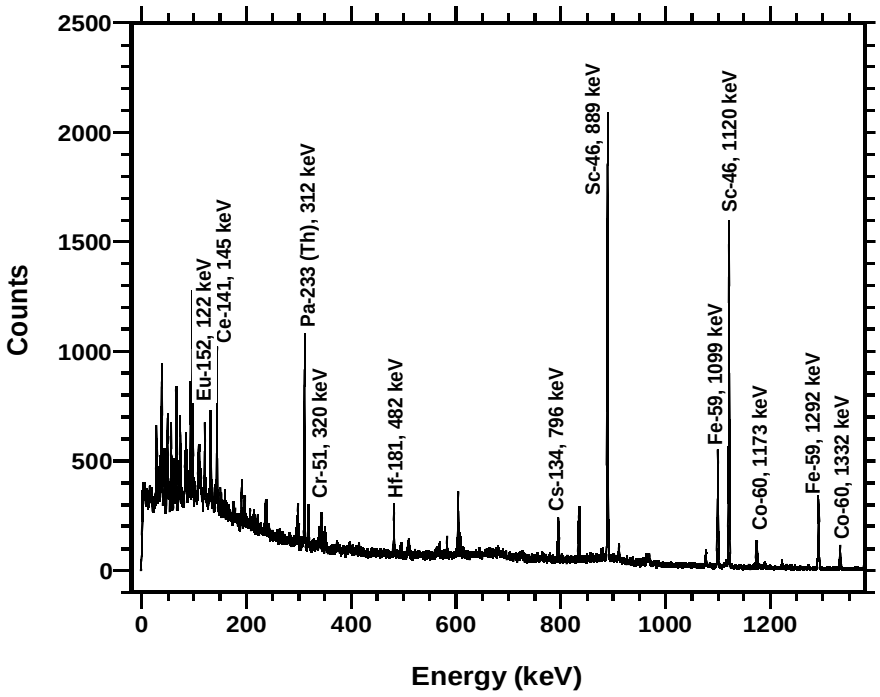

Fig. 3.14: A typical gamma-ray spectrum of a sediment core sample.

All of the irradiated samples and approved reference materials underwent gamma spectrometry analysis using digital gamma spectrometry equipment in conjunction with a

PC-based HPGe detector. The software Genie-2000 (Canberra) and MAESTRO-32 (ORTEC) were used for the data collection, and the gamma peak analysis was carried out.

3.3 SAMPLE ANALYSIS

3.3.1 ^{210}Pb Activity Determination

Using the constant rate of supply (CRS) model of the ^{210}Pb dating technique, sediment accumulation rates were computed [89, 90]. Through the measurement of ^{210}Po, the decay product of ^{210}Pb, an alpha spectrometer fitted with a passivated implanted planar silicon (PIPS) detector allowed for the indirect computation of ^{210}Pb's total activity (supported and unsupported). In sediment samples, the total ^{210}Pb was thought to be in radioactive equilibrium with the ^{210}Po. By utilizing a high-resolution HPGe detector setup to analyze ^{226}Ra activity, the $^{210}Pb_{sup}$ activity was determined. By examining the gamma-ray peak energies of its daughter nuclide, ^{214}Pb, at 185.9 keV (gamma intensity: 3.28%) and 351.9 keV (gamma intensity: 35.6%) in the ^{238}U-decay series, the activity concentration of ^{226}Ra was ascertained. The activity concentrations of $^{210}Pb_{ex}$ used to build the age models were computed using the difference between the activity concentrations of the total ^{210}Pb and ^{226}Ra ($^{210}Pb_{sup}$). The activity of ^{137}Cs was determined by analyzing the gamma-ray peak at 661.66 keV. By measuring the activity concentrations of ^{210}Pb in two approved reference materials, IAEA-368 and IAEA-300 (marine sediments), the accuracy of the radiometric process was assessed. Within 12% of their approved activity values, the obtained activity concentrations were found.

$$C_{Excess} = C_{tot} - C_{sup}$$
$$C_{Excess} = C_{Excess}(0)\, e^{-\lambda t}$$

Where C_{Excess} is the excess activity of ^{210}Pb isotope originating from precipitation, C_{sup} is activity along a vertical profile that is practically constant, and C_{tot} is the total activity of ^{210}Pb isotope.

3.3.2 Elemental Concentration Determination by INNA

The gamma peak analysis of samples and standards was performed using the gamma spectrum analysis software Hypermet PC version 5.12. The area under the peak of a gamma ray from a radionuclide of interest in a gamma-ray spectrum represents the total count for that peak. After getting the net count of a selected peak, it was put into the Excel sheet to calculate the concentration of the corresponding element in the sample.

The following equation, which was discussed in Chapter 2 was used to calculate the concentration, where the mass of the element in an unknown sample is

$$W = W' \frac{\text{Counts per second} \times F_i F_d F_c}{\text{Counts per second}' \times F_i' F_d' F_c'}$$

Where components with prime are referred to as related to standards.

3.3.3 Determination of Natural Radioactivity Concentration

The following equation was used to calculate the activity concentration.

Activity concentration $A = \frac{\text{CPS} \times 1000}{\text{WEI}}$

Where A = activity of the sample in $Bqkg^{-1}$, cps = the net counts per second, E = the counting efficiency of the gamma energy, I = the absolute intensity of the gamma ray, and W= the samples net weight (in kg).

3.3.4 Elemental Concentration Determination by AAS

One gram of each sediment sample and medicinal plant was utilized for AAS analysis, along with a soil sample and the same standards as were used for INAA digestion. Using standard protocols, a graphite furnace AAS (Varian Analytical Instruments, Models AA DUO 240 FS and AA 280 Z) assessed the elemental concentrations of the metals in medicinal plant and soil samples [28], [71]. Following the process of microwave digestion, the sample solutions underwent filtration and adjustments to a suitable volume with double-deionized water.

The acid digestion method is shown as a flowchart of the acid digestion method for AAS in Fig. 3.15.

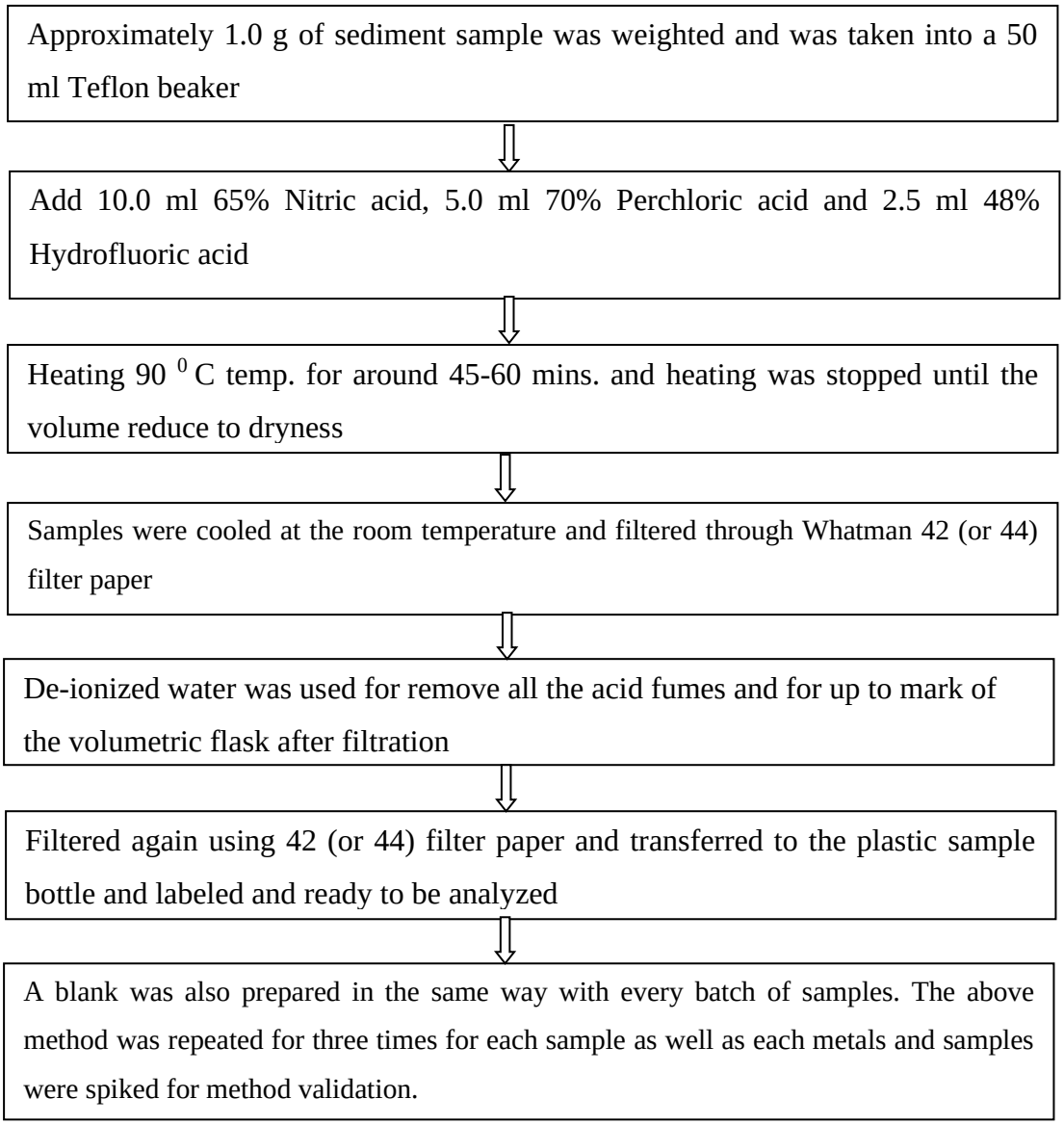

Fig. 3.15: Flowchart of acid digestion method for AAS.

3.4 MINIMUM DETECTABLE ACTIVITY CONCENTRATION

The minimum detectable activity concentration (MDAC) in natural radioactivity for the detector at a 95% confidence level was calculated using the following equation [91].

$$MDAC = \frac{\sqrt{B}K_{\alpha}}{\varepsilon_{\gamma} W t_s \rho_{\gamma}}$$

Where k_{α} is the statistical coverage factor (1.645), B is the background counts (cps), ε_{γ} is the photo peak efficiency, ρ_{γ} is the probability of gamma emission, t_s is the sample counting time in seconds, and w is the mass of the sample in kilograms. The MDAC values calculated in this study for ^{226}Ra, ^{232}Th, and ^{40}K were 0.45, 0.62, and 3.1 Bq kg^{-1}, respectively.

3.5 ASSESSMENT OF ELEMENTAL CONTAMINATION

Various indices have been developed to assess the contamination and environmental risk of trace elements in surface sediments based on their total contents. In this study, environmental contamination assessments for 20 environmentally important elements (Al, K, Ti, V, Cr, Mn, Fe, Co, Ni, Cu, Zn, As, Rb, Cd, Cs, Ba, Hg, Pb, Th and U) are discussed below.

i. Enrichment Factor

A common approach to estimate the anthropogenic impact on sediments is to calculate a normalized enrichment factor (EF) for metal concentrations above uncontaminated background levels. Thus, EF can be calculated by using the following equation [92]:

$$EF = \frac{\left(\frac{Metal}{Al}\right)_{Sample}}{\left(\frac{Metal}{Al}\right)_{Background}}$$

In this study, Al was used as a reference element for geochemical normalization, and upper continental crustal (UCC) average values from the literature [93] were used as the geochemical background concentration.

(1) Al is associated with a fine solid surface
(2) Its geochemistry is similar to that of many trace metals and
(3) Its natural concentration tends to be uniform.

The EF values close to unity indicate crusted origin, those less than 1.0 suggest a possible mobilization of depletion of metals, whereas EF > 1.0 indicates that the element is of anthropogenic origin. EF values 1.5-3.0, 3.0-5.0, 5.0-10 and >10 are the evidence of minor, moderate, severe, and very severe enrichment of the elements in sediments, respectively.

ii. Geo-accumulation Index

To characterize the pollution levels of sediments, the geo-accumulation index (I_{geo}) is an effective tool that can be defined by the following equation [93]:

$$I_{geo} = \log_2 \frac{C_n}{1.5 \times B_n}$$

Where C_n is the measured concentration of the metal n, B_n is the geochemical background matrix correction factor due to lithospheric effects. The geo-accumulation index consists of seven grades of classes [94]:

(i) Class 0 (practically uncontaminated): $I_{geo} \leq 0$
(ii) Class 1 (uncontaminated to moderately contaminated): $0 < I_{geo} < 0$
(iii) Class 2 (moderately contaminated): $1 < I_{geo} < 2$
(iv) Class 3 (moderately to heavily contaminated): $2 < I_{geo} < 3$
(v) Class 4 (heavily contaminated): $3 < I_{geo} < 4$
(vi) Class 5 (heavily to extremely contaminated): $4 < I_{geo} < 5$
(vii) Class 6 (extremely contaminated): $5 < I_{geo}$

Class 6 is an open class and comprises all values of the index higher than class 5.

iii. Mean ERM Quotient (M-ERM-Q)

To determine the possible biological effects of combined toxicant groups [95], use the M-ERM-Q method. The M-ERMQ is obtained by calculating mean quotients for a large range of contaminants [96] using the following equation:

$$M-ERM-Q=\frac{\sum_{i=1}^{n}\frac{C_i}{ERM_i}}{n}$$

Where C_i is the concentration of element i, ERM_i is the ERM value for the element i and n is the number of elements. According to the classification of M-ERM-Q: M-ERM-Q < 0.1 represents 9% probability of toxicity, 0.11 = M-ERM-Q < 0.5 represents 21% probability of toxicity, 0.51 = M-ERM-Q < 1.5 represents 49% probability of toxicity, and M-ERM-Q > 1.5 represents 76% probability of toxicity [95].

3.6 RADIONUCLIDE TRANSFER FACTOR

The transfer factor (TF) is frequently used to characterize the radionuclide transfer from soil to plant via plant roots [99]. The ratio of activity concentration (Bq kg^{-1}, dry weight) of a radionuclide in a plant or plant part to that in the rhizosphere soil of that plant is used to calculate the TF.

3.7 RADIOLOGICAL HAZARD INDICES

The description and equations of the radiological risk indices are given in Table 3.4.

Table 3.4: Description and equations of the radiological risk indices.

Index	Equation and description
Radium equivalent activity (Ra_{eq})	$Ra_{eq} = A_{Ra} + 1.43A_{Th} + 0.077A_K$ A_{Ra}, $A_{Th,}$ and A_K (in Bq kg^{-1}) represent the activity concentrations of ^{226}Ra, ^{232}Th, and ^{40}K, respectively.
Gamma representative level index (I_γ)	$I_\gamma = A_{Ra} / 150 + A_{Th} /100 + A_K / 1500$
Absorbed dose rate (D in $nGyh^{-1}$)	D ($nGyh^{-1}$) = $0.462A_{Ra} + 0.604A_{Th} + 0.042A_K$
Annual effective dose equivalent (AEDE)	AEDE ($mSvyr^{-1}$) = D($nGyh^{-1}$) × 8760 (h yr^{-1}) × O × C Here, C (in mSv/nGy) is the conversion coefficient from absorbed to effective dosage, and for outdoor exposure, O is the occupancy factor.
External hazard index (H_{ex})	$H_{ex}= A_{Ra}/370 + A_{Th}/259 + A_K/4810$
Internal hazard index (H_{in})	$H_{in}= A_{Ra}/185 + A_{Th}/259 + A_K/4810$
Annual effective ingestion dose rate (AE_{ingest})	AE_{ingest} (μSv y^{-1}) = C × I_{ingest}× IDF Where, C is the activity concentration of ^{226}Ra, ^{232}Th, and ^{40}K, I_{ingest} is the consumption rate of medicinal plants, and IDF is the uptake dose conversion factor for the corresponding radionuclides. I_{ingest} was calculated at 1.8 kg y^{-1} for medicinal plants Tettey-Larbi et al. [97], Harb et al. [98].
Excess lifetime cancer risk (ELCR)	ELCR = AEDE × ALT × RF Here, ALT is for an average lifetime, RF stands for risk factor, which is the number of additional cancers anticipated to the people of a given number, exposed to a carcinogen at a given dose, and is expected to be 70 years.

3.8 QUALITY CONTROL AND QUALITY ASSURANCE

Along with the core sediment, medicinal plant, and rhizosphere soil samples, repeated analyses of the reference materials IAEA-368, IAEA-300, IAEA-Soil-7, IAEA-SL-1, NIST-1633b, NIST-1547, and IAEA-336 were carried out to guarantee the stated data quality (accuracy and precision). U-score, Z-score, and relative bias from the certified/information values of the standards were computed to assess laboratory performance. The Z-score, U-score, and relative bias were determined using the following formulas, respectively [100]:

$$U-score=\frac{\left|X_{lab}-X_{ref}\right|}{\sqrt{\mu_{lab}^{2}-\sigma_{ref}^{2}}}$$

Where X_{lab}, X_{ref}, μ_{lab}, and σ_{ref} stand for the laboratory result, reference value, standard uncertainty with the reference value, and uncertainty resulting from the laboratory results, respectively. The laboratory performance is considered satisfactory if the U-score value is less than 1, and unsatisfactory if the U-score value is greater than 1, indicating a discrepancy between the certified value and the outcome.

$$Z-score=\frac{X_{lab}-X_{ref}}{\sigma_{ref}}$$

In this case, ref represents the uncertainty with the reference value, X_{ref} is the reference value, and X_{lab} is the laboratory value. The laboratory performance is considered excellent if the |Z|-score is greater than 2, dubious if the |Z|-score is less than 3, and unsatisfactory if the |Z|-score is greater than 3.

The relative bias is also calculated by using the following equation.

$$RB=\frac{X_{lab}-X_{ref}}{X_{ref}}$$

3.9 ESTIMATION OF UNCERTAINTIES

In all forms of measuring, its quantification is crucial [101]. The uncertainty budget estimated in INAA is shown in Table 3.5.

Table 3.5: Origin and typical magnitude of uncertainties in INAA.

Uncertainty Component		Origin	Typical relative standard uncertainty
		Sample and comparator preparation	
	U_{1a}	Mass determination of a sample	0.05 %
	U_{1b}	Mass determination of a comparator	0.2 %
	U_{1c}	Mass changes of samples due to moisture uptake during weighing	0.1 %
	U_{1d}	Blank variation and the necessary correction (due to analytical content in the irradiation vial)	0.5 %
U_2		**Irradiation**	
	U_{2a}	Irradiation geometry differences	0.10%
U_3		**Spectrometry measurement**	
	U_{3a}	Counting statistics	Depend on spectrum
	U_{3b}	Counting geometry difference	3 %
	U_{3c}	Pulse-pileup losses (random coincidences)	0.5 %
	U_{3d}	Peak integration method	0.3 %

$U_1 = \sqrt{\{(0.05)^2 + (0.2)^2 + (0.1)^2 + (0.5)^2\}}\% = 0.55\%$

$U_2 = 0.1\%$

$U_3 = \sqrt{\{ (U_{3a})^2_{sam} + (U_{3a})^2_{std} + (U_{3b})^2 + (U_{3c})^2 + (U_{3d})^2_{sam} + (U_{3d})^2_{std} \}}$

The combined uncertainty,

$U_c = \sqrt{\{U_1^2 + U_2^2 + U_3^2\}}\%$

This uncertainty is converted to absolute uncertainty as follows:

$U_{abs} = (U_c/100)$ * sample concentration, these uncertainties are added to the main result.

Uncertainty in Natural Radioactivity Concentration Data

Activity concentration can be expressed in the form of $x \pm \Delta x$, where x represents the activity of the sample and Δx represents the counting error (CE), which is equal to $\sqrt{x}$ according to Poisson distribution. If the average activity obtained from different photo peaks is taken as x, then Δx is represented by

$$CE = \sqrt{\frac{\Delta x_1^2 + \Delta x_2^2 + ... + \Delta x_N^2}{N-1}}$$

Where $\Delta x_1, \Delta x_2, \ldots \Delta x_N$ denotes counting error for $x_1. x_2, \ldots . x_N.$

3.10 DETECTION LIMITS

The detection limits represent the ability of a given INAA procedure to determine the minimum amounts of an element reliably. The detection limit depends on the irradiation, the decay, and the counting conditions. It also depends on the interference situation, including such things as the ambient background, the Compton continuum from higher energy γ-rays, and any γ-ray spectrum interference from such factors as the blank from pre-irradiation treatment and packing materials. The detection limit is calculated using Currie's formula.

$$D_L = 2.71 + 4.65\sqrt{B}$$

Where, D_L is the detection limit, and B is the background under a γ-ray peak.

It is valid only when the γ-ray background (counting statistical error) is the major interference. However, practically, the INAA detection limits depend on:

1. The amount of material to be irradiated and to be counted

2. The neutron fluxes and the duration of the irradiation time

4. The total induced radioactivity that can be measured

5. The duration of the counting time

7. The detector size, counting geometry, and background shielding.

Chapter 4: RESULTS AND DISCUSSION

4.1 MASS ACCUMULATION, ELEMENTAL CONTAMINATION HISTORY, AND ECOLOGICAL RISK ASSESSMENT OF THE SEDIMENT OF SUNDARBAN

In this study, alpha spectrometry, neutron activation analysis, atomic absorption spectrometry, and gamma-ray spectrometry systems have been applied to assess the mass accumulation rate, contamination history, and ecological risk of the Sundarban mangrove sediments.

4.1.1 Evaluation of Accuracy of the Analysis

The accuracy of the radiometric procedure was evaluated in an independent experiment by checking the activity of the determined radionuclide ^{210}Pb in two standard reference materials produced by the International Atomic Energy Agency: IAEA-368 and IAEA 300 (marine sediments). The obtained activity concentrations for certified radionuclide ^{210}Pb were close to the reported values with deviations of < 10 %. The result is tabulated in Table 4.1. In this study, the quality of the elemental analysis was also performed by determining the elemental contents of reference materials-NIST-SRM-1633b and IAEA-CRM-SL-1.

Table 4.1: Accuracy of the analysis by determining ^{210}Pb concentrations in the standard reference materials IAEA-368 (Pacific Ocean sediment) and IAEA-300 (Baltic Sea sediment).

Reference materials	Certified value (Bq kg^{-1})	Present work (Bq kg^{-1})	Deviation (%)
IAEA-368	23.2	24.9	7.3
IAEA-300	360	326	9.4

The reported uncertainties associated with the concentration values are due to counting statistics only. Since counting statistics mainly controls the total uncertainty in NAA, it was reported with concentration values.

However, in addition to this reported uncertainty, there was commonly 3% more uncertainty (estimated in our analysis) was also associated with the reported values, which included sample and standard preparation, irradiation, positioning in the detector, pulse-pileup losses, and peak integration. The deviations of the determined concentration values in the present study from the certified/Information values of the reference materials are shown in Tables 4.2 and 4.3. The studied element concentrations obtained in this study are in good agreement with their certified values, which ensures the accuracy of the analysis.

Table 4.2: Comparison of measured values with certified values (mg kg^{-1}) in the standard reference materials NIST-SRM-1633b.

Elements	Certified value[b]	This work value	Deviation (%)
Al %	15.05 ± 0.27	14.1 ± 1.2	-6.3
As	136.2 ± 2.6	131 ± 6	-3.8
Ca %	1.51 ± 0.06	1.68 ± 0.26	11
Cr	198.2 ± 4.7	189 ± 5	-4.6
Cu[a]	112.8 ± 2.6	106 ± 4	-6
Fe%	7.78 ± 0.23	7.94 ± 0.25	2.1
Hg[a]	0.143 ± 0.0018	0.147 ± 0.002	2.7
Ni[a]	120.6 ± 1.8	114 ± 5	-5.5
Pb[a]	68.2 ± 1.1	61.1 ± 4.7	-10
V	295.7 ± 3.6	301 ± 11.5	1.9
Zn	(210)	219 ± 10	4.2

[a]Determined by AAS technique; [b]Values within parenthesis are non-certified values;

Table 4.3: Comparison of measured values with certified values (mg kg^{-1}) in the certified reference materials IAEA-CRM-SL-1.

Elements	Certified value[b]	This work value	Deviation (%)
Al%	(8.9)	9.27 ± 0.36	4.2
As	27.5 ± 2.9	30.7 ± 1.6	11
Ca[c] %	4120 ± 2210	3630 ± 912	-11
Cr	104 ± 9	112 ± 4	8
Cu[a]	30 ± 5.6	27.4 ± 2.5	8.6
Fe%	6.74 ± 0.17	7.36 ± 0.23	9
Hg[a]	(0.13)	0.14 ± 0.02	7.7
Ni[a]	44.9 ± 8	40.1 ± 3.9	10
Pb[a]	37.7 ± 7.4	40.2 ± 4.1	6.3
V	170 ± 15	174 ± 6	2.1
Zn	223 ± 10	240 ± 9	8

[a]Determined by AAS technique; [b]Values within parenthesis are non-certified values; [c]From Georem database (2023).

4.1.2 Sediment Geochronology and Accumulation Rate

The ^{210}Pb dating method using the constant rate of supply (CRS) model was used for determining the age of sediments in the Sundarban mangrove ecosystem. The profiles of $^{210}Pb_{ex}$ with depth for the two sediment cores of the Sundarban are shown in Fig. 4.1. Due to the limited availability of the alpha spectrometry system, among the four sediment cores two of them were analyzed for ^{210}Pb dating. Since $^{210}Pb_{ex}$ activity profiles at both points are not decreasing in a proper exponential manner (Fig. 4.1), sedimentation rates are not constant with time; therefore, the CRS model was used in this study [102]. The maximum values of $^{210}Pb_{ex}$ at both points are a few layers beneath the surface sediments, which indicate disturbances at the top layers due to waves or activity of invertebrates [103]. In both cores, ^{137}Cs activity concentrations were found to be below the detection limit.

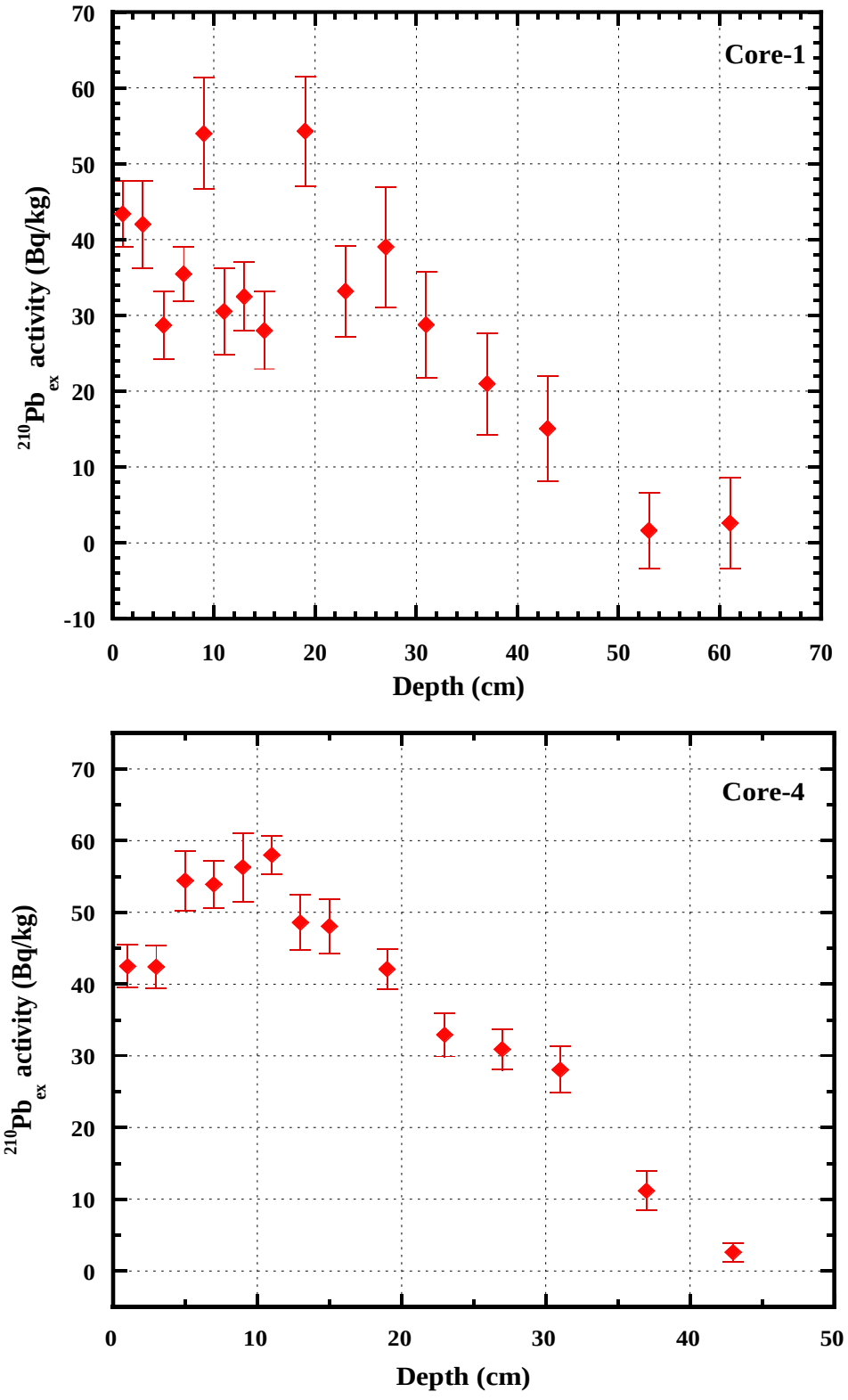

Fig. 4.1: The profiles of $^{210}Pb_{ex}$ vs. depth for the two sediment cores.

The calculated minimum detection activity (MDA) was 1.8 and 0.25 Bq kg^{-1} for ^{226}Ra and ^{137}Cs, respectively. The results of mass accumulation rates (MAR) with depth (and year) of the two sediment cores of the Sundarban obtained from the ^{210}Pb dating are plotted in Fig. 4.2. The bottom sediments of C1 (32 cm) and C4 (30 cm) were dated 1849 and 1856, respectively. The overall MAR increases over time, from the minimum value about 167 years ago to the maximum value at the sampling time (2018). For C1, the MAR increases from 0.06 to 2.61 kg m^{-2} y^{-1}, with an average of 0.60 k gm^{-2} y^{-1}. On the other hand, for C4, the MAR increases from 0.07 to 3.20 kg m^{-2} y^{-1}, with an average of 0.62 kg m^{-2} y^{-1}. Using the ^{210}Pb dating method, MAR was from 4.9 to 7.8 kg m^{-2} y^{-1} at the Indian part of the Sundarban near the Hooghly river estuary [104]. From the present study, the MAR at Bangladeshi Sundarban is lower than the results of the Indian part of the Sundarban. This can be attributed to the high sediment loads in the Hooghly river estuary brought by the Ganges River. Although the average MAR at both cores of the Bangladeshi Sundarban is almost the same (0.6 kg m^{-2} y^{-1}), the recent sediment accumulation rate at C4 is slightly higher than the C1. There is a sharp increase in the sediment accumulation rate after the year 2000 in both areas (Fig. 4.2). These changes could be related to the increase in industrial and human activities in the vicinity of the Sundarban area after the year 2000, which is caused by a change in the land use of that area. Alongi et al. [105] studied the rates of sediment accumulation in three mangrove forest areas of China, and MARs were rapid (10-62 kg m^{-2} y^{-1}) but decreased from the low- to the high-intertidal zone. The MARs at our mangrove are lower than those of the Chinese studied areas due to different inputs of organic material and processes resulting in sediment mixing, hence changes in sedimentation rates or erosion.

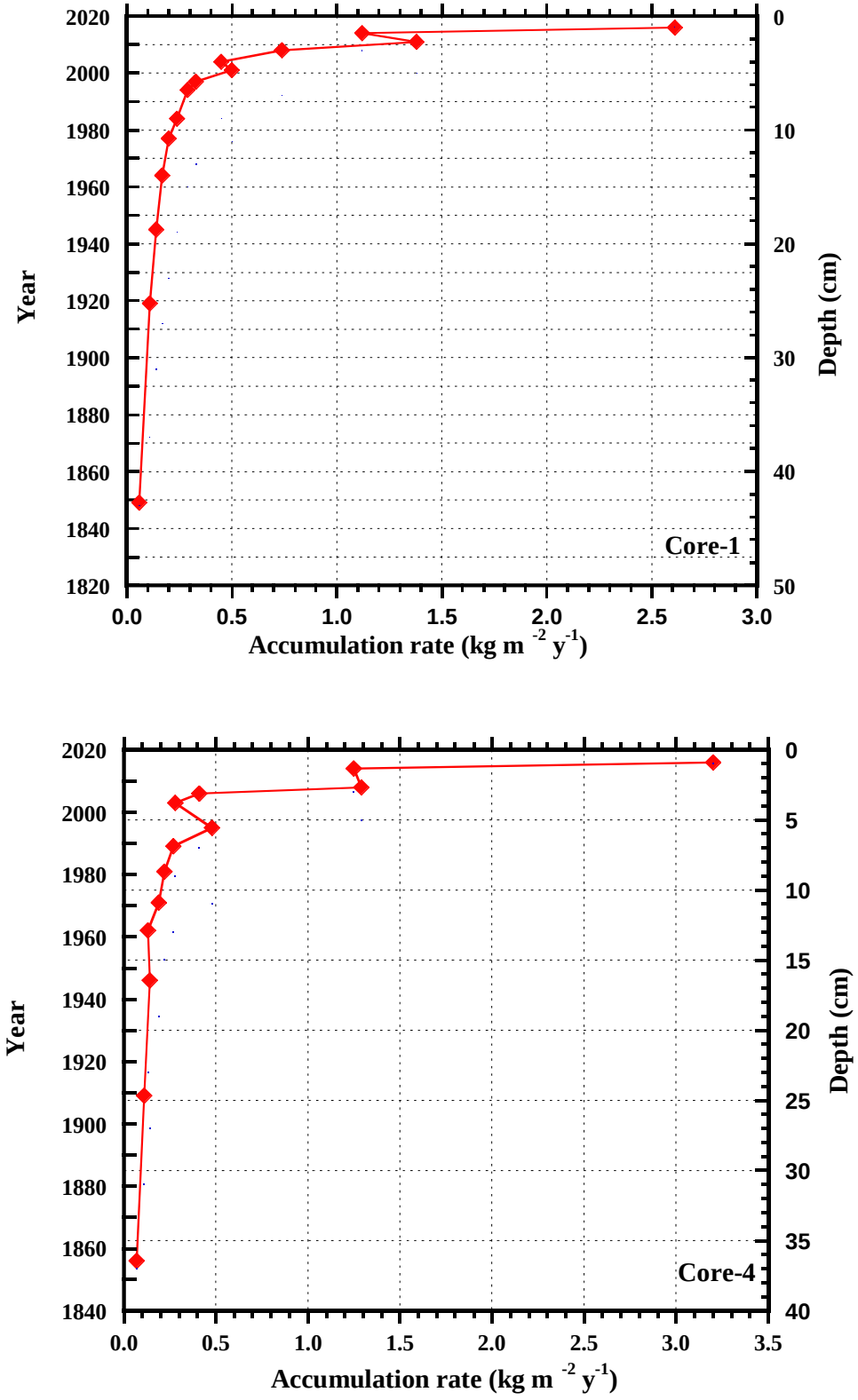

Fig.4.2: Depth (year) vs. mass accumulation rate for the sediment cores.

4.1.3 Spatiotemporal Distribution of Metals in the Sediment Cores

The descriptive statistics of the metal concentration data, along with the world mean values of UCC [106], and average shale values (ASV) [107], are tabulated in Tables 4.4 to 4.7. The available United States Environmental Protection Agency (USEPA) guideline values [108] of the respective metals are also tabulated in Tables 4.4 to 4.7. In this study, analytical data quality (accuracy and reproducibility) of the metals in sediments has been ensured by the repeated analysis of certified reference samples (NIST-SRM-1633b and IAEA-SL-1).

Table 4.4: Basic statistics of the metal concentration (% or mg kg^{-1}) data of the C1 core.

Elements in C1	Minimum	Maximum	Mean	SD	RSD, %	UCC[b]	ASV[c]	USEPA, 1999
Al,%	6.47	8.84	7.44	0.561	7.5	8.15	8.00	-
Ca,%	1.12	2.36	1.88	0.442	23	2.57	2.21	-
V	77.3	99.9	87.0	5.97	6.9	97	130	-
Cr	56.9	124	85.0	21.0	25	92.0	90.0	25
Fe,%	3.27	5.95	4.51	0.842	19	3.92	4.72	-
Ni[a]	26.3	40.6	35.2	4.40	13	47.0	68.0	16.0
Cu[a]	24.0	31.6	28.8	2.23	7.7	28.0	45.0	-
Zn	49.1	119	65.4	16.9	26	67.0	95.0	110
As	4.80	10.9	8.30	1.48	18	4.80	13.0	-
Hg[a]	0.012	0.038	0.020	0.007	33	0.050	0.40	-
Pb[a]	10.7	20.7	14.6	2.80	19	17	20	40

[a]Measured by AAS; all other metal concentrations are measured by INAA. [b]UCC: Upper continental crust [106]; [c]Average shale values [107], SD = standard deviation; RSD = relative standard deviation.

From Tables 4.4 to 4.7, it is observed that studied metal concentrations in different layers of the cores vary over different ranges (for C1, relative standard deviation (RSD): 6.9-

33%, for C2: 3.5-22.2%, for C3: 3.5 -51.7%, and for C4: 5.8-29%). The mean concentrations of Fe and As in C1, As and Pb in C4, Fe, As, Cr, and Zn in C2 and C3, show elevated values relative to UCC values. However, the mean concentrations of all studied metals are below the ASV values for C1 and C4 and except Cr and Zn for C2 and C3. When mean concentrations of the studied metals in cores of the Sundarban are compared to USEPA values [108], it is observed that Cr concentration is higher than the guideline values for all cores and Ni concentrations are higher than the guideline values for cores C1 and C4 (Tables 4.4 to 4.7). However, Pb concentrations range from 10.7-23.5 mg kg^{-1} for C1 and C4 cores and are below the Pb concentrations in clean coastal sediments (lower than 25 mg kg^{-1}) [109]. The Chandpai range near the Mongla seaport area has experienced more anthropogenic impact than the Satkhira area, as shown by the higher mean concentrations of all metals at C1 than at C4, with the exception of Pb.

Table 4.5: Basic statistics of the metal concentration (% or mg kg^{-1}) data of the C2 core.

Elements in C2	Minimum	Maximum	Mean	SD	RSD,%	UCC[b]	ASV[c]	USEPA, 1999
Al,%	6.99	8.17	7.66	0.27	3.5	8.15	8.00	-
Ca,%	0.453	0.998	0.686	0.154	22.2	2.57	2.21	-
V	98.9	103	96.2	4	4.4	97	130	-
Cr	88.2	116	97	7	7.7	92.0	90.0	25
Fe,%	1.21	5.02	4.34	0.835	19.2	3.92	4.72	-
Zn	98.0	116	106	6	5.3	67.0	95.0	110
As	7.54	12.9	10	1	10.9	4.80	13.0	-

[a]Measured by AAS; all other metal concentrations are measured by INAA. [b]UCC: Upper continental crust [106]; [c]Average shale values [107], SD = standard deviation; RSD = relative standard deviation.

Table 4.6: Basic statistics of the metal concentration (% or mg kg^{-1}) data of the C3 core.

Elements in C3	Minimum	Maximum	Mean	SD	RSD,%	UCC[b]	ASV[c]	USEPA, 1999
Al,%	5.92	8.52	7.40	0.652	3.5	8.15	8.00	-
Ca,%	0.301	1.28	0.951	0.264	27.7	2.57	2.21	-
V	79.6.	135	95.6	13	14	97	130	-
Cr	71.6	112	93.2	8	9.1	92.0	90.0	25
Fe,%	4.15	6.84	4.70	0.635	13.5	3.92	4.72	-
Zn	82.8	207	100	31	30.5	67.0	95.0	110
As	5.69	33.4	12	6	51.7	4.80	13.0	-

Table 4.7: Basic statistics of the metal concentration (% or mg kg^{-1}) data of the C4 core.

Elements in C4	Minimum	Maximum	Mean	SD	RSD,%	UCC[b]	ASV[c]	USEPA, 1999
Al,%	6.39	7.69	7.20	0.415	5.8	8.15	8.00	-
Ca,%	0.968	2.16	1.45	0.323	22	2.57	2.21	-
V	74.0	100	87.9	9.01	10	97	130	-
Cr	49.3	95.1	71.5	12.4	17	92.0	90.0	25
Fe,%	2.84	4.73	3.76	0.592	16	3.92	4.72	-
Ni[a]	22.2	31.6	28.1	3.46	12	47.0	68.0	16.0
Cu[a]	18.4	26.2	23.2	2.74	12	28.0	45.0	-
Zn	42.6	63.0	56.0	6.92	12	67.0	95.0	110
As	6.99	9.45	8.08	0.848	10	4.80	13.0	-
Hg[a]	0.010	0.025	0.014	0.0041	29	0.050	0.40	-
Pb[a]	15.9	23.5	19.9	2.42	12	17	20	40

[a]Measured by AAS; all other metal concentrations are measured by INAA. [b]UCC: Upper continental crust [106]; [c]Average shale values [107], SD = standard deviation; RSD = relative standard deviation.

The vertical distributions of the metal concentrations in both cores are shown in Fig. 4.3. The concentrations of Al, Zn, As and Hg did not show pronounced variations in the sediment cores, except for the concentration of Zn at 10 cm and Hg at 12 cm depth of the

C1. In this study, the overall elevated concentrations of Al, Ca, V, Cr, and Fe in C1 from the bottom to top sediment layers (Fig. 4.3) could be attributed to the increase in natural weathering of soil materials and the increase in anthropogenic activities in recent years [104, 110, 111].

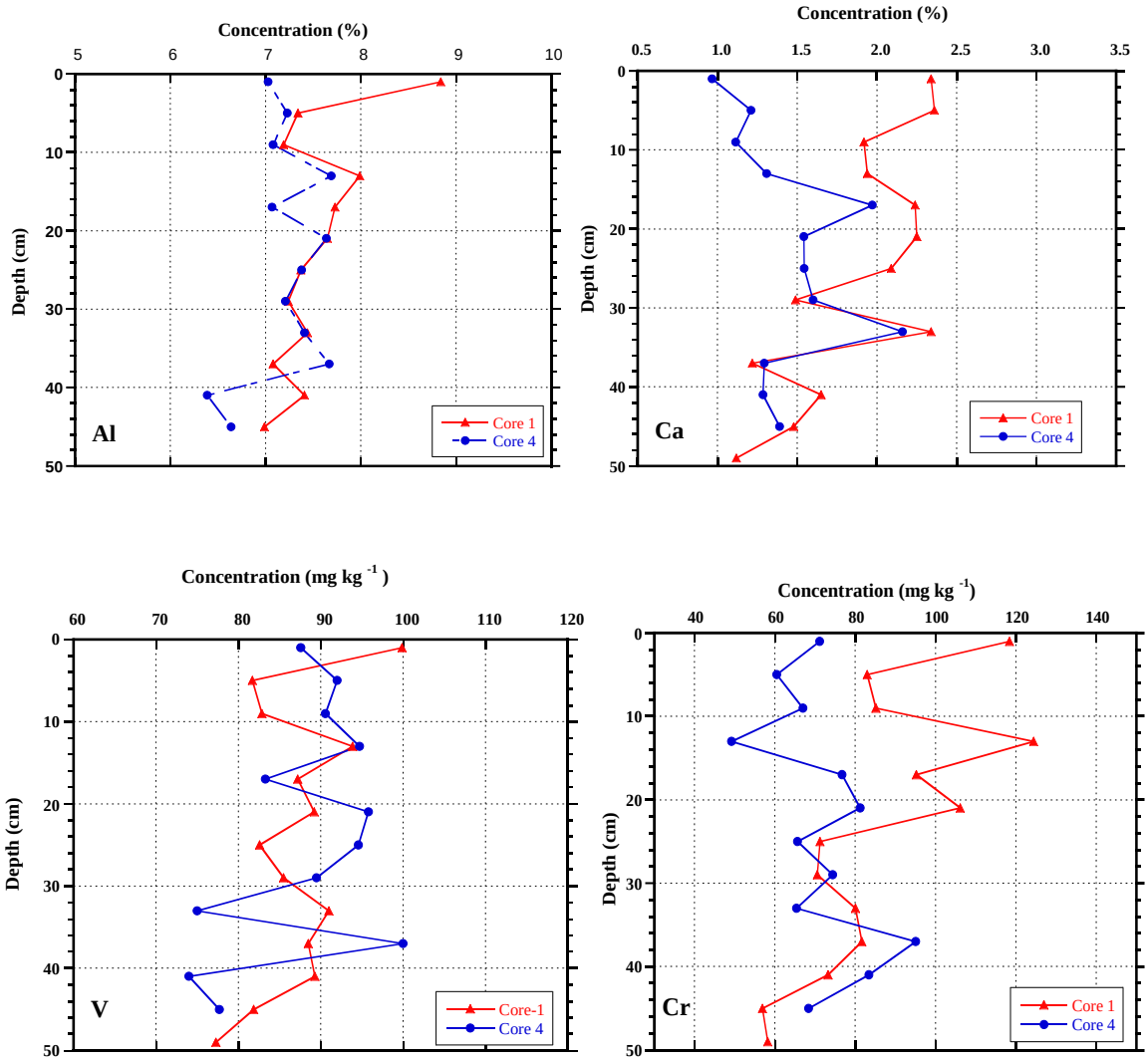

Fig. 4.3: Vertical metal concentration variations in two cores.

The increase in the concentration of Ca in core-1 (C1) indicates a high biological production rate in this area. For most of the metals at C1, there is an increase in concentration trend from 10 cm depth (1980) to the surface of the core. This is due to the increase in Mongla port activities, and industrial and human activities since 1980 in this area of the Sundarban [112].

In comparison, the concentrations of Cr, Ni, and Fe in the surface sediments of this study are higher than those of the mangrove sediments of India, Senegal, Brisbane, Brazil, and Hong Kong [113-117].

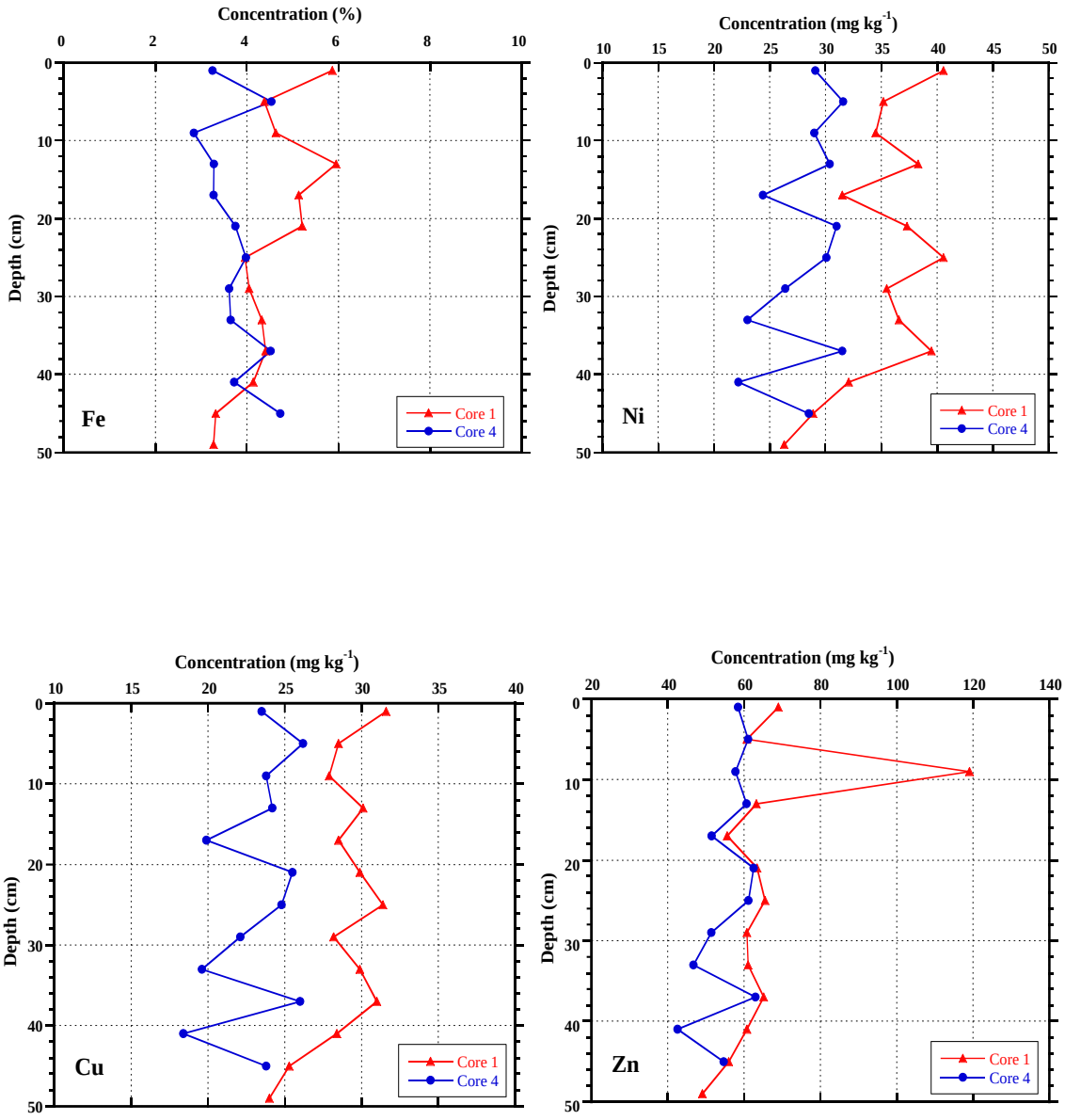

Fig. 4.3: Continued.

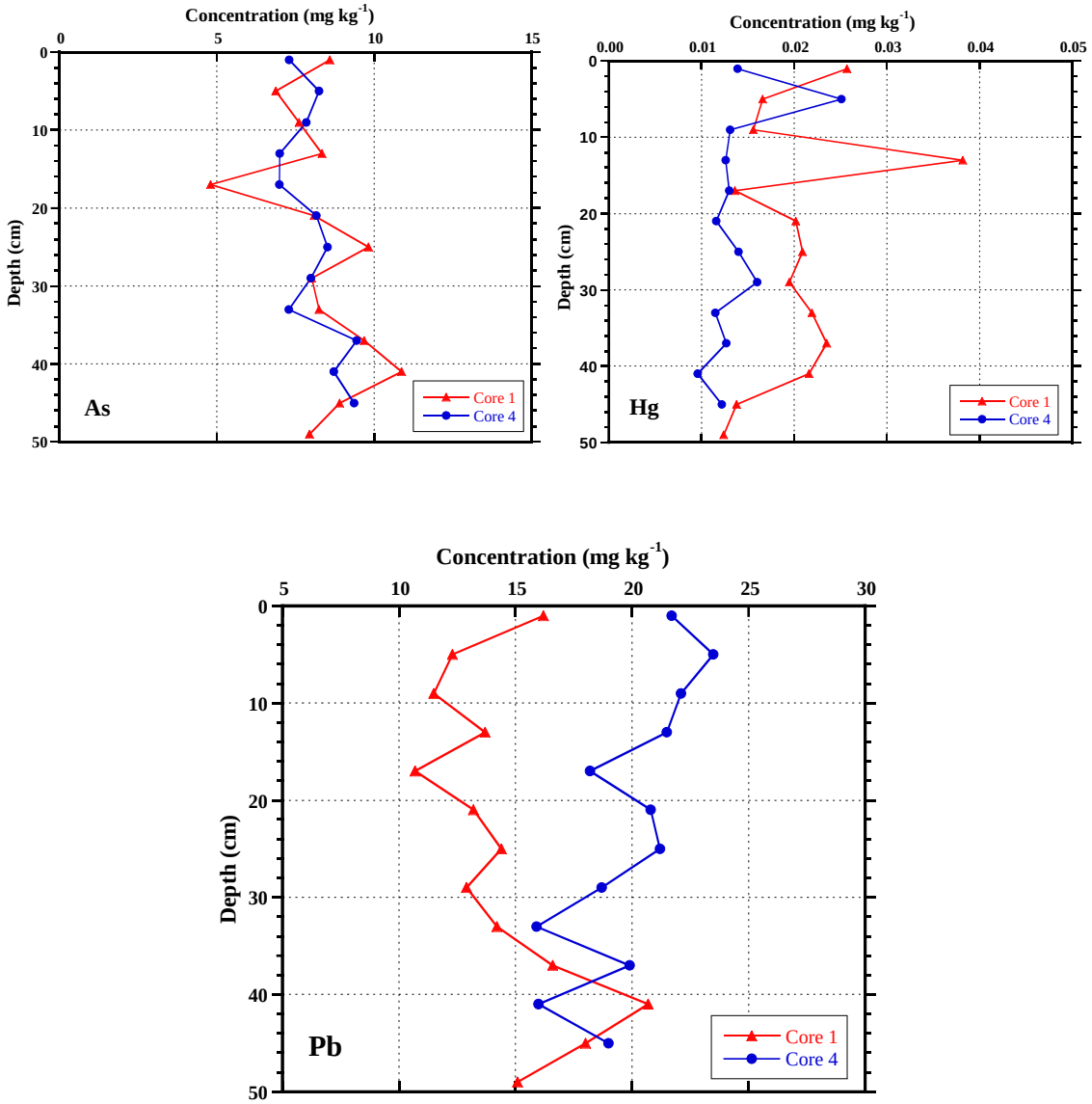

Fig. 4.3: Continued.

However, Cu and Hg concentrations in the Indian Sundarban [113], and Zn and Pb concentrations in Brisbane mangrove sediments [114] are higher than those of the results of this study. Some studies on trace metals in sediments (core and surface) of the Sundarban mangrove forest have been carried out by different authors [113, 114, 118-122]. For comparison, their data are given in Table 4.8.

Table 4.8**:** Comparison of metal concentrations (% or mg kg^{-1}) in sediments from Bangladeshi and Indian parts of the Sundarban mangrove forest.

Location	Sediment	V	Cr	Fe, %	Ni	Cu	Zn	As	Hg	Pb
This Study (Bangladesh)	Core-1	77.3 - 99.9 (87.0) [99.9]	56.9 - 124 (85.0) [118]	3.27- 5.95 (4.51) [5.87]	26.3-40.6 (35.2) [40.6]	24.0 - 31.6 (28.8) [31.6]	49.1- 11.9 (65.4) [69.0]	4.80 - 10.9 (8.30) [8.60]	0.01 - 0.04 (0.02) [0.0257]	10.7 - 20.7 (14.6) [16.2]
	Core-4	74.0 - 100 (87.9) [87.6]	49.3- 95.1 (71.5) [71.2]	2.84- 4.73 (3.76) [3.25]	22.2- 31.6 (28.1) [29.1]	18.4- 26.2 (23.2) [23.5]	42.6 – 63.0 (56.0) [58.4]	6.99 - 9.45 (8.08) [7.30]	0.01 - 0.03 (0.01) [0.0139]	15.9 - 23.5 (19.9) [21.7]
India [104]	Core1	–	35.5- 56.7 (48.8)	5.14- 4.59 (4.10)	44.9 – 62 (56.1)	38 - 46.5 (42.9)	70.1- 91.4 (81.4)	–	–	26.8 - 36.3 (33.6)
	Core2	–	37.5- 48.0 (43.0)	3.2- 4.4 (3.85)	44.9- 55.4 (50.9)	33.2- 41.1 (38.0)	69.5- 99.6 (84.2)	–	–	22.9 - 32.1 (28.1)
	Core3	–	35.2- 48.4 (40.6)	2.24- 3.93 (3.31)	39.9- 52.7 (44.2)	31.1- 41.6 (34.3)	49.1- 75.8 (61.9)	–	–	23.7- 32.4 (28.6)
India [120]	Surface	–	77.9	3.33	39.3	22.46-45.49 (46.5)	81.0	–	–	32.64- 55.26 (46.2)
Bangladesh [120]	Surface	–	70.1	3.03	33.7	28.65-41.21 (34.35)	67.1	–	–	33.41- 48 (42.4)
Bangladesh [119]	Surface	86.9	67.0	3.81	28.6	22.3	67.7	6.76	0.0308	19.7
Bangladesh [118]	Surface	–	38.7	3.43	167	31.7	58.6	14.0	–	17.9
India [113]	Surface	–	28.3	0.29	34.5	38.31	34.4	3.82	0.07	15.8
India [121]	Surface	–	50.0	–	43.8	32.5	–	9.88	–	18.3
Bangladesh [122]	Surface	bld[a]-52 (32.9)	3-115 (15.7)	0.003-24.8 (17.4)	8-1127 (76.1)	2-44 (10.5)	bld-112 (73.6)	bld-10 (4.60)	bld- 0.0833 (0.0064)	bld-34 (19.3)

[a]bld means below the limit of detection

The concentration values within the first brackets are mean values, and the data within the third brackets are concentrations of the corresponding metals in the surface sediments of the core. It is observed that concentrations of V and Cr in surface sediments at our studied points are higher than in the previous studies (Table 4.8). The overall concentrations of the other studied metals are comparable to the previous data. Some exceptions are Fe (17.4%) and Ni (76.1 mg kg^{-1}) concentrations by Antizar-Ladislao et al. [121], which are higher than those of the other studies. Relatively high concentrations of Ni (167 mg kg^{-1})

were also reported by Kumar et al. [118]. From this study, the average concentration of Cu in surface sediments (27.5 mg kg^{-1}) of the cores is higher than the average concentration of Cu (10.5 mg kg^{-1}) reported by Antizar-Ladislao et al. [121] but slightly lower than the data (34.3 mg kg^{-1}) reported by Ranjan et al.[120]. From Table 4.8, it is also observed that the average Pb concentration (18.9 mg kg^{-1}) in surface sediments of this study is comparable to all reported data; however, it is lower than the data (42.4 mg kg^{-1}) reported by Ranjan et al. [120]. It should be mentioned that though a wide range of increase in sediment MAR was observed over time, metal concentrations in different layers of the cores did not vary over a wide range (5.8-33%). Metal concentrations of sediments mainly depend on geomorphology, anthropogenic activities, and climatic conditions, but for the MAR of an area, it also needs to consider sediment mixing, erosion, land use patterns, etc.

4.1.4 Metal Contamination and Ecological Risk Assessment

EF and I_{geo} are two widely used approaches to characterize the degree of anthropogenic metal pollution in sediments. The EF and I_{geo} profiles of the studied metals over time are shown in Fig. 4.4. In this study, EF values of As at C1 are more than 1.5 whereas Fe and Zn values around the year 2000 are above 1.5. The EF values for the rest of the metals at C1 are below 1.5 which indicates no contamination by these metals over dated time. It is observed that I_{geo} values for all studied metals at C1 are from 0 to 1 (except Hg), which indicates uncontaminated to moderate contamination of the sediments by these metals (Fig. 4.4). The enrichment of As over the last century in the Ganges floodplains is supposed to be of geological origin [123, 124]. On the other hand, the values of EF and I_{geo} for core 2 also indicate minor contamination by As. However, the contamination level for As at C1 is higher than that at C4 over time (Fig. 4.4). In this study, some metals, including Ca, Ni, and Hg, have enrichment factors that are less than one. The biological uptake of these metals may be the cause of their decrease in comparison to crustal abundances [125, 126]. In this study, potential ecological risk assessments for the metals Cr, Ni, Cu, Zn, As, Hg, and Pb are performed and given in Table 4.9.

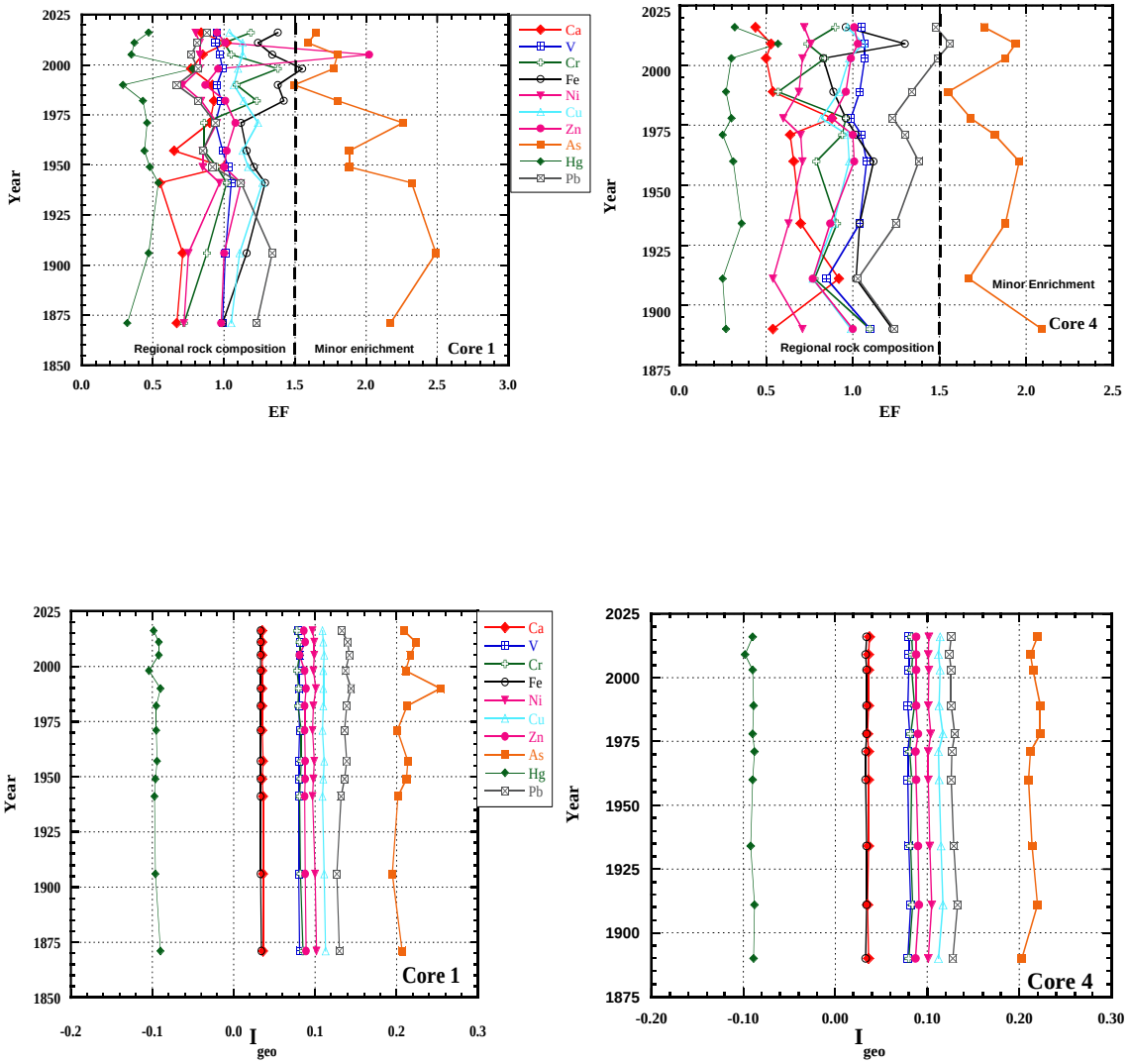

Fig. 4.4: Profiles of EF and I_{geo} values of the elements over time at sediment cores.

It is observed that the potential ecological risk factors (E_r) for the studied metals at both cores of the Sundarban pose a low risk (E_r < 40) over the dated time. The combined potential ecological risk index (PERI) values for the studied metals at both cores are also low (PERI <100). Moreover, to evaluate the quality of the sediments of the Sundarban mangrove forest, metal concentrations in the sediments were compared with TEL (Threshold Effect Level) and PEL (Probable Effect Level) [127], and ERL (Effect Range Low) and ERM (Effect Range Medium) [128] guiding values for marine sediments (Table 4.9). The percentage of samples under different SQG values is shown in Fig. 4.5.

Table 4.9: Ecological risk factors for the potentially toxic metal(loid)s in sediment cores.

Depth (cm) for C1	E_r							PERI
	Cr	Ni	Cu	Zn	As	Hg	Pb	
1	2.57	4.32	5.63	1.03	17.92	20.57	4.75	56.8
5	1.80	3.74	5.10	0.91	14.34	13.25	3.63	42.8
9	1.85	3.67	4.97	1.78	15.87	12.46	3.39	44.0
13	2.70	4.07	5.37	0.95	17.39	30.56	4.02	65.1
17	2.07	3.35	5.08	0.83	14.17	10.85	3.16	39.5
21	2.31	3.97	5.35	0.95	16.88	16.14	3.87	49.5
25	1.55	4.32	5.60	0.98	20.45	16.74	4.23	53.9
29	1.54	3.78	5.04	0.91	16.71	15.59	3.79	47.3
33	1.74	3.90	5.34	0.91	17.19	17.55	4.18	50.8
37	1.78	4.21	5.53	0.97	20.19	18.82	4.87	56.4
41	1.59	3.42	5.07	0.91	22.66	17.25	6.09	57.0
45	1.24	3.08	4.52	0.84	18.56	11.02	5.29	44.5
49	1.27	2.80	4.29	0.73	16.56	9.95	4.43	40.0

[a]Concentration in mg kg^{-1}: [b]TEL= Threshold Effect Level; PEL= Probable Effect Level [127]: [c]ERL= Effect Range Low; ERM= Effect Range Medium [128]

According to TEL-PEL SQG, any site is considered contaminated if 10% of the samples exceed the TEL value. It is observed that for C1, concentrations of Cr, Cu, and Ni at all layers exceeded the TEL values, whereas concentrations of As at 85% of the layers exceeded the TEL value, indicating occasional adverse biological effects on the biota of the mangrove system. According to ERL-ERM SQG, concentrations of Cr, Ni, and As fall in the range of ERL-ERM values, for the 54%, 100%, and 54% samples, respectively. However, concentrations for these metals did not exceed the PEL/ERM values.

Table 4.9: Continued.

Depth (cm) for C4	E_r							PERI
	Cr	Ni	Cu	Zn	As	Hg	Pb	
1	1.55	3.10	4.20	0.87	15.21	11.08	6.37	42.4
5	1.31	3.36	4.69	0.91	17.19	20.05	6.91	54.4
9	1.46	3.09	4.25	0.86	16.36	10.47	6.49	43.0
13	1.07	3.24	4.32	0.91	14.59	10.12	6.32	40.6
17	1.67	2.59	3.55	0.77	14.55	10.40	5.35	38.9
21	1.77	3.29	4.55	0.93	17.03	9.25	6.11	42.9
25	1.43	3.20	4.43	0.91	17.75	11.16	6.25	45.1
29	1.62	2.81	3.94	0.77	16.64	12.82	5.51	44.1
33	1.42	2.44	3.50	0.70	15.19	9.18	4.67	37.1
37	2.07	3.36	4.64	0.94	19.69	10.20	5.84	46.7
41	1.81	2.37	3.28	0.64	18.16	7.69	4.71	38.7
45	1.49	3.03	4.26	0.82	19.53	9.80	5.57	44.5
TEL[a,b]	52.3	15.9	18.7	124	7.24	0.130	30.2	
PEL[a, b]	160	42.8	108	271	41.6	0.700	112	
ERL[a, c]	81	20.9	34	150	8.2	0.15	46.7	
ERM[a, c]	370	51.6	270	410	70	0.71	218	

[a]Concentration in mg kg^{-1}: [b]TEL= Threshold Effect Level; PEL= Probable Effect Level [127]: [c]ERL= Effect Range Low; ERM= Effect Range Medium [128]

The concentrations of Zn, Hg, and Pb at all layers of C1 were below the TEL/ERL values indicating rare toxic effects of these metals on the biota of the Sundarban mangrove system. On the other hand, for C4, the concentrations of Cr, Cu, Ni, and As at most of the layers exceeded their corresponding TEL values but were below the PEL values.

According to ERL-ERM guideline values, concentrations of Cr, Ni, and As fall in the range of ERL-ERM values (but below the ERM value) for 25%, 100%, and 42% layers, respectively, indicating occasional biological effects on the biota of that core.

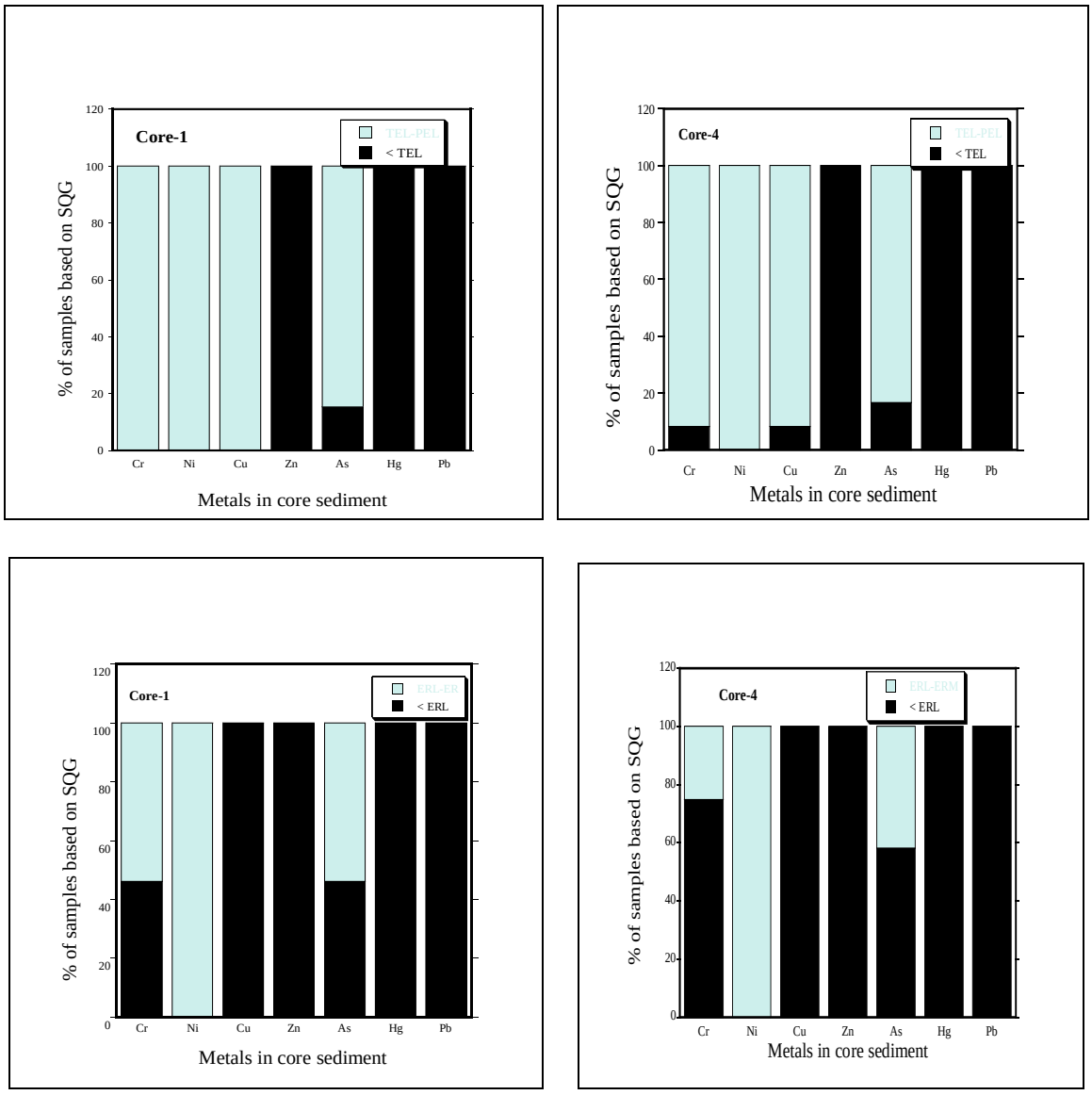

Fig. 4.5: Percentage of samples under different SQG values for sediment cores.

Similar to the concentrations in C1, concentrations of Zn, Hg, and Pb at all layers of C4 are below the PEL/ERL values. These results suggest that Zn, Hg, and Pb have rare toxic effects on the biota of the Sundarban because their concentration values obtained are below TEL/ERL (also $E_r < 40$) values.

However, sediments at some layers of the cores can be classified as presenting some extent of threat to the organisms due to the high concentrations of Cr, Cu, Ni, and As. For evaluating the combined toxicity level of different toxic metals retained in the sediments, the mean ERM quotient (ERM-Q) was also calculated for the studied metals. The mean ERM-Q value for C1 was 0.20, and for C2, it was 0.17. According to the mean ERM-Q criteria (Table 4.9; [129]; the quotient values indicate that the combination of the studied metals has a 21% probability of being toxic ($0.11 \leq$ M-ERM-Q < 0.5) at two sites of the Sundarban. Therefore, the results of the mean ERM-Q suggest that it is a proper time for routine monitoring of the toxic metal pollution of the Sundarban to protect aquatic life in this sensitive mangrove ecosystem.

4.1.5 Statistical Analysis for Source Apportionment and Transport Behavior of Metals

Correlation Analysis

To study the inter-metal relationships and their transport behavior in the mangrove sediments, the Pearson correlation matrix was calculated for the two sediment cores, and the result is tabulated in Table 4.10. With the exception of Zn, As, and Pb, it is shown that Al has strong positive correlations with most metals in C1, indicating that aluminosilicate minerals are the primary geochemical carriers of these metals [119]. Likewise, Fe shows strong positive correlations with the majority of the other metals (Table 4.10), showing that these metals' distributions were influenced by the same variables, such as clay minerals and Fe oxy-hydroxides. The negative or poor correlations of some metals with Al and/or Fe in mangrove sediments are due to their association with organic detritus [130, 131]. Zinc has negative or poor correlations with all metals at C1 whereas; at C4, it has strong positive correlations with V (0.89; $p < 0.01$), Ni (0.98; $p < 0.01$), Cu (0.95; $p < 0.01$), and Pb (0.86; $p < 0.01$). From Table 4.10, it is observed that As has a negative or poor correlation with most of the metals, which may indicate the different origins of this metal in Sundarban mangrove core sediments. However, a strong positive correlation of As with Pb (0.82; $p < 0.01$) in C1 indicates common sources of metals like pigments and antifouling paints, the movement of fishing boats, and commercial ships in this area [132].

Table 4.10: Pearson correlation coefficients for the metal(loid)s in sediment cores

Core 1	Al	Ca	V	Cr	Fe	Ni	Cu	Zn	As	Hg	Pb
Al	1.00										
Ca	0.68	1.00									
V	**0.88**	0.44	1.00								
Cr	**0.85**	0.58	**0.79**	1.00							
Fe	**0.87**	0.60	**0.81**	**0.99**	1.00						
Ni	0.62	0.46	0.62	0.59	0.60	1.00					
Cu	**0.69**	0.54	**0.70**	0.63	0.66	**0.96**	1.00				
Zn	0.08	0.16	0.01	0.18	0.22	0.24	0.15	1.00			
As	-0.08	-0.38	0.14	-0.23	-0.25	0.26	0.21	-0.02	1.00		
Hg	0.58	0.18	**0.73**	**0.69**	0.66	0.66	0.64	-0.01	0.35	1.00	
Pb	-0.07	-0.44	0.16	-0.30	-0.32	-0.13	-0.08	-0.30	**0.82**	0.13	1.00

Core 4	Al	Ca	V	Cr	Fe	Ni	Cu	Zn	As	Hg	Pb
Al	1.00										
Ca	0.19	1.00									
V	**0.75**	-0.36	1.00								
Cr	-0.12	0.03	0.04	1.00							
Fe	-0.04	-0.03	0.04	0.23	1.00						
Ni	0.55	-0.56	**0.86**	-0.14	0.30	1.00					
Cu	0.54	-0.51	**0.83**	-0.11	0.39	**0.99**	1.00				
Zn	0.65	-0.44	**0.89**	-0.12	0.20	**0.98**	**0.95**	1.00			
As	-0.23	-0.29	0.08	0.51	**0.78**	0.26	0.34	0.14	1.00		
Hg	0.13	-0.23	0.32	-0.34	0.32	0.43	0.47	0.36	-0.01	1.00	
Pb	0.38	-0.63	**0.75**	-0.37	0.00	**0.88**	**0.85**	**0.86**	-0.04	0.60	1.00

Marked correlations are significant at $p < 0.01$

The major metal Ca displays weak or negative correlations with the majority of the other metals in both sediment cores, indicating that these metals may originate from a variety of sources of pollution [133]. To identify metal abundance clustering in the sediment cores of the Sundarban, cluster analysis (CA) was employed [134] using linkage distance among the metals, and the results are displayed in Fig. 4.6. It is observed that the studied metals are distributed into two main clusters, with Zn, Cr, and V in one cluster, and the rest of the metals in another cluster. Considering Fe and Al as indicators of detritus materials, it is evident that the origin of Cu, Ni, Pb, Hg, Ca, and As in both sediment cores is mostly from lithogenous sources [135].

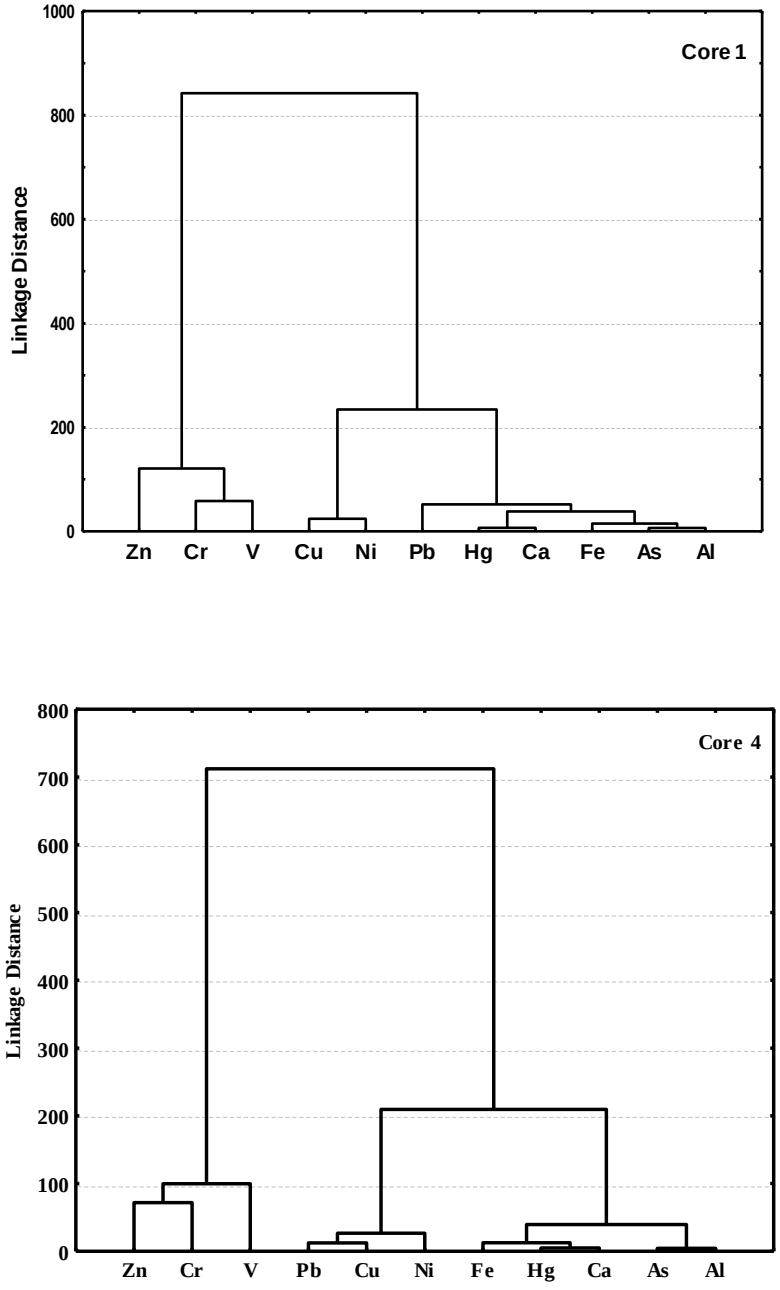

Fig. 4.6: Dendogram plot of the metals for both sediment cores.

Principal Component Analysis

In this study, datasets were analyzed by principal component analysis (PCA) to further examine metal associations and their possible sources. The varimax rotated factor loading matrix of 11 metal(loid)s (variables) for Sundarban core sediment samples is given in Table 4.11. This study revealed that the first three factors (PC1, PC2, and PC3) for C1 explained a cumulative variance of 84% of the total variance (Table 4.11).

Table 4.11**:** Varimax rotated factor loading matrix of 11 metal(loid)s (variables) for Sundarban core sediment samples.

Elements	Core 1				Core 4		
	PC1	PC2	PC3		PC1	PC2	PC3
Al	**0.924**	-0.163	-0.043		**0.898**	-0.227	-0.214
Ca	0.587	-0.531	0.155		-0.126	-0.229	**-0.727**
V	**0.931**	0.117	-0.099		**0.933**	0.051	0.207
Cr	**0.897**	-0.304	0.040		0.020	0.661	-0.503
Fe	**0.900**	-0.328	0.075		0.060	**0.807**	0.183
Ni	**0.763**	0.155	0.491		**0.812**	0.203	0.529
Cu	**0.824**	0.121	0.371		**0.792**	0.278	0.521
Zn	0.020	-0.148	**0.867**		**0.889**	0.102	0.403
As	0.068	**0.969**	0.141		0.004	**0.965**	0.104
Hg	**0.804**	0.318	0.034		0.179	-0.031	0.699
Pb	-0.027	**0.875**	-0.321		0.626	-0.120	**0.747**
Eigen value	5.80	2.36	1.12		5.54	2.21	1.40
% variance explained	52.7	21.4	10.2		50.3	20.1	12.7
% cumulative variance	52.7	74.1	84.4		50.3	70.5	83.1

Bold values represent higher factor loadings.

For core 1, the largest loadings in PC1 are for Al, V, Cr, Fe, Ni, Cu, and Hg, which account for 52.7% of the variance. Geological factors govern the majority of these metals

[136-138]. Therefore, the contribution of geological origin is intended to be reflected in PC1. The low EF values and cluster analysis results discussed in the earlier section also confirmed these findings. The component PC2 shows high loadings of As (0.97) and Pb (0.87), and it explains 21% of the variance. The metals As and Pb are toxic metal(loid)s and are supposed to originate from anthropogenic sources; therefore, PC2 represents the contribution from anthropogenic origin. The possible sources of As are due to the burning of fossil fuels, the use of agrochemicals, oil from boats and ships, and anti-fouling paints [139, 140]. However, As contamination in the southwestern region of Bangladesh is of geological origin, so there may be the contribution of geological origin of As in the Mangrove sediments. The sources of Pb can be the combustion of coal and oil in different industrial and naval activities in this area [141, 142]. The PC3 shows high positive loadings of Zn. According to EF values, sediments at C1 are slightly enriched by Zn around the year 2000. The enrichment of Zn may be derived from both geogenic and anthropogenic origins. Therefore, PC3 for C1 represents a contribution from mixed sources (geogenic and anthropogenic). The PCA results for C4 show that the first 3 components explain a cumulative variance of 83% of the total variance (Table 4.11). For C4, PC2 shows high loadings of Fe and As whereas PC3 shows high loadings of Ca and Pb.

4.2. ELEMENTAL CONTAMINATION AND HEALTH RISK ASSESSMENT OF THE MEDICINAL PLANTS

In this study, neutron activation analysis, atomic absorption spectrometry, and gamma spectrometry systems were applied to assess the elemental concentration, natural radioactivity, and health risk due to consumption of medicinal plants of the Sundarban.

4.2.1 Accuracy Level of the Analysis

In this study, the quality of the analysis was performed by determining the elemental contents of SRM-1547 (peach leaves). The reported uncertainties associated with the concentration values are due to counting statistics only. Since counting statistics mainly control the total uncertainty in NAA, it was reported with concentration values.

However, in addition to this reported uncertainty, there was commonly 3% uncertainty (estimated in our analysis) also associated with the reported values, which included sample and standard preparation, irradiation, positioning in the detector, pulse-pileup losses, and peak integration. The deviations of the determined concentration values in this study from certified/Information values of the reference materials are shown in Table 4.12.

Table 4.12: Comparison of measured values with certified values (mg kg^{-1}) in the standard reference materials of SRM-1547 (peach leaves).

Elements	Certified value[b]	This work value (n =3)	U-score	Z-score	Deviation (%)
Al	248.9 ± 6.5	248 ± 9	0.04	0.06	0.2
As	0.062 ± 0.014	0.0706 ± 0.0140	0.38	0.62	-13
Br	(11)	10.9 ± 1	0.01	0.02	0.1
Ca	15590 ± 160	14200 ± 1230	1.08	1.09	8.6
Cd[a]	0.0261 ± 0.0022	0.0235 ± 0.0103	0.25	0.25	10
Ce	(10)	9.26 ± 0.72	0.99	1.03	7.4
Co	(0.07)	0.0582 ± 0.0083	0.38	1.41	16
Cr	(1)	1.12 ± 0.11	0.82	1.11	-12
Fe	219.8 ± 6.8	204 ± 27	0.62	0.75	6.9
K	24330 ± 380	26100 ± 2100	0.87	0.88	-7.4
La	(9.0)	9.57 ± 0.75	0.69	0.76	-6.4
Mn	97.8 ± 1.8	93.9 ± 3.3	0.86	1.15	3.9
Na	(23.8 ± 1.6)	26.9 ± 2.3	1.01	1.33	-12
Pb[a]	0.869 ± 0.018	0.818 ± 0.052	0.77	0.98	5.9
Sb	(0.02)	0.0226 ± 0.0034	0.03	0.76	-12
Sc	(0.04)	0.0437 ± 0.036	0.01	1.02	-9.1
Sm	(1)	0.928 ± 0.072	0.96	1.00	7.2
Th	(0.05)	0.0560 ± 0.0059	0.96	1.01	-12
V	0.367 ± 0.038	0.351 ± 0.046	0.29	0.35	-4.4
Zn	17.97 ± 0.53	19.6 ± 1.7	0.98	1.01	-9.2

[a]Determined by AAS technique; [b]Non certified value (information value)

The studied elements obtained in this study are in good agreement with their certified/information values, which ensures the accuracy of the analysis. Elemental concentrations (mg kg^{-1}) of the studied medicinal plants *A. ilicifolius*, *A. officinalis*, and *X. mekongensis*, and rhizosphere soil samples were determined using INAA and AAS techniques.

Twenty chemical elements (Al, As, Br, Ca, Cd, Ce, Co, Cr, Fe, K, La, Mn, Na, Pb, Sb, Sc, Sm, Th, V, and Zn) were identified in the studied medicinal plants and rhizospheric soil samples tabulated in Table 4.13 and Table 4.14. These elements could be divided into three categories: essential elements (Ca, Co, Fe, K, Mn, Na, and Zn); potentially toxic elements (As, Br, Cd, Cr, and Pb); other elements (Al, Ce, La, Sb, Sc, Sm, Th, and V). The human body desires several elements that are taken into consideration as important for its growth; these elements are necessary components and play an important physiological function in which Ca is a vital mineral for human health, contributing to the formation of bones and teeth. The concentrations of Ca in *A. ilicifolius, A. officinalis,* and *X. mekongensis* were obtained 3220, 3520, and 6580 mg kg^{-1} respectively. The K is the most common place for intracellular ion in human and animal cells and is also abundant in dietary counts [143, 144]. It is noteworthy that, the contents of K in *A. ilicifolius, A. officinalis,* and *X. mekongensis* were found to be 20600, 15300, and 25300 mg kg^{-1}which indicate that they are the potential sources for K. Among the studied medicinal plants, the highest concentrations of Ca and K were found in the *X. mekongensis* plant. Iron is a vital element, which is an important component of hemoglobin that transports oxygen [145]. In the present study, Fe concentrations varied from 157 to 1160 mg kg^{-1}; the maximum concentration of iron was found in *A. ilicifolius,* (1160 mg kg^{-1}) as shown in Table 4.13. Therefore, *A. ilicifolius* could be a possible natural source/supplement for this micronutrient. Zinc is another vital trace element needed for proper growth, thyroid function, blood clotting, and protein and DNA synthesis. But excessive Zn can be harmful and cause toxicity to human health [146]. Excessive amounts of Zn may also lead to abdominal pain, diarrhea, vomiting, and nausea [147], while Zn deficiency leads to hypogonadism and growth retardation [148]. The Zn concentrations for this study were found to be 41.2 mg kg^{-1}, 18.7 mg kg^{-1}, and 11.2 mg kg^{-1} for *A. ilicifolius, A. officinalis,* and *X. mekongensis* respectively (Table 4.13). The Zn concentration in *A. ilicifolius* is greater than the WHO maximum permissible limit (27 mg kg^{-1}) [149]. Concentrations of Zn were obtained to be 111 mg kg^{-1}, and 97.4 mg kg^{-1} for *A. ilicifolius* and *A. officinalis* medicinal plants in the Indian part of Sundarban, which were higher than the presently studied values. Besides this, Co is an important micronutrient needed for the metabolic processes of humans, animals, and plants.

It is available with vitamin B12, which is required in producing red blood cells and in the prevention of anemia [147]. In this study, Co concentrations were found to be 0.431 mg kg^{-1}, 0.664 mg kg^{-1}, and 0.532 mg kg^{-1} for *A. ilicifolius, A. officinalis,* and *X. mekongensis* plants, respectively.

Table 4.13: Mean values (n = 3) of elemental concentrations (mg kg^{-1}) determined in three medicinal plants by the INAA and AAS.

Elements	*A. ilicifolius*	*A. officinalis*	*X. mekongensis*	WHO /FAO values [144]
Essential elements				
Ca	3220 ± 154	3520 ± 430	6580 ± 1180	
Co	0.431 ± 0.015	0.664 ± 0.099	0.532 ± 0.087	0.48
Fe	1160 ± 122	157 ± 34	837 ± 403	
K	20600 ± 1710	15300 ± 5190	25300 ± 2990	
Mn	104 ± 22	54.5 ± 17.8	37.4 ± 10.3	
Na	16700 ± 1800	13600 ± 790	12900 ± 2500	
Zn	41.2 ± 10.1	18.7 ± 0.3	11.2 ± 1.6	27
Potential toxic elements				
As	0.0182 ± 0.0047	0.0433 ± 0.0164	0.0144 ± 0.0071	5.0
Br	132 ± 4	122 ± 11	146 ± 22	
Cd[a]	0.026 ± 0.002	0.021 ± 0.002	0.020 ± 0.002	0.3
Cr	3.35 ± 0.37	0.829 ± 0.271	4.02 ± 2.30	2
Pb[a]	0.939 ± 0.079	1.01 ± 0.09	1.12 ± 0.10	10
Other elements				
Al	1790 ± 173	207 ± 62	1820 ± 1020	
Ce	1.99 ± 0.15	< 0.187	1.88 ± 1.11	
La	1.49 ± 0.23	0.325 ± 0.060	1.47 ± 0.72	
Sb	0.0458 ± 0.0151	0.0313 ± 0.0048	0.0180 ± 0.0134	
Sc	0.376 ± 0.051	0.0388 ± 0.0081	0.273 ± 0.138	
Sm	0.167 ± 0.038	< 0.024	0.147 ± 0.053	
Th	0.603 ± 0.047	0.0406 ± 0.0027	0.633 ± 0.379	
V	2.75 ± 0.32	< 0.648	3.10 ± 2.05	

[a]Determined by AAS technique. Uncertainties are due to standard deviation (n = 3, 1σ).

Therefore, the concentrations of Co except in *A. ilicifolius* in all medicinal plants were slightly higher than the WHO permissible limit of 0.48 mg kg^{-1} [149]. Although Co is a vital element, it can be harmful if consumed in larger amount. Excess consumption of Co can cause blood pressure, cardiomyopathy, diarrhea, pulmonary disorders, vomiting,

slowed respiration, and so on, whereas, its deficiency consequences in anemia, loss of weight, and retarded growth [147]. Besides this, Al is an element that has a negative impact on plants [150]. Besides this, Al is an element that has a negative impact on plants. The Al concentrations were obtained in the present study by 1790 mg kg^{-1}, 207 mg kg^{-1}, and 1820 mg kg^{-1} in *A. ilicifolius*, *A. officinalis*, and *X. mekongensis* plants, respectively. Manganese is an important element as well as a significant activator of the enzyme. The concentrations of Mn were found to be 104 mg kg^{-1}, 54.5 mg kg^{-1}, and 37.4 mg kg^{-1} for *A. ilicifolius, A. officinalis,* and *X. mekongensis* plants, respectively, whereas the concentrations of the same element in *A. ilicifolius,* and *A. officinalis,* plants were found to be 178 mg kg^{-1}, and 163 mg kg^{-1} in the Indian part of Sundarban [151] which are much greater than the same plants in the Bangladeshi part of Sundarban. The elements As, Cd, and Pb are considered toxic elements, and Br, Sb, and Cr are occasionally considered toxic elements. Arsenic is carcinogenic and can lead to cancer of the liver, bladder, lungs, and skin; besides this, inorganic arsenic intake at lower concentrations can cause abnormal heart rhythm and reduced red and white blood cell production [152]. The As concentrations in the present study were obtained for *A. ilicifolius, A. officinalis,* and *X. mekongensis* plants as 0.018 mg kg^{-1}, 0.043 mg kg^{-1}, and 0.014 mg kg^{-1}, respectively, which are below the WHO / FAO permissible limit of 5 mg kg^{-1} [149]. Besides this, the Cd concentrations were found to be 0.026 mg kg^{-1}, 0.021 mg kg^{-1}, and 0.020 mg kg^{-1} for *A. ilicifolius, A. officinalis,* and *X. mekongensis* plants, whereas the WHO / FAO permissible limit is 0.3 mg kg^{-1} [149], and the concentration of the same element for *A. ilicifolius,* and *A. officinalis* in the Indian part of Sundarban [151] was determined to be 1.6 mg $kg^{-1}$and 1.9 mg kg^{-1} which are greater than the Bangladeshi part of Sundarban. Among the toxic elements, Pb is very harmful to humans, plants, and microorganisms [153]. Exposures to Pb can cause serious disturbances, resulting in permanent complications with brain problems [147]. In the present study, the Pb concentrations in *A. ilicifolius, A. officinalis,* and *X. mekongensis* plants were obtained to be 0.94 mg kg^{-1}, 1.01 mg kg^{-1}, and 1.1 mg kg^{-1} respectively, where the WHO / FAO permissible limit for medicinal plants is 10 mg kg^{-1} [149], but in the Indian part of Sundarban, the concentration of this element for *A. ilicifolius,* and *A. officinalis,* was estimated at 27.3 mg kg^{-1} and 36.6 mg kg^{-1}, which are higher than the Bangladeshi part of Sundarban as well as WHO / FAO permissible limit.

Table 4.14: Elemental concentrations (mg kg^{-1}) in the rhizosphere soil samples.

Elements	*A. ilicifolius*	*A. officinalis*	*X. mekongensis*
Al	87300 ± 9100	96200 ± 3700	88700 ± 3600
As	9.58 ± 0.05	10.2 ± 0.1	8.87 ± 0.82
Br	18.1 ± 4.8	16.9 ± 1.2	21.1 ± 7.2
Ca	10600 ± 3700	15500 ± 1200	12100 ± 2000
Ce	77.9 ± 2.9	94.3 ± 3.3	90.2 ± 2.3
Cd[a]	0.43 ± 0.03	0.45 ± 0.02	0.36 ± 0.01
Co	15.7 ± 0.7	18.9 ± 0.2	18.2 ± 0.1
Cr	82.7 ± 4.8	99.3 ± 2.4	96.0 ± 0.9
Fe	38900 ± 1800	47500 ± 1000	44300 ± 1900
K	33000 ± 3500	36000 ± 1600	37300 ± 1400
La	42.0 ± 3.7	42.7 ± 1.7	40.1 ± 3.0
Mn	740± 51	927 ± 16	943 ± 12
Na	9100 ± 690	8900 ± 1600	8400 ± 890
Pb[a]	15.8 ± 0.5	19.9 ± 0.3	14.6 ± 0.4
Sb	0.794 ± 0.043	1.42 ± 0.72	0.856 ± 0.068
Sc	14.2 ± 0.8	16.9 ± 0.2	16.1 ± 0.4
Sm	6.75 ± 0.92	6.40 ± 0.18	6.52 ± 0.18
Th	17.6 ± 0.8	20.8 ± 0.8	20.1 ± 0.6
V	108 ± 8	122 ± 7	116 ± 2
Zn	90.2 ± 11.2	100 ± 1	89.1 ±12.7

[a]Determined by AAS technique. Uncertainties are due to standard deviation (n=3, 1σ).

Likewise, the Cr concentrations in *A. ilicifolius, A. officinalis,* and *X. mekongensis* were 3.3 mg kg-1, 0.8 mg kg^{-1}, and 4 mg kg^{-1} respectively. According to the WHO / FAO, the maximum permissible limit of Cr is 2 mg kg^{-1} [149]; the concentration levels of Cr obtained from this study for *A. ilicifolius,* and *X. mekongensis* were found to be higher than the tolerable limit of the WHO/FAO limit. Therefore, it can be said that the metal concentrations of studied plants were higher in the Indian part of Sundarban compared to the Bangladeshi part of Sundarban. On the other hand, the elemental concentrations in the rhizosphere soil samples are given in Table 4.14, where most of the elemental concentrations were higher than the determined values in the previous study for surface sediments in Sundarban [119].

The average concentrations of As, Cr, and Pb were obtained in the present study as 8.47 mg kg^{-1}, 92.6 mg kg^{-1}, and 16.8 mg kg^{-1} whereas the concentrations of the same elements were found in the previous study [119] as 6.76 mg kg^{-1}, 67 mg kg^{-1}, and 15.8 mg kg^{-1} respectively. Therefore, concentrations of these toxic elements in Sundarban soils have increased, which may affect their concentrations in medicinal plants in this mangrove ecosystem.

Table 4.15: Comparison of the average daily intake (ADI, mg day^{-1}) of the elements in medicinal plants with the corresponding maximum tolerable daily intake (MTDI) in the Bangladeshi population.

Elements	*A. ilicifolius*	*A. officinalis*	*X. mekongensis*	MTDI value
As	2.7×10^{-6}	6.5×10^{-6}	2.2×10^{-6}	0.126
Cd	3.9×10^{-6}	3.2×10^{-6}	3.0×10^{-6}	0.021
Cr	5.0×10^{-4}	1.2×10^{-4}	6.0×10^{-4}	0.2
Mn	1.6×10^{-2}	8.2×10^{-3}	5.6×10^{-3}	2-5
Pb	1.4×10^{-4}	1.5×10^{-4}	1.7×10^{-4}	0.21
Zn	6.1×10^{-3}	2.8×10^{-3}	1.7×10^{-3}	60

MTDI means a maximum tolerable daily intake.

4.2.2. Health Risk Assessments

4.2.2.1 Average Daily Intake

The estimated ADI values for *A. ilicifolius, A. officinalis,* and *X. mekongensis* were tabulated in Table 4.15. The ADI value of As in these medicinal plants was found in the range of 2.2×10^{-6} to 6.5×10^{-6} mg day^{-1}, whereas the maximum tolerable daily intake (MTDI) is 0.126 mg day^{-1} [154]. Similarly, ADI values for Cd, Cr, Mn, Pb, and Zn in *A. ilicifolius, A. officinalis,* and *X. mekongensis*, plants were obtained in the range of 3.0×10^{-6} to 3.9×10^{-6} mg day^{-1}, 1.2×10^{-4} to 6.0×10^{-4} mg day^{-1}, 5.6×10^{-3} to 1.6×10^{-2} mg day^{-1}, 1.4×10^{-4} to 1.7×10^{-4} mg day^{-1}, and 1.7×10^{-3} to 6.1×10^{-3} mg day^{-1}, respectively while maximum daily allowance for above elements is 0.021, 0.2, 2- 5, 0.21 and 60 mg day^{-1} [155, 156]. Therefore, the ADI values of the elements for all studied medicinal plants were found less than the MTDI values.

4.2.2.2 Target Hazard Quotient

The target hazard quotient values for the As, Cd, Cr, Mn, and Zn are given in Table 4.16. It is observed that THQ values for the elements are below 1.0. The total target hazard quo-tient values for the considered elements in *A. ilicifolius, A. officinalis,* and *X. mekongensis* samples were found to be 3.5×10^{-1}, 1.6×10^{-1}, and 2.8×10^{-1}, respectively (Table 4. 16). In the present study, the total THQ value for every medicinal plant was found below 1.0, which indicates that no non-carcinogenic risk is associated to consume these medicinal plants [156, 157].

4.2.2.3 Target Carcinogenic Risk

The TCR values for As and Cr in *A. ilicifolius, A. officinalis,* and *X. mekongensis* samples were calculated and also given in Table 4.16. According to the latest regional screening level (RSL) Tables of the US-Environmental Protection Agency (EPA) [158], among the considered elements only these two elements have available CSF values. It should be mentioned that calculations of THQ and TCR values for As and Cr were done based on RfD and CSF values of inorganic As and Cr (VI) contents because of the unavailability of these values for total As and Cr contents in the latest RSL tables of EPA. So, THQ and TCR values calculated in this study may be overestimated. The range of TCR values for As and Cr of *A. ilicifolius, A. officinalis,* and *X. mekongensis* were 3.2×10^{-6} to 9.7×10^{-6} and 6.2×10^{-5} to 3.0×10^{-4}, respectively. If the TCR value is above 1×10^{-6}, it indicates the carcinogenic risk associated with the consumption of these medicinal plants [156, 159]. It is observed that the estimated TCR values of As and Cr for the studied medicinal plants were found above 1.0×10^{-6}. This indicates some extent of carcinogenic risk to consume these medicinal plants by people. However, the carcinogenic risk also depends on different factors like exposure frequency, duration, and amounts of consumption of medicinal plants.

Table 4.16: Target hazard quotient (THQ) and target carcinogenic risk (TCR) values of the elements for consuming medicinal plants.

Target hazard quotient (THQ)				Target carcinogenic risk (TCR)		
Elements	*A. ilicifolius*	*A. officinalis*	*X. mekongensis*	*A. ilicifolius*	*A. officinalis*	*X. mekongensis*
As	9.1×10^{-3}	2.2×10^{-2}	7.2×10^{-3}	4.1×10^{-6}	9.7×10^{-6}	3.2×10^{-6}
Cd	3.9×10^{-2}	3.2×10^{-2}	3.0×10^{-2}	-	-	-
Cr	1.7×10^{-1}	4.1×10^{-2}	2.0×10^{-1}	2.5×10^{-4}	6.2×10^{-5}	3.0×10^{-4}
Mn	1.1×10^{-1}	5.8×10^{-2}	4.0×10^{-2}			
Zn	2.1×10^{-2}	9.4×10^{-3}	5.6×10^{-3}			
Total	3.5×10^{-1}	1.6×10^{-1}	2.8×10^{-1}			

4.2.2.4 Transfer Factor and Pollution Index

The capability of a plant species to transfer metal from the soil into the plant is indicated as a transfer factor (TF). The factors are considered on the root uptake of the metal and reduce the foliar absorption of atmospheric metal deposits. Higher TF values (≥ 1) indicate higher metal absorption from the soil by plants that can cause harm to human health due to the consumption of the plants. On the contrary, a TF value below 1 indicates a poor plant response to metal absorption [160]. The estimated TF value is given in Table 4.17. In this study, the TF values obtained for three medicinal plants were 0.002–0.021 (Al), 0.002–0.004 (As), 6.93–7.29 (Br), 0.277–0.545 (Ca), 0.046–0.061 (Cd), 0.027–0.035 (Co), 0.008–0.042 (Cr), 0.003–0.030 (Fe), 0.425–0.679 (K), 0.008–0.037 (La), 0.001–0.141 (Mn), 1.52–1.83 (Na), 0.051–0.077 (Pb), 0.021–0.058 (Sb), 0.002–0.026 (Sc), 0.002–0.034 (Th) and 0.125–0.457 (Zn), respectively.

The TF value for Br and Na were higher than 1.0 (Table 4.17) indicating the absorption of Br and Na were higher than the other elements for studied medicinal plants. Besides this,

the TF values obtained for all heavy metals were below 1.0, which implied the low absorption capacity of the heavy metals by the medicinal plants.

Table 4.17: Transfer factor for medicinal plant samples *A. ilicifolius*, *A. officinalis*, and *X. mekongensis*.

Elements	*A. ilicifolius*	*A. officinalis*	*X. mekongensis*
Al	0.021	0.002	0.021
As	0.002	0.004	0.002
Br	7.29	7.24	6.93
Ca	0.305	0.227	0.545
Cd	0.061	0.046	0.056
Co	0.027	0.035	0.029
Cr	0.040	0.008	0.042
Fe	0.030	0.003	0.019
K	0.624	0.425	0.679
La	0.036	0.008	0.037
Mn	0.141	0.001	0.040
Na	1.83	1.52	1.54
Pb	0.059	0.051	0.077
Sb	0.058	0.022	0.021
Sc	0.026	0.002	0.017
Th	0.034	0.002	0.031
Zn	0.457	0.186	0.125

*Concentrations of Ce, Sm, and V in plant leaves were below the detection limits of INAA.

It is also observed that for an element, transfer factors for different medicinal plant species were different. The safety level consideration by using PI value was divided into five categories: safe ($PI \leq 0.7$), guard line ($0.7 < PI < 1$), mild contamination ($1 < PI < 2$), moderate contamination ($2 < PI < 3$), and serious contamination ($PI \geq 3$) [161]. The PI values obtained in this study are shown in Table 4.18.

For *A. officinalis*, the PI values of As, Cd, Cr, Pb, and Zn were below the safety level. On the other hand, for *X. mekongensis*, the PI value of Cr was 2.0 which indicates mild contamination whereas PI for other elements is within safe limits. Besides this, for A. ilicifolius, the value of PI for As, Cd, and Pb was at a secure level but for Zn, it was in the guard line, and for Cr, it was at a mild contamination level.

Table 4.18: Pollution index value for heavy metals in medicinal plants.

Elements	*A. ilicifolius*	*A. officinalis*	*X. mekongensis*
As	0.002	0.004	0.001
Cd	0.13	0.10	0.10
Cr	1.7	0.41	2.0
Pb	0.094	0.10	0.11
Zn	0.82	0.37	0.2

4.2.3 Statistical Analysis of the Elemental Data of Medicinal Plants

Pearson correlation matrix was calculated to study the inter-metal relationships in the medicinal plants of the Sundarban and tabulated in Table 4.19 - 4.21. For *A. ilicifolius* and *X. mekongensis* plants, it is observed that Al has strong positive correlations with most of the elements, and for *A. ilicifolius* plant Fe has also strong positive correlations with most of the metals (Table 4.19). This can be attributed that Al and Fe-oxides in the plant soils are one of the main factors that affect plant uptake of trace elements from soils [162]. Zinc has negative or poor correlations with every metal at *A. officinalis* (except Co and Mn) whereas, at *X. mekongensis*, it has strong positive correlations with most metals. This indicates the complex correlation nature of the elements in different species of medicinal plants [163]. From Table 4.19 - 4.21, it is also observed that for *A. ilicifolius and A. officinalis,* As has a negative or poor correlation with the majority of the elements which may show the different sources of this metal in Sundarban mangrove soils and also in plants.

Table 4.19: Pearson correlation coefficients for the metals in plant sample (*A. ilicifolius*).

	Al	As	Br	Ca	Ce	Cd	Co	Cr	Fe	K	La	Mn	Na	Pb	Sb	Sm	Sc	Th	V	Zn
Al	1.00																			
As	**-0.96**	1.00																		
Br	**0.87**	**-0.97**	1.00																	
Ca	**0.97**	**-0.87**	**0.74**	1.00																
Ce	0.44	-0.17	-0.06	0.63	1.00															
Cd	0.36	-0.61	**0.78**	0.15	-0.68	1.00														
Co	0.45	-0.68	**0.83**	0.24	-0.61	**0.99**	1.00													
Cr	0.22	-0.48	0.67	-0.01	**-0.78**	**0.99**	**0.97**	1.00												
Fe	**0.88**	**-0.98**	**0.99**	**0.74**	-0.05	**0.77**	**0.82**	0.66	**1.00**											
K	**0.99**	**0.91**	**-0.79**	**-0.99**	-0.56	-0.23	-0.32	-0.08	**-0.80**	1.00										
La	0.14	0.14	-0.36	0.36	**0.95**	**-0.87**	**-0.82**	**-0.93**	-0.35	-0.28	1.00									
Mn	-0.65	**0.84**	**-0.94**	-0.46	0.40	**-0.95**	**-0.97**	**-0.89**	**-0.93**	0.54	0.66	1.00								
Na	**-0.81**	**0.94**	**-0.99**	-0.66	0.17	**-0.84**	**-0.89**	**-0.75**	**-0.99**	**0.72**	0.46	**0.97**	1.00							
Pb	0.03	0.26	-0.47	0.25	**0.91**	**-0.92**	**-0.88**	**-0.97**	-0.46	-0.16	**0.99**	**0.75**	0.56	1.00						
Sb	**0.96**	**-0.99**	**0.97**	**0.87**	0.16	0.61	0.68	0.49	**0.98**	**-0.91**	-0.14	**-0.84**	**-0.94**	-0.26	1.00					
Sc	**0.86**	**-0.97**	**0.99**	**0.72**	-0.08	**0.79**	**0.84**	0.69	**0.99**	**-0.78**	-0.38	**-0.95**	**-0.99**	-0.49	**0.97**	1.00				
Sm	-0.32	0.57	**-0.74**	-0.09	**0.71**	**0.99**	**-0.99**	**-0.99**	**-0.74**	0.18	**0.89**	**0.93**	**0.81**	**0.94**	-0.57	**-0.76**	1.00			
Th	**0.99**	**-0.93**	**0.83**	**0.99**	0.51	0.29	0.38	0.14	**0.84**	**-0.99**	0.22	-0.59	**-0.76**	0.10	**0.93**	**0.82**	-0.24	1.00		
V	**0.73**	**-0.89**	**0.97**	0.56	-0.29	**0.90**	**0.94**	**0.82**	**0.97**	**-0.63**	-0.57	**-0.99**	**-0.99**	-0.66	**0.90**	**0.98**	**-0.88**	0.68	1.00	
Zn	0.20	-0.47	**0.66**	-0.02	**-0.79**	**0.99**	**0.97**	**0.99**	0.65	-0.07	**-0.94**	**-0.88**	-0.74	**-0.97**	0.47	0.68	**-0.99**	0.13	**0.82**	1

Bold correlations are significant at $p < 0.01$

The major element Ca exhibits negative or poor correlations with most of the metals at *A. ilicifolius and A. officinalis* which indicates that they can result from diverse sources of contamination of the Sundarban soils.

Table 4.20: Pearson correlation coefficients for the metals in plant sample (*A. officinalis*).

	Al	As	Br	Ca	Cd	Co	Cr	Fe	K	La	Mn	Na	Pb	Sb	Sc	Th	Zn
Al	1.00																
As	**-0.98**	1.00															
Br	-0.10	-0.09	1.00														
Ca	**-0.84**	**0.73**	0.62	1.00													
Cd	0.61	-0.45	**-0.85**	**-0.94**	1.00												
Co	**-0.85**	**0.93**	-0.44	0.43	-0.10	1.00											
Cr	**0.96**	**-0.99**	0.18	-0.67	0.37	**-0.96**	1.00										
Fe	**0.85**	**-0.94**	0.43	-0.44	0.11	**-0.99**	**0.96**	1.00									
K	**-0.86**	**0.75**	0.59	**0.99**	**-0.93**	0.46	-0.69	-0.47	1.00								
La	0.62	-0.46	**-0.84**	**-0.94**	**0.99**	-0.11	0.38	0.12	**-0.93**	1.00							
Mn	-0.65	**0.78**	-0.69	0.14	0.21	**0.95**	**-0.83**	**-0.95**	0.17	0.20	1.00						
Na	0.63	-0.47	**-0.83**	**-0.95**	**0.99**	-0.13	0.40	0.14	**-0.94**	**0.99**	0.18	1.00					
Pb	-0.54	0.37	**0.89**	**0.91**	**0.99**	0.02	-0.29	-0.03	**0.89**	**-0.99**	-0.29	**-0.99**	1.00				
Sb	0.49	-0.32	**-0.92**	**-0.88**	**0.99**	0.04	0.23	-0.03	**-0.87**	**0.99**	0.34	**0.99**	**-0.99**	1.00			
Sc	**0.96**	**-0.99**	0.17	-0.67	0.37	**-0.96**	**0.99**	**0.96**	**-0.69**	0.38	**-0.83**	0.40	-0.30	0.24	1.00		
Th	-0.28	0.09	**0.98**	**0.75**	**-0.93**	-0.27	0.01	0.26	**0.73**	**-0.93**	-0.55	**-0.92**	**0.96**	**-0.97**	-0.01	1.00	
Zn	-0.54	0.69	**-0.79**	0.01	0.35	**0.90**	**-0.75**	**-0.90**	0.03	0.33	**0.99**	0.32	-0.42	0.47	**-0.74**	-0.66	1.00

Bold correlations are significant at $p < 0.01$

For *A. officinalis* significant positive correlation between Cd and Pb ($r = 0.99$, $P < 0.1$) points to their geochemical similarities (chalcophile behavior) in the soil as well as their similar transfer factors (discussed in the previous section) for the medicinal plants.

Table 4.21**:** Pearson correlation coefficients for the elements in plant sample (*X. mekongensis*).

	Al	As	Br	Ca	Ce	Cd	Co	Cr	Fe	K	La	Mn	Na	Pb	Sb	Sm	Sc	Th	V	Zn
Al	1.00																			
As	**0.93**	1.00																		
Br	**0.84**	0.59	1.00																	
Ca	**0.99**	**0.93**	**0.84**	1.00																
Ce	**0.99**	**0.90**	**0.89**	**0.99**	1.00															
Cd	**0.91**	**0.99**	0.54	**0.91**	**0.87**	1.00														
Co	0.03	0.40	-0.51	0.04	-0.05	0.45	1.00													
Cr	**0.99**	**0.98**	**0.74**	**0.99**	**0.97**	**0.96**	0.20	1.00												
Fe	0.24	-0.13	**0.73**	0.24	0.33	-0.19	**-0.96**	0.08	1.00											
K	**-0.98**	**-0.98**	**-0.74**	**-0.99**	**-0.97**	**-0.97**	-0.21	**-0.99**	-0.07	1.00										
La	**0.99**	**0.98**	**0.74**	**0.99**	**0.97**	**0.97**	0.21	**0.99**	0.07	**-0.99**	1.00									
Mn	**0.98**	**0.98**	**0.73**	**0.98**	**0.96**	**0.97**	0.21	**0.99**	0.06	**-0.99**	0.99	1.00								
Na	0.59	0.25	**0.93**	0.59	0.66	0.19	**-0.79**	0.45	**0.93**	-0.44	0.44	0.43	1.00							
Pb	**-0.93**	**-0.72**	**-0.98**	**-0.92**	**-0.96**	**-0.68**	0.35	**-0.85**	-0.59	**0.85**	**-0.85**	**-0.84**	**-0.85**	1.00						
Sb	0.24	-0.13	**0.72**	0.23	0.32	-0.19	**-0.96**	0.08	**0.99**	-0.07	0.07	0.06	**0.93**	-0.59	1.00					
Sm	0.26	-0.11	**0.74**	0.26	0.34	-0.17	**-0.96**	0.10	**0.99**	-0.09	0.09	0.08	**0.93**	-0.60	**0.99**	1.00				
Sc	**0.90**	0.67	**0.99**	**0.90**	**0.93**	0.63	-0.41	**0.81**	0.64	**-0.81**	**0.81**	**0.80**	**0.89**	**-0.99**	0.64	0.66	1.00			
Th	**0.99**	**0.94**	**0.83**	**0.99**	**0.99**	**0.92**	0.06	**0.99**	0.21	**-0.99**	**0.99**	**0.99**	0.57	**-0.91**	0.21	0.23	**0.88**	1.00		
V	**0.99**	**0.92**	**0.85**	**0.99**	**0.99**	**0.90**	0.02	**0.98**	0.26	**-0.98**	**0.98**	**0.98**	0.60	**-0.93**	0.26	0.28	**0.91**	**0.99**	1.00	
Zn	**0.96**	**0.99**	0.66	**0.96**	**0.93**	**0.99**	0.31	**0.99**	-0.04	**-0.99**	**0.99**	**0.99**	0.34	**-0.78**	-0.04	-0.02	**0.74**	**0.97**	**0.95**	1.00

Bold correlations are significant at $p < 0.01$

4.3. NATURAL RADIOACTIVITY AND RADIOLOGICAL RISK ASSESSMENT OF THE CORE SEDIMENTS AND MEDICINAL PLANTS OF SUNDARBAN

4.3.1 Depth-wise Radioactivity Concentrations

The calculated depth-wise activity concentrations of natural radionuclides (^{226}Ra, ^{232}Th, and ^{40}K) of four core samples from Sundarban have been presented in Table 4.22-4.25. The minimum, maximum, and mean activity concentration of natural radionuclides of core samples is given in Table 4.26.

The mean activity concentrations of ^{232}Th were higher than those of ^{226}Ra in the majority of the studied samples (Table 4.26).

Table 4.22: Activity concentrations (Bq kg^{-1}) of radionuclides in the core-1.

Sample	^{226}Ra	^{232}Th	^{40}K
C-1.1	32.7 ± 8.1	36.1 ± 7.4	1350 ± 37
C-1.2	66.2 ± 11.5	59.2 ± 9.4	935 ± 31
C-1.3	33.0 ± 8.1	36.4 ± 7.4	1460 ± 38
C-1.4	36.8 ± 8.6	15.8 ± 4.9	1560 ± 39
C-1.5	22.6 ± 6.7	33.1 ± 7.0	1310 ± 36
C-1.6	20.0 ± 6.3	32.9 ± 7.0	784 ± 28
C1.7	23.5 ± 6.9	49.8 ± 8.6	433 ± 20
C-1.8	51.7 ± 10.2	44.8 ± 8.2	1210 ± 35
C-1.9	40.7 ± 9.0	53.5 ± 9.0	1890 ± 43
C-1.10	16.9 ± 5.8	23.9 ± 6.0	1340 ± 37
C-1.11	23.0 ± 6.8	36.2 ± 7.4	173 ± 13
C-1.12	83.3 ± 12.9	79.4 ± 10.9	1520 ± 39
C-1.13	37.9 ± 8.7	15.6 ± 4.8	936 ± 31
C-1.14	93.6 ± 13.7	79.0 ± 10.9	1780 ± 42
C-1.15	49.4 ± 9.9	76.6 ± 10.7	1750 ± 42
C-1.16	26.3 ± 7.2	34.1 ± 7.2	999 ± 32

In this study, the activity concentrations of ^{226}Ra and ^{232}Th in the studied soils were not identical, which denotes the variations in the geological characteristics of the area under study. However, since K is the most abundant radioactive element in the environment and is widely used as part of an NPK fertilizer medium in intensive farming and agricultural activities to support the rapid growth of crops [164], its activity far outweighed that of ^{232}Th and ^{226}Ra. The analyzed samples' overall mean activities of ^{226}Ra, ^{232}Th, and ^{40}K

were found to be greater than the corresponding global mean values of 35, 30, and 400 Bq kg^{-1}[165].

Table 4.23: Activity concentrations (Bq kg^{-1}) of radionuclides in the core-2.

Sample	^{226}Ra	^{232}Th	^{40}K
C2-1	46.0 ± 9.6	76.2 ± 10.7	854 ± 29
C2-2	101 ± 14	100 ± 12	1660 ± 41
C2-3	102 ± 14	80.6 ± 11.0	1330 ± 36
C2-4	68.0 ± 11.7	108 ± 12	1470 ± 38
C2-5	78.6 ± 12.5	89.3 ± 11.6	864 ± 29
C2-6	46.4 ± 9.6	63.6 ± 9.8	2260 ± 48
C2-7	47.7 ± 9.8	110 ± 12	2750 ± 52
C2-8	44.5 ± 9.4	48.8 ± 8.6	706 ± 26
C2-9	46.6 ± 9.7	44.8 ± 8.2	1600 ± 40
C2-10	43.4 ± 9.3	40.4 ± 7.8	910 ± 30
C2-11	53.8 ± 10.4	60.4 ± 9.5	867 ± 29
C2-12	25.5 ± 7.1	15.4 ± 4.8	388 ± 19
C2-13	43.0 ± 9.3	36.7 ± 7.4	186 ± 13

Due to its high water solubility, ^{226}Ra may experience surface runoff over muddy terrain, whereas ^{232}Th sticks to the soil more due to its limited geochemical mobility [166, 167]. Every location in the world has unique geological and topographical features that affect soil radioactivity [168, 169]. In addition to geology, regional geological events, industrial wastes, mineral processing, soil drainage, use of pesticides and fertilizers, use of fossil fuels, rate and amount of rainfall, and natural occurrences like volcanic eruptions, earthquakes, and forest fires can alter the distribution of radionuclides in soils [136, 170, 171].

Table 4.24: Activity concentrations (Bq kg^{-1}) of radionuclides in the core-3.

Sample	^{226}Ra	^{232}Th	^{40}K
C-3.1	46.1 ± 9.60	92.1 ± 11.8	2090 ± 46
C-3.2	53.4 ± 10.34	103 ± 12	1950 ± 44
C-3.3	36.3 ± 8.5	99.5 ± 12.2	2380 ± 49
C-3.4	62.5 ± 11.2	87.5 ± 11.5	1740 ± 42
C-3.5	52.3 ± 10.2	110 ± 13	2150 ± 46
C-3.6	62.8 ± 11.2	107.± 13	1810 ± 43
C-3.7	33.6 ± 8.2	111 ± 13	2130 ± 46
C-3.8	51.0 ± 10.1	118 ± 14	1890 ± 43
C-3.9	57.6 ± 10.7	81.8 ± 11.1	1340 ± 37
C-3.10	45.9 ± 9.6	90.9 ± 11.7	1770 ± 42
C-3.11	51.5 ± 10.1	79.9 ± 10.9	1560 ± 40
C-3.12	50.7 ± 10.1	87.5 ± 11.5	1260 ± 36
C-3.13	50.3 ± 10.0	71.5 ± 10.4	1080 ± 33
C-3.14	38.3 ± 8.8	65.4 ± 9.9	1090 ± 33

The average activity of ^{226}Ra, ^{232}Th, and ^{40}K in this study was higher for the studied cores (except for the ^{226}Ra and ^{232}Th values in core-1) than those of the Indian Sundarban [172]. The depth-wise variation of the activity concentration of natural radionuclides ^{226}Ra, ^{232}Th, and ^{40}K is shown in Fig. 4.7. It is observed that depth-wise activity concentration variation of ^{226}Ra, ^{232}Th, and ^{40}K activities for core-2 and core-4 increase from the deeper layer to the surface soils, which indicates an increase in radiological contamination in recent years. The activity concentration variations for the other cores are haphazard or overall show no change over the studied soil layers.

Table 4.25: Activity concentrations (Bq kg^{-1}) of radionuclides in the core-4.

Sample	^{226}Ra	^{232}Th	^{40}K
C-4.1	129 ± 16	114 ± 13	1870 ± 43
C-4.2	84.2 ± 13.0	121 ± 14	1900 ± 44
C-4.3	58.4 ± 10.8	135 ± 14	2440 ± 49
C-4.4	108 ± 14	163 ± 16	1850 ± 43
C-4.5	86.7 ± 13.2	134 ± 14	2050 ± 45
C-4.6	84.7 ± 13.0	142 ± 15	337 ± 18
C-4.7	114 ± 15	122 ± 14	1870 ± 43
C-4.8	70.6 ± 11.9	90.8 ± 11.7	1440 ± 38
C-4.9	62.7 ± 11.2	91.7 ± 11.7	1490 ± 39
C-4.10	59.8 ± 10.9	70.7 ± 10.3	1230 ± 35
C-4.11	55.6 ± 9.5	78.3 ± 10.8	1150 ± 34
C-4.12	55.4 ± 10.5	73.1 ± 10.5	1210 ± 35
C-4.13	47.1 ± 9.7	66.7 ± 10.0	673 ± 26
C-4.14	49.0 ± 9.9	62.7 ± 9.7	890 ± 30
C-4.15	49.4 ± 9.9	63.7 ± 9.8	821 ± 29

The comparison of available activity concentrations at different mangrove ecosystems in the world to those of the present study is given in Table 4.27. The activity of both ^{226}Ra and ^{232}Th in the Bangladeshi Sundarban was higher than those of most of the reported mangroves in the world. It is observed that the average activity concentrations of ^{226}Ra and ^{232}Th in the present study were relatively higher than those of the previously reported activity concentrations of the surface soil of the Bangladeshi Sundarban [173, 174].

Table 4.26: Radioactivity concentrations (Bq kg^{-1}) of the naturally occurring radionuclides in the soil core samples.

Sample	Value	^{226}Ra	^{232}Th	^{40}K
Core-1 (32 cm)	Min	16.9 ± 5.8	15.6 ± 4.8	173 ± 13
	Max	93.6 ± 13.7	79.4 ± 10.9	1893 ± 43
	Mean (n = 16)	41.1 ± 8.8	44.2 ± 7.9	1210 ± 34
Core-2 (26 cm)	Min	25.5 ± 7.1	15.4 ± 4.8	186 ± 13
	Max	102 ± 14	110 ± 13	2750 ± 52
	Mean (n = 13)	57.5 ± 10.5	67.3 ± 9.8	1220 ± 33
Core-3(28 cm)	Min	33.6 ± 8.2	65.4 ± 9.9	1080 ± 33
	Max	62.8 ± 11	118 ± 13	2380 ± 50
	Mean (n = 14)	49.5 ± 9.9	93.2 ± 11.8	1730 ± 41
Core-4 (30 cm)	Min	47.1 ± 9.5	62.7 ± 9.7	337 ± 18
	Max	128 ± 16	163 ± 16	2440 ± 49
	Mean (n = 15)	74.3 ± 12	102 ± 12	1410 ± 37
	World Average [169]	35	30	400
	Indian Sundarban [175]	48	58	866

A major portion of the Bangladeshi Sundarban has been reclaimed and is primarily agriculture-based. Phosphate fertilizers are used to increase agricultural productivity. Uranium and thorium are present in significant amounts in phosphate fertilizers. In fact, the concentrations of ^{226}Ra and ^{232}Th in NPK fertilizer could reach as high as 380 and 300 Bq kg^{-1}, respectively [175]. The activity concentrations of ^{232}Th in this study are the same as within the reported uncertainty for the activity concentrations in Pichavaram Mangrove [176].

Table 4.27: Comparison of ^{226}Ra and ^{232}Th activities (Bq kg^{-1}) in soils of different mangrove ecosystems of the world.

Location	^{226}Ra Bq kg^{-1}	^{232}Th Bq kg^{-1}	Reference
Chico Science Mangrove; Pernambuco, Brazil	24 ± 4	41 ± 6	Paiva et al., 2016 [176]
Pichavaram Mangrove; South eastcoast of India	25.9 ± 15.8	65.1±34.5	Satheeshkumar et al., 2011 [177]
Sundarban Mangrove; Eastern part of India	48.9 ± 2.6	58.3 ± 3.1	Chaudhuri et al., 2017 [178]
Payyanur mangrove, Kerala, India	2.6±0.9	13.4±2.8	Benny et al., 2023 [179]
Bangladeshi Sundarban	26±3	33 ±6	Siraz et al., 2023 [173]
Bangladeshi Sundarban	22±2	32±3	Al-mahmud et al., 2024 [180]
Bangladeshi Sundarban	55.6 ± 10.3	76.7 ± 10.4	Present study

The Sundarban deltaic area lies at the tip of the Gangetic plain. At the mouth of the Bay of Bengal, where a network of interconnected bays, creeks, and rivers converge, there is a considerable likelihood that agro-industrial waste from upstream may accumulate alongside locally utilized agrochemicals, leading to an elevated level of ^{226}Ra and ^{232}Th. The high natural radioactivity concentrations relative to Siraz et al., 2023 [173] and Mahmud et al., 2024 [180] could be attributed to the different sampling sites of the Sundarban. They analyzed topsoil samples, whereas we analyzed core sediments from rivers of the Sundarban. The river sediments of the Sundarban may contain higher radioactivity concentrations than those of the soil samples.

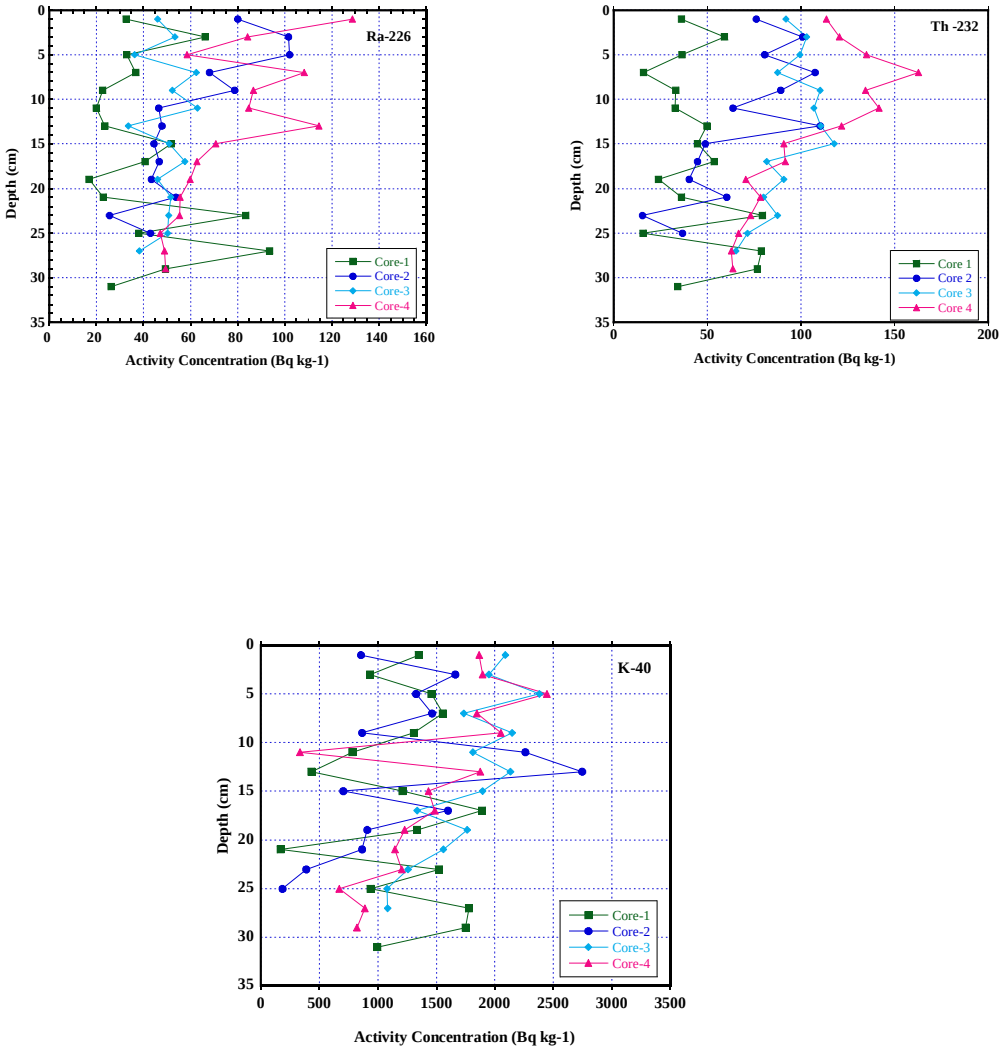

Fig. 4.7: Depth-wise variations of the activity concentrations of the radionucleides ^{226}Ra, ^{232}Th, and ^{40}K .

4.3.2 Radiological Hazard Parameters

The radiological hazard indices calculated for the soils of the Sundarban in this study are given in Table 4.28. The mean Ra_{eq} for four cores was found to be 197 Bq kg^{-1}, 247 Bq kg^{-1}, 315 Bq kg$^{-1,}$ and 328 Bq kg^{-1}, respectively.

Due to natural radionuclides, the average external absorbed dose rate (D) in four core samples was obtained as 96.7 nGy h^{-1}, 118 nGy h^{-1}, 151 nGy h$^{-1,}$ and 155 nGy h^{-1}, respectively, whereas a world average value is 55 nGy h^{-1}[165].

Table 4.28: Radiological hazard indices of core soils of the Sundarban and the corresponding recommended values.

Sample	Value	Ra_{eq} [Bq kg^{-1}]	H_{ex}	H_{in}	D [ηGyh^{-1}]	AED [mSv y^{-1}]	I_γ	ELCR ($x10^{-4}$)
Core-1	Mean	197	0.53	0.65	96.7	0.12	1.53	0.41
	Min	88.1	0.24	0.30	39.8	0.05	0.63	0.17
	Max	343	0.93	1.18	166	0.20	2.60	0.71
Core-2	Mean	247	0.67	0.82	118	0.15	1.87	0.51
	Min	77.3	0.21	0.28	37.4	0.05	0.58	0.16
	Max	416	1.13	1.28	204	0.25	3.25	0.88
Core-3	Mean	315	0.85	0.99	151	0.19	2.42	0.65
	Min	215	0.58	0.69	102	0.13	1.63	0.44
	Max	375	1.01	1.16	181	0.22	2.89	0.78
Core-4	Mean	328	0.89	1.09	155	0.19	2.46	0.67
	Min	194	0.52	0.65	90.3	0.11	1.43	0.39
	Max	483	1.31	1.60	226	0.28	3.58	0.97
	Recommended values	370 [181]	< 1 [165]	< 1 [165]	55 [165]	0.46 [182]	1 [165]	2.9×10^{-4} [165]

Stdev. means standard deviation (1σ).

To maintain insignificant radiation hazards, the values of the H_{ex} and H_{in} hazard indices should be less than unity. In the present study, the H_{in} value for core-4 was found to be slightly higher than unity, and others were less than unity (Table 4.28). The calculated average values of ELCR for the core samples were below the recommended value of $2.9x10^{-4}$ [165]. Thus, among the studied radiological hazard indices, some values higher than the recommended values infer regular monitoring of the activity

concentration levels of the Sundarban soils to save this sensitive ecosystem.

4.3.3 Radioactivity and Associated Radiological Risk of The Medicinal Plants

The activity concentrations of the radionuclides in the medicinal plants, their rhizosphere soils, and radionuclide transfer factors are given in Table 4.29. Among the studied medicinal plants of the Sundarban, a maximum activity concentration of ^{226}Ra was observed at *Acanthus ilicifolius*, whereas maximum activity concentrations of ^{232}Th and ^{40}K were observed at *Xylocarpus mekongensis.*

Table 4.29: Average activity concentrations (Bq kg^{-1}, n = 3) of the radionuclides in medicinal plant leaves, rhizosphere soils, and transfer factor of the radionuclides in the mangrove ecosystem.

Sample ID	Activity concentration (Bq kg^{-1}) in plant sample			Activity concentration (Bq kg^{-1}) in rhizosphere soils			TF		
	^{226}Ra	^{232}Th	^{40}K	^{226}Ra	^{232}Th	^{40}K	^{226}Ra	^{232}Th	^{40}K
A. ilicifolius	66.9 ± 8.2	25.3 ± 5.0	68.1 ± 8.3	49.3 ± 7.0	95.2 ± 11.9	1890 ± 43	1.36	0.27	0.036
A. officinalis	9.03 ± 3.01	27.9 ± 9.2	114 ± 10	46.1 ± 6.8	33.7 ± 9.6	1050 ± 32	0.20	0.83	0.108
X. mekongensis	21.4 ± 6.5	155 ± 16	139 ± 12	63.0 ± 7.9	74.5 ± 10.6	1410 ± 37	0.34	2.08	0.098

The activity concentrations of ^{226}Ra and ^{232}Th in the present study are comparable to the previous studies on the medicinal plants of Thailand [183], Turkey [171], and Ghana [184]. However, the ^{40}K concentration is lower than of the medicinal plants of Ghana [184]. The natural radioactivity levels of medicinal plants are determined to assess the concomitant radiological risks posed to the animals and humans who consume these plants directly or indirectly. The calculated radiological risk parameters and their comparison with the world average values are given in Table 4.30. The computed radiological hazard parameters were determined to be below the permitted limit values when compared to the

worldwide mean values [165]. Hence, this study suggests that the use of these medicinal plants for therapeutic purposes is unlikely to present any health risks to consumers due to radioactivity.

Table 4.30: Average radioactivity concentrations and radiological risk parameters for the studied medicinal plants.

Location	^{226}Ra Bq kg^{-1}	^{232}Th Bq kg^{-1}	^{40}K Bq kg^{-1}	Ra_{eq} Bq kg^{-1}	D nGy h^{-1}	AED µSv y^{-1}	H_{ex}	AE_{ingest} µSv y^{-1}	ELCR 10^{-3}
Sundarban (Present Study)	32	69	107	140	61	75	0.38	46	0.17
World Average [165]	32	45	412	370 [181]	84	410	1	285	0.29

4.3.4 Radionuclide Transfer Factor for the Medicinal Plants

The phytoremediation capacity of terrestrial plants in radionuclide-contaminated soil is significantly indicated by the transfer factor. It is also employed to assess radioactivity transport to plants [185, 186]. A high ability to transmit radionuclides from the soil to the plant is indicated by TF values greater than 1 [187]. In the Sundarban mangrove forest, the TF values of the medicinal plants varied from 0.20 to 1.36, 0.27 to 2.08, and 0.036 to 0.108 for ^{226}Ra, ^{232}Th, and ^{40}K, respectively (Table 4.30). All of the TF values exceeded the default values of 0.04 and 0.05 for ^{226}Ra and ^{232}Th, respectively [188]. The highest TF value of 2.08 was determined for ^{232}Th in *Xylocarpus mekongensis*. The spectrum of TFs in plant organs depends on physiological characteristics, such as species-specific metabolic rates [189]. For phytoremediation, the TF capacity of a plant can be used to enhance radionuclide removal capability [190, 191]. Therefore, phytostabilization is the best option for managing the root system-mediated dispersion of pollutants in mangrove environments. In this study, the high TF values of the studied medicinal plants invoke proper monitoring of their radioactivity levels to prevent health risks for consumers. Moreover, they can be used for phytoremediation of radionuclides in the mangrove ecosystem.

4.3.5 Statistical Analysis of Radiological Data

In this study, statistical analysis of the radioactivity and radiological parameters was done using the software Statistica. To elucidate the potential association and linear relationship between the activity of the radionuclides and their associated radiological indices in the soils, Pearson's correlation analysis was performed in this study. The correlation coefficients between the radionuclides and their associated radiological parameters are given in Tables 4.31- 4.34. From this study, it is observed that ^{226}Ra and ^{232}Th show strong positive correlations for the studied soil cores (except core-3), which denotes radium and thorium content being of the same origin and occurring together [192, 193]. On the other hand, weak and negative correlations between ^{226}Ra and ^{40}K indicate their different source(s) of origin [194] (Table 4.31-4.34).

Table 4.31: Pearson's correlations between radionuclides and associated radiological hazard parameters for core-1.

	^{226}Ra	^{232}Th	^{40}K	Ra_{eq}	D	AED	I_γ	H_{ex}	H_{in}	ELCR
^{226}Ra	**1.00**									
^{232}Th	**0.66**	**1.00**								
^{40}K	0.23	**0.63**	**1.00**							
Ra_{eq}	**0.63**	**0.91**	**0.86**	**1.00**						
D	**0.60**	**0.89**	**0.89**	**1.00**	**1.00**					
AED	**0.60**	**0.89**	**0.89**	**1.00**	**1.00**	**1.00**				
I_γ	0.59	**0.89**	**0.90**	**1.00**	**1.00**	**1.00**	**1.00**			
H_{ex}	**0.63**	**0.91**	**0.86**	**1.00**	**1.00**	**1.00**	**1.00**	**1.00**		
H_{in}	**0.74**	**0.92**	**0.79**	**0.99**	**0.98**	**0.98**	**0.98**	**0.99**	**1.00**	
ELCR	**0.60**	**0.89**	**0.89**	**1.00**	**1.00**	**1.00**	**1.00**	**1.00**	**0.98**	**1.00**

Marked correlations are significant at $p < 0.05$

The strong positive correlations between ^{226}Ra, ^{232}Th, and ^{40}K activities and all radiological parameters ($r > 0.7$) for most of the cores indicate that these radionuclides contribute to the emission of gamma radiation for the cores and influence associated radiological risks in the mangrove soils [195]. For the core soils, principal component (PC) analysis was carried out to investigate the relationship between the radionuclides and related radiological parameters. The major components (PC-1 and PC-2) that were acquired after varimax rotation are given in Table 4.35. It is observed that the first principal component, PC-1 explained about 87.1 to 91.2 % variance for the analyzed cores.

Table 4.32: Pearson's correlations between radionuclides and associated radiological hazard parameters for core-2.

	^{226}Ra	^{232}Th	^{40}K	Ra_{eq}	D	AED	I_γ	H_{ex}	H_{in}	ELCR
^{226}Ra	1.00									
^{232}Th	**0.77**	**1.00**								
^{40}K	0.46	0.35	**1.00**							
Ra_{eq}	**0.86**	**0.82**	**0.79**	**1.00**						
D	**0.83**	**0.78**	**0.83**	**1.00**	**1.00**					
AED	**0.83**	**0.78**	**0.83**	**1.00**	**1.00**	**1.00**				
I_γ	**0.83**	**0.79**	**0.83**	**1.00**	**1.00**	**1.00**	**1.00**			
H_{ex}	**0.86**	**0.82**	**0.79**	**1.00**	**1.00**	**1.00**	**1.00**	**1.00**		
H_{in}	**0.92**	**0.83**	**0.73**	**0.99**	**0.98**	**0.98**	**0.98**	**0.99**	**1.00**	
ELCR	**0.83**	**0.78**	**0.83**	**1.00**	**1.00**	**1.00**	**1.00**	**1.00**	**0.98**	**1.00**

Table 4.33: Pearson's correlations between radionuclides and associated radiological hazard parameters for core-3.

	^{226}Ra	^{232}Th	^{40}K	Ra_{eq}	D	AED	I_γ	H_{ex}	H_{in}	ELCR
^{226}Ra	1.00									
^{232}Th	0.03	**1.00**								
^{40}K	-0.22	**0.80**	**1.00**							
Ra_{eq}	0.05	**0.94**	**0.93**	**1.00**						
D	0.02	**0.92**	**0.95**	**1.00**	**1.00**					
AED	0.02	**0.92**	**0.95**	**1.00**	**1.00**	**1.00**				
I_γ	0.01	**0.93**	**0.95**	**1.00**	**1.00**	**1.00**	**1.00**			
H_{ex}	0.05	**0.94**	**0.93**	**1.00**	**1.00**	**1.00**	**1.00**	**1.00**		
H_{in}	0.22	**0.92**	**0.87**	**0.99**	**0.98**	**0.98**	**0.98**	**0.99**	**1.00**	
ELCR	0.02	**0.92**	**0.95**	**1.00**	**1.00**	**1.00**	**1.00**	**1.00**	**0.98**	**1.00**

Marked correlations are significant at $p < 0.05$

The PCA values for ^{226}Ra, ^{232}Th, and ^{40}K show high loading in PC-1 for every core (except for ^{226}Ra in core-3). Similarly, PC-1 shows the highest loading for all of the radiological parameters (Table 4.35). The high loadings of the parameters in PC 1 imply that the level of natural radioactivity (^{226}Ra, ^{232}Th, and ^{40}K) and associated radiological hazards in the investigated core samples can be traced to the activity concentrations of

^{226}Ra, ^{232}Th, and ^{40}K. The PC 2 has a total variance of 7.64 to 11 % with low loading for practically all of the radiation parameters.

Table 4.34: Pearson's correlations between radionuclides and associated radiological hazard parameters for core-4.

	^{226}Ra	^{232}Th	^{40}K	Ra_{eq}	D	AED	I_γ	H_{ex}	H_{in}	ELCR
^{226}Ra	1.00									
^{232}Th	**0.71**	**1.00**								
^{40}K	0.48	0.55	**1.00**							
Ra_{eq}	**0.81**	**0.90**	**0.83**	**1.00**						
D	**0.79**	**0.87**	**0.86**	**1.00**	**1.00**					
AED	**0.79**	**0.87**	**0.86**	**1.00**	**1.00**	**1.00**				
I_γ	**0.78**	**0.88**	**0.86**	**1.00**	**1.00**	**1.00**	**1.00**			
H_{ex}	**0.81**	**0.90**	**0.83**	**1.00**	**1.00**	**1.00**	**1.00**	**1.00**		
H_{in}	**0.87**	**0.89**	**0.78**	**0.99**	**0.99**	**0.99**	**0.99**	**0.99**	**1.00**	
ELCR	**0.79**	**0.87**	**0.86**	**1.00**	**1.00**	**1.00**	**1.00**	**1.00**	**0.99**	**1.00**

Marked correlations are significant at $p < 0.05$

Table 4.35: Factor loadings of the radioactivity and radiological parameters of soils.

Radiological Parameters	Core-1		Core-2		Core-3		Core-4	
	PCA 1	PCA 2	PCA 1	PCA 2	PCA 1	PCA 2	PCA 1	PCA 2
^{226}Ra	**-0.867**	0.348	**-0.649**	0.733	-0.029	0.997	**-0.819**	0.453
^{232}Th	**-0.817**	0.490	**-0.913**	0.186	**-0.936**	0.025	**-0.888**	0.259
^{40}K	**-0.791**	-0.612	**-0.856**	-0.490	**-0.940**	-0.259	**-0.832**	-0.541
Ra_{eq}	**-1.000**	-0.003	**-1.000**	-0.023	**-1.000**	0.023	**-0.999**	-0.005
D	**-0.997**	-0.073	**-0.997**	-0.074	**-0.999**	-0.007	**-0.998**	-0.057
AED	**-0.997**	-0.073	**-0.997**	-0.074	**-0.999**	-0.007	**-0.998**	-0.057
I_γ	**-0.997**	-0.076	**-0.996**	-0.085	**-0.999**	-0.021	**-0.998**	-0.063
H_{ex}	**-1.000**	-0.003	**-1.000**	-0.023	**-1.000**	0.023	**-0.999**	-0.005
H_{in}	**-0.994**	0.082	**-0.992**	0.126	**-0.981**	0.191	**-0.995**	0.092
ELCR	**-0.997**	-0.073	**-0.997**	-0.074	**-0.999**	-0.007	**-0.998**	-0.057
% variance explained	90.1	7.64	89.4	8.52	87.1	11.0	91. 2	7.95

Chapter 5: CONCLUSIONS

In this study, sediment chronology, MARs, elemental characterization, and natural radioactivity levels of the Sundarban mangrove ecosystem were evaluated using different nuclear techniques. In addition, some chemical elements (Al, As, Br, Ca, Cd, Ce, Co, Cr, Fe, K, La, Mn, Na, Pb, Sc, Sb, Sm, Th, V, and Zn) were determined in medicinal plants by INAA and AAS techniques. The present study indicates that Cr concentrations were slightly higher than WHO/FAO tolerable levels in *A. ilicifolius*, and *X. mekongensis*. However, average daily intake (ADI) values compared with MTDI and target hazard quotient (THQ) values were within the safe levels. Finally, the radioactivity concentrations of natural radionuclides (^{226}Ra, ^{232}Th, and ^{40}K) in medicinal plants and core soils were also estimated for the first time in the Sundarban mangrove forest.

5.1 KEY FINDINGS

According to the obtained results of this study, the following conclusions could be drawn:

- In this study, sediment accumulation rate and temporal variations of natural radioactivity concentrations in sediments of the Bangladeshi Sundarban ecosystem were reported for the first time.
- From this study, sediment accumulation rates for the last one and a half centuries were assessed and indicated that an increase in accumulation rate was observed in recent years, which may be attributed to an increase in human activities and changes in patterns of water circulation in this mangrove system.
- The metal concentration data of the mangrove soils showed that the mean concentrations of Cr and Ni were higher than those of the international guideline values.
- The contamination history of the studied metals for the last century indicated that metal contaminations were higher in recent years than in the past, which should be considered to develop an enlarged management strategy to save this ecosystem from metal pollution.
- The evaluation of ecological risk by different SQGs and PERI indicated low ecological risk (PERI < 100) to the organisms of this ecosystem due to the studied toxic metals.
- The source apportionment of the heavy metals by principal component analysis and correlation analysis revealed that both man-made and natural sources of contamination were present in the studied region.

- ❖ The health risk assessments of the heavy metal contents of medicinal plants from Sundarban indicated that target carcinogenic risk (TCR) values of Cr for *A. ilicifolius* and *X. mekongensis* plants were higher than those of the recommended levels, which reveals some extent of risk to consumers if consumed for a long time.
- ❖ Although studied medical plant leaves might be considered a good source of Ca, K, and Zn, the consumption rate of those leaves must be monitored and strictly controlled by the proper authority to avoid potential toxicity to the consumers.
- ❖ Natural radioactivity and radiological hazard index assessments of the medicinal plants of the Sundarban elucidate that consumption of these plants is radiologically safe.
- ❖ Finally, the results of this study will give valuable data on elemental, ecological, and radiological risks to develop future strategies and enlarge management practices to save the mangrove ecosystem.

5.2 LIMITATION OF STUDY

Since the use of the alpha spectrometry system was limited in this study for a large number of sediment samples, two sediment cores were analyzed using this technique. Mineralogical analysis of the sediments could be applied to find out their mineralogical contents so that the mineral assemblage of the toxic elements would be cleared.

5.3 PRACTICAL IMPLICATION

The findings of this study will facilitate the implementation of sustainable management strategies to protect the sensitive Sundarban mangrove ecosystem from metal and radioactive pollution.

5.4 RECOMMENDATION FOR FURTHER STUDY

- Further research work can be done on a large scale to know the spatial metal pollution status of the whole region including the surrounding area of the Sundarban.
- Water and fish samples from rivers and creeks of the Sundarban can be analyzed in the future to investigate the bioaccumulation of heavy metals and radioactivity in this ecosystem.

BIBLIOGRAPHY

[1] S. Sandilyan, K. Kathiresan, Biodivers Conser, 21 (2012) 523.

[2] K. W. Krauss, C. E. Lovelock, K. L. Mckee, L. Lopez-Hoffman, S. M. L. Ewe, W. P. Sousa, Aquat Bot., 89 (2008) 105.

[3] A. R. Karbassi, R. Amirnezhad, Int. J. Environ. Sci. Technol., 1 (2004) 191.

[4] M. J. Leng, J. D. Marshall, Quat. Sci. Rev., 23 (2004) 811.

[5] I. Sert, M. Eftelioglu, F. E. Ozel, J. Radioanal. Nucl. Chem., 314 (2017) 2155.

[6] J. Shi, D. Zhao, F. Ren, L. Huang, Sci. Total Environ. 871, (2023) 161768.

[7] L. YiYi, C. HaiYang, Z. ZhiRou, W. JinSheng, Chemosphere, 364 (2024) 143299.

[8] A. K. Pathak, R. Kumar, P. Kumar, S. Yadav, India. J. Geochem. Explor., 159 (2015) 169.

[9] A. L. Mariet, C. Bégeot, F. Gimbert, J. Gauthier, P. Fluck, A. V. Walter-Simonnet, The Holocene, 26 (2016) 1225.

[10] M. E. T. Turk, M. Abdullah, R. M. Zakaria, N. K. A Bakar, Estuar. Coast. Shelf Sci., 226 (2019) 106266.

[11] M. Chai, R. Li, Z. Qiu, Z. Niu, X. Shen, Estuar. Coast. Shelf Sci., 240 (2020) 106770.

[12] A. M. Iordache, C. Nechita, R. Zgavarogea, C. Voica, M. Varlam, R. E. Ionete, Sci. Rep., 12 (2022) 880.

[13] F. Moore, M. J. Nematollahi, B. Keshavarzi, Environ. Monit. Assess., 187 (2015), 411.

[14] M. Frignani, L. G. Bellucci, M. Favotto, S. Albertazzi, Environ. Int., 31 (2005) 1011.

[15] M. Maghrebi, A. Karbassi, R. Lak, R. Noori, M. Sadrinasab, Mar. Pollut. Bull., 135 (2018) 880.

[16] A. P. Figols, D. M. Bonotto, J. Radioanal Nucl. Chem., 331 (2022) 89.

[17] J. A. Robbins, D. N. Edgington, Geochim. Cosmochim. Acta, 39 (1975) 285.

[18] A. A. Lubis, J. Coast. Dev., 10 (2006) 9.

[19] M. Baskaran, J. Environ. Radioact., 102 (2011) 13.

[20] J. F.Ontiveros-Cuadras, A.C. Ruiz-Fernández, J. A. Sanchez-Cabeza, L. H. Pérez-Bernal, J. L. Sericano, M. Preda, L. L.M. Kwong, F. Páez-Osuna. Science of the total environment, 468 (2014) 677.

[21] P. G. Appleby, F. Oldfield, Catena, 5 (1978) 1.

[22] M. J. Crickmore, G. S. Tazioli, P. G. Appleby, F. Oldfield, International Hydrological Programme, UNESCO, Paris, (1990) 131.

[23] A. Chowdhury, A. Naz, S. K. Maiti, Environ. Sci. Pollut. Res., 28 (2021) 1.

[24] M. Trifuoggi, L. Ferrara, M. Toscanesi, P. Mondal, J. M. Ponniah, S. K. Sarkar, M. Arienzo, India. Environ. Sci. Pollut. Res., 29 (2021) 6929.

[25] R. J. Daoust, T. R. Moore, G. L. Chmura, J. F. Magenheimer, J. Coast. Res., 12 (1996) 520.

[26] S. Sarkar, Nature, The Third Pole, London, UK, (2018).

[27] A. Kumar, A. L. Ramanathan, M. B. K Prasad, D. Datta, M. Kumar, S. M. Sappal, Environ. Sci. Pollut. Res., 23 (2016) 8985.

[28] M. A. Islam, A. Al-Mamun, F. Hossain, S. B. Quraishi, K. Naher, R. Khan, S. Das, U. Tamim, S. M. Hossain, F. Nahid, Mar. Pollut. Bull., 124 (2017) 356.

[29] J. C. Tilburta, T. J. Kaptchuk, Bulletin of the World Health Organization, 86 (2008).

[30] J. G. F. Macedo, I. R. A. Menezes, D. A. Ribeiro, M. O. Santos, D.G. Mâcedo, M. J. F. Macêdo, B. V. Almeida, L. G. S. Oliveira, C. P. Leite, M. M. A. Souza, Evid Based Complement Alternat Med., (2018) 6769193.

[31] M. Ekor, Front Pharmacol, 4 (2013) 177.

[32] S. Javied, F. Arshad, M. Tufail, J. Radioanal. Nucl. Chem., 331 (2022) 4615.

[33] F. Karahan, I. I. Ozyigit, I. A. Saracoglu, Biol. Trace Elem. Res., (2019) 1.

[34] R. Teschke, C. Frenzel, X. Glass, J. Schulze, A. Eickhoff, Br. J. Clin Pharmacol, 75 (2013) 630.

[35] S. Begaa, M. Messaoudi, L. Radiochim. Acta, 106 (2018) 769.

[36] K. Pytlakowska, A. Kita, P. Janoska, M. Połowniak, V. Kozik, Food Chem., 135 (2012) 494.

[37] R. Proshad, D. Zhang, M. Uddin, Y. Wu, China. Environ. Sci. Pollut. Res., 27 (2020) 18355.

[38] A. E. Mohamed, M. N. Rashed, A. Mofty, Ecotoxicol Environ. Saf., 55 (2003) 251.

[39] M. L. Alonso, F. P. Montana, M. Miranda, C. Castillo, J. Hernandez, J. L. Benedito, Biometals, 17 (2004) 389.

[40] L. Jarup, Br. Med. Bul., l68 (2003) 167.

[41] R. N. Malik, N. Zeb, Ecotoxicol, 18 (2009) 522.

[42] M. Rahman, M. A. Islam, M. M. Zaved, Biol. Trace Elem. Res., 198 (2020) 707.

[43] S. Raut, S. Khan, Adv. Plant. Sci., 25 (2012) 749.

[44] W. M. Bandaranayak, Mangroves and Salt. Marshes, 2 (1998) 133.

[45] A. Simlai, A. Roy, Pharmacogn Rev., 7 (2013) 170.

[46] A. I. Robertson, D. M. Alongi, K. G. Boto, Tropical mangrove ecosystems, (1993) 293.

[47] J. A. Duke, K. K. Wain, Encyclopaedia Americana, Grolier, 3 (1981) 25.

[48] S. Ganesh, J. J. Vennila, Res. J. Phytochem., 5 (2011) 60.

[49] M. T. Islam, J. Sharifi-Rad, M. Martorell, E. S. Ali, M. N. Asghar, F. Deeba, K. Chelapram, C. K. Firoz, M. S. Mubarak, J. Ethnopharmacol., 15 (2020) 112958.

[50] M. M. M. Siraz, A. M. Jubair, M. S. Alam, R. MdBazlar, Z. Hossain, U. K. Mayeen, D. A. Bradley, S. Yeasmin, Plos one, 18 (2023) 0289113.

[51] V. Ramasamy, M. Sundarrajan, K. Paramasivam, V. Meenakshisundaram, G. Suresh, Appl. Radiat. Isot., 73 (2013) 21.

[52] H. M., Zakaly, A., Abbasi, N., Almousa, A. Savaşan, J. Radioanal. Nucl. Chem., 333 (2024) 1073

[53] G. Hevesy, H. Levi, Danske Videnskabernes Selskab, Mathematisk-fysiske Meddelelser, 14 (1936) 3.

[54] L. C. Laul, Atomic Energy Rev.,17 (1979) 3.

[55] D. Soete, D. Gijbels, R. Hoste, New York, (1972).

[56] M. J. Crickmore, G. S.Tazioli, P. G Appleby, F. Oldfield, International Hydrological Programme, UNESCO, Paris, (1990) 131.

[57] M. Ivanovich, R. S. Harmon, Uranium-series Disequilibrium: Applications to Earth, Marine and, Environmental Sciences, Clarendon Press-Oxford, (1992) 1250.

[58] S. Ballestra, T. Hamilton, Basic Procedures Manual Radiochemistry, IAEA-Marine Environment Laboratory, Monaco, (1994)75.

[59] J. A. Sanchez-Cabeza, P. Masque, I. A. Ragolta, J. Merino, M. Frignani, F. Alvisi, A. Palanques, P. Puig, Pro. Oceanogr., 44 (1999) 313332.

[60] G. J. Hancock, J. R. Hunter, Australia, Mar Fresh. Wat. Res., 50 (1999) 533.

[61] D. Pittauerova, B. Hettwig; H. W. Fischer, Supported lead in Pb-210 chronology, Institute of Environmental Physics, University of Bremen, Bremen, GERMANY.

[62] D. G. Wren, J. R. Rigby, G. R. Davidson, M. A. Locke, J. Soil Water Conserv., 71 (2016) 137.

[63] A. Kumar, A. L. Ramanathan, M. B. K. Prasad, D. Datta, M. Kumar, S. M. Sappal, Environ. Sci. Pollut. Res., 23 (2016) 8985.

[64] A. Borrell, V. Tornero, D. Bhattacharjee, A. Aguilar, Sci. Total Environ., 545 (2016) 414.

[65] E. V. Silva Filho, M. P. Jonathan, M. Chatterjee, S. K. Sarkar, S. M. Sella, A. Bhattacharya, K. K. Satpathy, Environ. Earth Sci., 63 (2011) 1213.

[66] B. D. Bhattacharya, D. C. Nayak, S. K. Sarkar, S. N. Biswas, D. Rakshit, M. K. Ahmed, J. Clean. Prod., 96 (2015) 233.

[67] R. Chowdhury, P. J. C. Favas, J. Pratas, M. P. Jonathan, P. S. Ganesh, S. K., Sarkar, Int. J. Phytoremediation, 17 (2015) 885.

[68] R. R. Harris, M. C. Santos, Mar. Biol., 137 (2000) 691.

[69] S. D. Sasmito, Y., Kuzyakov, A. A. Lubis, D. Murdiyarso, L. B. Hutley, S., Bachri, D. A. Friess, C. Martius, N. Borchard, Catena, 187 (2020) 104414.

[70] M. A. Islam, B. Das, S. B. Quraishi, R. Khan, K. Naher, S. M. Hossaina, S. Karmakerd, S. A. Latife, M. B. Hossen, Mar. Polluti. Bull., 160 (2020) 111649.

[71] M. Rahman, M. A. Islam, M. M. Zaved, Biol. Trace Elem. Res., 198 (2000) 707.

[72] M. Rahman, M. A. Islam, A. K. Ruhul, J. Radioanal. Nucl. Chem., 318 (2018) 1347.

[73] M. A. Islama, A. Al-mamun, F. Hossainc, S. B. Quraishid, K. Nahera, R. Khana, S. Dasa, U. Tamima, S.M. Hossaina, F. Nahid, Mar. Pollut. Bull., 124 (2017) 356.

[74] C. A. Tannus, F. S. Dias, F. B. Santana, D. C. M. B. Santos, H. I. F. Magalhães, F. S. Dias, A. F. S. Júnior, Biol. Trace Elem. Res., 199 (2021) 2330.

[75] A. Chowdhury, A. Naz, S. K. AMaiti, Environ. Sci. Pollut. Res., 28 (2021) 33042.

[76] J. Gao, D. Zhang, E. E. Uwiringiyimana, R. Proshad , A. Ugurlu, Biol. Trace Elem. Res., 199 (2021) 4342.

[77] M. U. Khandaker, K. Asaduzzaman, A. F. B. Sulaiman, D. A. Bradley, M. O. Isinkaye, Mar. Pollut. Bull., 127 (2018) 654.

[78] E. N. Naskar, S. Lahiri, P. Chaudhuri, J. Radioanal. Nucl. Chem., 1 (2019) 213.

[79] D. J. Stanley, A. K. Hait, J. Coast. Res., 16 (2000) 26.

[80] A. Chowdhury, A Naz, S. K. Maiti, Environ. Sci. Pollut. Res., 28 (2021) 1.

[81] A. Chowdhury, A. Naz, S. K. Maiti, Environ. Sci. Pollut. Res., 189 (2023) 106042.

[82] FAO/UNDP, Integrated resource management plan of the Sundarbans Reserved Forest. Project BGD/84/056, 1 (1998) 323.

[83] S. L. Goodbred, S. A., Kuehl, M. S. Steckler, M. H. Sarker, Sedimentary Geology, 155 (2003) 301.

[84] S. Das, J. R. Vincent, Proceedings of the National Academy of Sciences, 106 (2009) 7357.

[85] M. R. Ali, M. A. Islam., M. F. Hossain, S. M. Hossain, S. M. R. Khan, K. Naher,U. Tamim, F. Nahid, Bangladesh. J.Radioanal. Nucl. Chem., 328 (2021) 1349.

[86] T. R. Choudhury, N. Acter, N. Uddin, M. Kamal, A. M. S. Chowdhury, M. S. Rahman, Environ. Nanotechnol. Monit. Manag., 16 (2021) 100484.

[87] A. A. Lubis, J Coast Dev., 10 (2006) 9.

[88] S. D. Sasmito, Y. Kuzyakov, A. A. Lubis, D. Murdiyarso, L. B. Hutley, S. Bachri, D. A. Friess, C. Martius, N. Borchard, Catena, 187 (2020) 104414.

[89] J. Carroll, M. Williamson, I. Lerche, E. Karabanov, D. F. liams, Appl. Rad. Isotop., 50 (1999) 1105.

[90] J. Sanchez-Cabeza, A. Ruiz-Fernández, Cosmochim. Acta, 82 (2012) 183.

[91] H. M., Zakaly, A., Abbasi, N., Almousa, A. Savaşan, J. Radioanal. Nucl. Chem., 333 (2024) 1073.

[92] G. M. S., Abrahim, R. J. Parker, Environ. Monit. Assess., 136 (2008) 227.

[93] M. Chatterjee, S. Massolo, S. K. Sarkar, A. K. Bhattacharya, B. D. Bhattacharya, K. K. Satpathy, S. Saha, Environ. Monit. Assess., 150 (2009) 307.

[94] M. A. H. Bhuiya, L. Parvez, M. A. Islam, S. B. Dampare. S. Suzuki, J. Hazard. Mater, 173 (2010) 384.

[95] E. R. Long, D. D. MacDonald, C. G. Severn, B. C. Hong, Environ. Toxicol., 19 (2000) 2598.

[96] X. Gao, C. T. A. Chen, Water Res., 46 (2012) 1901.

[97] L. Tettey-Larbi, E.O. Darko, C. Schandorf, A. A. Appiah, Springer Plus. 2 (2013) 157.

[98] S. R. Harb, Radiat. Protect. Environ., 38 (2015) 35.

[99] International Atomic Energy Agency (IAEA), Soil–plant transfer of radionuclides in non-temperate environments. IAEA-TECDOC-1979, Vienna, Austria, (2021).

[100] P. Bode, Instrumental and organizational aspects of a neutron activation analysis laboratory. Interfaculty Reactor Institute, Delft University of Technology, Delft, (1996) 147.

[101] J. Kucera, V. Stypanek, P. Bode, J. Radioanal. Nucl. Chem., 245 (2000) 115.

[102] J. A. Sanchez-Cabeza, P. Masque, I. Ani-Ragolta, J. Merino, M. Frignani, F. Alvisi, A. Palanques, P. Puig, Progress in Oceanography, 44 (1999) 313.

[103] G. J. Hancock, J. R. Hunter, Mar Fresh. Wat. Res., 50 (1999) 533.

[104] K. Banerjee, B. Senthilkumar, R. Purvaja, R. Ramesh, Environ. Geochem. Health, 34 (2012) 27.

[105] D. M. Alongi, J. Pfitzner, L. A. Trott, F. Tirendi, P. Dixon, D. W. Klumpp, Coast. Shelf Sci., 63 (2005) 605.

[106] R. L. Rudnick, S. Gao, Composition of the continental crust. In: Treatise on Geochemistry, second ed. (2014) 1 (chapter 4).

[107] K. K. Turekian, K. H. Wedepohl, Geol. Soc. Am. Bull., 72 (1961) 175.

[108] United States Environment Protection Agency (USEPA): Screening-level Ecological Risk Assessment Protocol for Hazardous Waste Combustion Facilities. Appendix E Toxicity Ref Values, 3 (1999).

[109] United Nations Environment Programme (UNEP), GESAMP: Cadmium, lead and tin in marine environment. United Nations Environment Programme: Regional Seas Reports and Studies No., 56 (1999) 90.

[110] Sk. A. Latif, D. Afroj, S. M. Hossain, M. S. Uddin, M. A. Islam, K. Begum, Y. Oura, M. Ebihara, M. Katada, Bull Environ Contam Toxicol., 82 (2009) 384.

[111] M. R. Ali, M. A. Islam, M. F. Hossain, S. M. Hossain, R. Khan, K. Naher, U. Tamim, F. Nahid, J. of Radioanal. Nucl. Chem., 328 (2021) 1349.

[112] K. Ahmed, Y. Mehedi, R. Haque, P. Mondol, Environ. Monit. Assess., 177 (2011) 505.

[113] R. Chowdhury, P. J. C. Favas, J. Pratas, M. P. Jonathan, P. S. Ganesh, S. K. Sarkar, Int. J. Phytoremediation, 17 (2015) 885.

[114] N. Bodin, R. Ka. S. Gom-Ka, O. T. Thiaw, L. Tito de Morais, F. Le-Loch, E., Rozuel-Chartier, D. Auger, J. F. Chiffoleau, West Africa. Chemosphere, 90 (2013)150.

[115] A. P. Mackey, M. C. Hodgkinson, Environ. Pollut., 90 (1995) 181.

[116] R. R. Harris, M. C. Santos, 2000. Trace metal contamination and physiological variability in the Brazilian mangrove crabs Ucidescordatus and Callinectesdanae (Crustacea: Decapoda). Mar. Biol., 137 (2000) 691.

[117] N. F. Y. Tam, Y. S. Wong, Environ. Pollut., 110 (2000) 195.

[118] A. Kumar, A. L. Ramanathan, M. B. K. Prasad, D. Datta, M. Kumar, S. M. Sappal, Environ. Sci. Pollut. Res., 23 (2016) 8985.

[119] M. A. Islam, A. Al-Mamun, F. Hossain, S. B. Quraishi, K. Naher, R. Khan, S. Das, U. Tamim, S. M. Hossain, F. Nahid, Mar. Pollut. Bull., 124 (2017) 356.

[120] P. Ranjan, A. L. Ramanathan, A. Kumar, R. K. Singhal, D. Datta, M., Venkatesh, Mar. Pollut. Bull., 127 (2018) 541.

[121] B. Antizar-Ladislao, P. Mondal, S. Mitra, S. K. Sarkar, Mar. Pollut. Bull., 101 (2015) 886.

[122] M. A. Awal, W. H. Hale, B. Stern, Mar. Pollut. Bull., 58 (2009) 1944.

[123] S. K. Acharyya, S. Lahiri, B. C. Raymahashay, A., Bhowmik, Environ. Geol., 39 (2000)1127.

[124] M. Chakraborty, A. Mukherjee, K. M. Ahmed, Current Pollution Reports, 1 (2015) 220.

[125] M. V. S. F. E., Chatterjee, E. V. Silva Filho, S. K. Sarkar, S. M. Sella, A. K. K. Bhattacharya Satpathy, M. V. R. Prasad, S. Chakraborty, B. D. Bhattacharya, Environ. Int., 33 (2007) 346.

[126] M. Chatterjee, S. Massolo, S. K. Sarkar, A. K. Bhattacharya, B. D. Bhattacharya, K. K. Satpathy, S. Saha, Environ. Monit. Assess., 150 (2009) 307.

[127] Canadian sediment quality guidelines for the protection of aquatic life: mercury, zinc, lead, copper, chrome and cadmium. In: Canadian Environmental Quality Guidelines, 1999. Winnipeg, Canadian Council of Ministers of the Environment (CCME) (1999).

[128] National Oceanic and Atmospheric Administration (NOAA), USA (2012), (Chapter 173–204 WAC, 1991/95, WA Dept. of Ecology).

[129] E. R. Long, D. D. MacDonald, C. G. Severn, B. C. Hong, Environ. Toxicol., 19 (2000) 2598.

[130] P. J. Hanson, D. W. Evans, D. R. Colby, Mar. Environ. Res., 36 (1993) 237.

[131] K. D. Daskalakis, T. P. O'Connor. Environ. Sci. Technol., 29 (1995) 470.

[132] F. R. Siegel, Environmental Geochemistry of Potentially Toxic Metals. Springer-Verlag Berlin Heidelberg GmbH, New York (2002) 30.

[133] R. Khan, M. S. Islam, A. R. M. Tareq, K. Naher, A. R. M. T. Islam, M. A. Habib, M. A. B. Siddique, M. A. Islam, S. Das, M. B. Rashid, A. A., Ullah, Environ. Nanotechnol. Monit. Manag., 14 (2020) 100318.

[134] M. A. Ahsan, F. Satter, M. A. B. Siddique, M. A. Akbor, S. Ahmed, M. Shajahan, R. Khan, Environ. Monit. Assess., 191 (2019) 575.

[135] M. Maghrebi, A. Karbassi, R. Lak, R. Noori, M. Sadrinasab, Mar. Pollut. Bull., 135 (2018) 880.

[136] M. A. Islam, B. Das, S. B. Quraishi, R. Khan, K. Naher, S. M. Hossain, S. Karmaker, S. A. Latif, M. B. Hossen, Mar. Pollut. Bull., 160 (2020) 111649.

[137] L. Boruvka, O. Vacek, J. Jehlicka, Geoderma, 128 (2005) 289.

[138] R. Sajn, J. Halamić, Z. Peh, L. Galović, J. Alijagić, Geochem. Explor., 110 (2011) 278.

[139] G. R. Wu, H. L. Hong, C. L. Yan, Int. J. Environ. Res. Public Health, 12 (2015) 7244.

[140] S. D. U. Islam, M. A. H. Bhuiyan, Environ. Sustain., 1 (2018) 113.

[141] J. E. Zhang, J. L. Liu, Y. Ouyang, B. W. Liao, B. L. Zhao, Ecological Engineering, 36 (2010) 807.

[142] W. Cheng, S. Le, Z. Bian, Y. Zhao, Y. Li, Y. Gan, J. Hazard Mater. 387 (2020) 121666.

[143] J. A. Beto, The role of calcium in human aging. Clin Nutr Res, 4 (2015) 1.

[144] K. Szentmihályi, Á. Kéry, M. Then, B. Lakatos, Z. Sándor, P. Vinkler, Phyther Res, 12 (1998) 163.

[145] A. Arzani, H. Zeinali, K. Razmjo, Plant Physiol Biochem, 45 (2007) 323.

[146] R. Dghaim, S. Al Khatib, H. Rasool, M. Ali Khan, J Environ Public Health, (2015).

[147] H. Begum, M. Humayun, K. Zaman, Z. Shinwari, A. Hussain, Pak J. Bot., 49 (2017) 1155.

[148] M. A. Nkansah, S. T. Hayford, L. S. Borquaye, J. H. Ephraim, Cogent. Environ. Sci., 2 (2016) 1234660.

[149] World Health Organization WHO guidelines for assessing quality of herbal medicines with reference to contaminants and residues (2007).

[150] S. K. Panda, F. Baluska, H. Matsumoto, Aluminum stress signaling in plants. Plant Signal Behav, 4 (2009) 592.

[151] A. Chowdhury, A. Naz, S. K. Maiti, Environ. Sci. Pollut. Res. 28 (2021) 1.

[152] B. K. Mandal, K. T. Suzuki Arsenic round the world: a review. Talanta, 58 (2002) 201.

[153] K. Annan, R. A. Dickson, I. K. Amponsah, I. K. Nooni, Pharm Res., 5 (2013) 103.

[154] Summary and conclusions of the 61st meeting of the Joint FAO/WHO Expert Committee on Food Additives (JECFA), JECFA/61/SC. Rome, Italy, (2003).

[155] N. Shaheen, N. M. Irfan, I. N. Khan, S. Islam, M. S. Islam, M. K. Ahmed, Chemosphere, 152 (2016) 431.

[156] M. Rahman, M. A. Islam, Biol. Trace Elem. Res., 191 (2019) 243.

[157] N. Saha, M. R. Zaman, Environ. Monit. Assess., 185 (2013) 3867.

[158] Regional Screening Level Tables of the EPA, Accessed, 5 (2023).

[159] M. Rahman, M. A. Islam, R. A. Khan, J. Radianal. Nucl. Chem., 318 (2018) 1347.

[160] S. S. Rangnekar, S. K. Sahu, G.G. Pandit, V. B. Gaikwad, Int. Res. J. Environ. Sci., 2 (2013) 1.

[161] J. L. Y. Wang, H. Yang, P. Yu, Y. Tang, Ecol. Risk Assess., 24 (2018) 2288.

[162] S. Dudka, W. P. Miller, J. Environ. Sci. Health, Part B, 34 (1999) 681.

[163] W. Liu, X. Yang, L. Duan, R. Naidu, K. Yan, Y. Liu, X. Wang, Y. Gao, Y. Chen, Scientific Reports, 11 (2021) 2064.

[164] I. H. Saleh, A. F. Hafez, N. H. Elanany, H. A. Motaweh, M. A. Naim, J. Environ. Eng. Sci., 31 (2007) 9.

[165] UNSCEAR, Sources and effects of Ionizing Radiations, United Nations. Report to the General Assembly, with Scientific Annexes, United Nations (A/55/46), New York, (2000).

[166] G. Suresh, V. Ramasamy V. Meenakshisundaram, R. Venkatachalapathy, V. Ponnusamy, Appl. Radiat. Isot., 69 (2011) 1466.

[167] R. Khan, M. S. Parvez, Y. N. Jolly, M. A. Haydar, M. F. Alam, M. A. Khatun, M. M. R. Sarker, M. A. Habib, U. Tamim, S. Das, S. Sultana, M. A. Islam, K. Naher, D. Paul, S. Akter, M. H. R. Khan, F. Nahid, R. Huque, M. Rajib, S. M. Hossain, Environ. Nanotechnol. Monit. Manag.,12 (2019) 100225.

[168] S. J. A. Dos, S. A. R. Dos, D. N. Santos, J. M. Da Silva, L. A. V. Rojas, M. O. Milan, M. N. De Almeida, J. Bezerra, E. E. N. D. Araújo, Radiat. Prot. Dosimetry, 182 (2018) 448.

[169] M. Tanha, B. Riebe, A. Ikeda-Ohno, M. Schulze, F. R. Khalid, A. Storai, C. Walther, J. Radioanal. Nucl. Chem., 318 (2018) 2425.

[170] A. Abbasi, H. M. Zakaly, F. Mirekhtiary, Mar. Pollut. Bull., 161 (2020) 111793.

[171] A. Guven, G. B. Cengiz, I. Caglar, S. Ates, Appl. Radiat. Isot., 200 (2023) 110939.

[172] N. Nabanita, L. Susanta, C. Punarbasu, J. Radioanal. Nucl. Chem., (2019).

[173] M. M. M. Siraz, A. M. Jubair, M. S. Alam, R. MdBazlar, Z. Hossain, U. K. Mayeen, D. A. Bradley, S. Yeasmin, Plos one, 18 (2023) 0289113.

[174] FAO/UNDP, Integrated resource management plan of the Sundarbans Reserved Forest. Project BGD/84/056, 1 (1998) 323.

[175] C. H. Saueia, B. P. Mazzilli, D. I. T. Favaro, J. Radioanal. Nucl. Chem., 264 (2005) 445.

[176] J. D. S. Paiva, E. E. Sousa, E. E. G. Farias, A. M. Carmo, E. M. Souza, E. J. Franca, J. Radioanal. Nucl. Chem., 307 (2016) 883.

[177] G. Satheeshkumar, P. S. Hameed, M. Meeramaideen, V. Kannan, Radiation Protection Environment, 34 (2011) 96.

[178] P. Chaudhuri, N. Nabanita, L. Susanta, J. Radioanal. Nucl. Chem., 311 (2017) 194.

[179] S. P. Benny, T. K. Prasad, V. Vineethkumar, K. P. Shimod, S. Das, M. D. Sajeev, Materials Today: Proceedings, (2023).

[180] J. Al Mahmud, M. M. Siraz, M. S. Alam, M. J. Dewan, M. B. Rashid, M. U. Khandaker, H. Osman, N. Tamam, S. Yeasmin, Mar. Pollut. Bull., 202 (2024) 116349.

[181] OECD (Organization for Economic Cooperation and Development), Exposure to Radiation from Natural Radioactivity in Building Materials. In: Report by the NEA (Nuclear Energy Agency) Group of Experts. OECD, Paris, France, (1979).

[182] UNSCEAR, United Nations Scientific Committee on the Effects of Atomic Radiation, Sources and Effects of Ionizing Radiation. United Nations, New York, (2008).

[183] K. Saenboonruang, E. Phonchanthuek, K. Prasandee, J. Environ. Radioact., 184 (2018) 1.

[184] L. Tettey-Larbi, E.O. Darko, C. Schandorf, A. A. Appiah, Springer Plus., 2 (2013) 157.

[185] V. A. Pulhani, S. Dafauti, A. G. Hegde, R. M. Sharma, U. C. Mishra, J. Environ. Radioact., 79 (2005) 331.

[186] H. P. Aung, Y. S. Aye, A. D. Mensah, R. A. Omari, S. Djedidi, Y. Oikawa, N. Ohkama-Ohtsu, T. Yokoyama, S. D. Bellingrath-Kimura, J. Environ. Radioact., 150 (2015) 203.

[187] N. Hu, D. Ding, G. Li, J. Li. L. Zheng, W. Zhao, Y. Wang, J. Environ. Radioact., 129 (2014) 100.

[188] IAEA, Handbook of parameter values for the prediction of radionuclide transfer in temperate environments. Technical Reports Series No.364, Vienna, (1994).

[189] S. B. Chen, Y. G. Zhu, Q. H. Hu, J. Environ. Radioact., 82 (2005) 223.

[190] F. W. Whicker, G. Shaw, G. Voigt, E. Holm, Environ. Pollut., 100 (1999) 133.

[191] P. Kotrba, M. Mackova, T. Macek. Microbial Biosorption of Metals. Springer, the Netherlands, (2011).

[192] I. Tanaskovic, D. Golobocanin, N. Miljevic, J. Geochem. Explor., 112 (2012) 226.

[193] A. S. M. Sayam, M. A. Islam, M. R. Ali, M. M. H. Khan, M. F Ishrak, Applied Radiation and Isotopes, 196 (2023) 110784.

[194] C. G. Bilgici, I. Çaglar, Acta Pharmaceutica Sciencia, 57 (2019) 133.

[195] R. Ravisankar, J. Chandramohan, A. Chandrasekaran, P. J. J. Prince, I. Vijayalakshmi, P. Vijayagopal, B. Venkatraman, Mar. Pollut. Bull., 97 (2015) 419.